HOKKAIDO UNIVERSITY

Title	Design of Wide Area Monitoring Systems for Securing Voltage Stability
Author(s)	Putranto, Lesnanto Multa Putranto
Citation	北海道大学. 博士(工学) 甲第12656号
Issue Date	2017-03-23
DOI	10.14943/doctoral.k12656
Doc URL	http://hdl.handle.net/2115/65980
Type	theses (doctoral)
File Information	Lesnanto_Multa_Putranto.pdf

Instructions for use

Hokkaido University Collection of Scholarly and Academic Papers : HUSCAP

SSI-DT79145049

Doctoral Thesis

Design of Wide Area Monitoring System for Securing Voltage Stability

Lesnanto Multa Putranto

March, 2017

Power and Energy System Laboratory
Division of Systems Science and Informatics
Graduate School of Information Science and Technology
Hokkaido University

Doctoral Thesis
submitted to Graduate School of Information Science and Technology,
Hokkaido University
in partial fulfillment of the requirements for the degree of
Doctor of Information Science.

Lesnanto Multa Putranto

Thesis Committee: Professor Hiroyuki Kita
Professor Hajime Igarashi
Professor Satoshi Ogasawara
Associate Professor Ryoichi Hara

Design of Wide Area Monitoring System for Securing Voltage Stability

Lesnanto Multa Putranto

ABSTRACT

The trend of renewable energy integration, power system size and complexity growth, occurrence of line contingencies, and more stressed loading conditions for power systems increase the threat of voltage stability, which has recently been among the main problems in power systems. Those factor cause uncertainty in power system, which make the existing conventional systems and control strategy insufficient to warrant the secure operation. For obtaining securer operation, design of wide area monitoring system (WAMS), which has more reliable performance than conventional system, is proposed in this work. The originalities of this thesis are described in two major parts, which are WAMS applications and phasor measurement units (PMUs) configuration, including the state estimation process.

First, the WAMS application is focused on how to secure the voltage stability under the uncertainty scenario. Scenarios are built as the combination of line contingency and renewable energy source (RES) power fluctuation for the upcoming time-slot. For that purpose, a multistage preventive scheme based on voltage stability and security monitoring and control is developed for securing all of selected scenarios for the upcoming time-slot. A stochastic security-constrained optimal power flow considering voltage stability and renewable energy generation uncertainty, reactive power compensator tap re-operation minimization, and load shedding minimization problems are hierarchically implemented. Considering huge number of scenarios, the optimization problem size will become huge, for that a hybrid computation approach for solving optimal power flow (HC-OPF) is proposed, which make the problem can be solved within reasonable computation time. Furthermore, the problem is extended for re-scheduling of energy storage system (ESS) operation if a power system operates the ESS.

Second, WAMS is correlated to the PMUs configuration since they are the main component to warrant the WAMS performance. PMUs have advantages comparing to the conventional measurement in sampling rate and uniform sampling time. Design for PMU-based WAMS and WAMS hybrid are described in the second

part. For PMU-based WAMS, novel PMU placement and state estimation procedure for PMU-based WAMS are proposed. A new PMU placement algorithm, which can minimize the number of PMU, considering network connectivity, ZIB, N-1 line contingency, system reliability and voltage stability level is proposed. By introducing the concept of system reliability, the proposed method can effectively reduce the number of PMU while ensuring the observability for major contingencies. Furthermore, state estimation technique considering measurement errors to increase the estimation accuracy based on time-series PMU data LAV estimator is proposed. Proposed state estimation method can minimize the estimation error which has been proven in fast system condition. For WAMS hybrid, the procedure to upgrade SCADA into WAMS systems by installing sufficient number of PMUs in the existing SCADA system and state estimation for PMU-SCADA data combination are described. Optimal PMU placement is subjected to the improvement of estimation accuracy under contingencies considering some important buses. State estimation for WAMS hybrid manages the initial state variable and modifies the weighting factor strategy which is suitable for hybrid system especially during fast system condition change.

Several cases based on a modified IEEE 57-bus test system are used to demonstrate the effectiveness of the contributions. The simulation results show that the proposed methods can make an important contribution to improve voltage stability and security performance under uncertainty condition. Furthermore, the estimation accuracy of the overall power system is also increasing, which can improve the preciseness of the monitoring and controlling process. Optimal PMUs placement in a power system can be flexibly decided since the proposed methods give some option in selecting the important consideration.

Keywords : power system uncertainty, multistage preventive control scheme, stochastic security-constrained optimal power flow, optimal PMU placement, state estimation

TABLE OF CONTENT

LIST OF FIGURE

LIST OF TABLE

I. INTRODUCTION

1.1. Research Background

Renewable energy source (RES) has been integrated into the power system all over the word as the response of the energy sustainability and environmental friendly issues. RES integration can give more reliability to the power system and for some cases can result in more economical generation cost. On the other hand, fluctuations are still remained as the RES nature, which can lead into potential violation. Furthermore, RES power installation will increase more in the future power system, which will also increase the magnitude of the fluctuations. The fluctuation of RES power becomes one of the uncertainty sources. Another source of the uncertainty is transmission line contingency, which was caused the voltage stability problem and led so many major black out in the past. For that reason, N-1 contingency criteria of transmission line should be considered when the power system has the mission to secure uncertainty.

Considering the uncertainty, the power system state for the upcoming time interval is unknown, whether the line contingency or RES power fluctuations will occur or not. Power system operation condition can go in some possible directions. The expected direction occurs when power system in non-contingency condition and RES power output the same as the prediction data. However, power systems can probably goes into contingency condition and RES power output higher/ lower than the predicted data, which might be not expected by power system utility. In power system uncertainty, all of those possible directions (combination of line-contingency and RES output state) are called scenario. Considering the uncertainty, the important mission of modern power system is to warrant the security of all scenarios, including the voltage stability. For those reasons, the multistage preventive scheme strategy is needed.

Power system uncertainty is strongly correlated to the fast condition change in the system, which is difficult to be monitored by the conventional platform of power system, in example supervisory control and data acquisition (SCADA) system. Nowadays, wide area monitoring system (WAMS) which is based on the phasor measurement unit (PMU) data is existed. WAMS has the ability to monitor the whole power system accurately due to the high accuracy, fast sampling time and synchronous sampling time of PMUs. Having these advantages, WAMS platform with PMUs will be capable to monitor the fast condition change and probably the

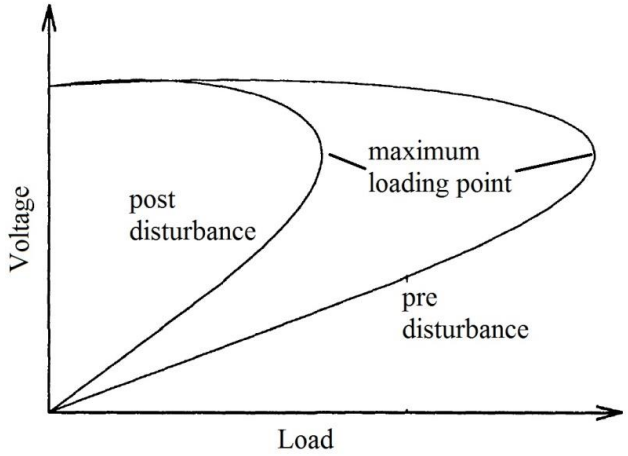

Figure 1.1 P-V curve generated by different operating condition

dynamic phenomena. Furthermore, WAMS will become the platform the future power systems.

1.2. Voltage Stability Problem in Power System

Among the security issues, voltage stability problem is becoming a major threat as the impact of modern power system operation, which tends to operate the power system close to the limit. Voltage stable is defined as power system' voltages which close to the voltages at normal operating condition after the disturbance happened [1]. The voltage stability of a power system is greatly dependent upon the amount, location and type of reactive power sources available.

Unstable condition/voltage collapse will happen in power system when the voltages uncontrollably decrease because of sudden removal of generation or a transmission line, an increase of load without an adequate increase of reactive power, or the slow clearing of a system fault [2]. A voltage collapse may occur rapidly or more slowly, depending on the system dynamics. Installation of RES would improve the supply reliability from the adequacy viewpoint. However, it also brings additional uncertainty which can trigger the voltage collapse, especially in the heavy loading condition.

For assessing the voltage stability, P-V curve/ Nose curve, which can be estimated is utilized as presented in Figure 1.1. Secure operating condition in power system network is upper the nose of P-V curve that is maintain the bus voltage above the limit. This part of PV-curve is statically and dynamically stable. The nose of the curve is called the maximum loading point. Maximum loading point is the critical point where the solutions unit is the voltage collapse point [1]. The power systems become voltage unstable after this point. The lower part of the PV-curve, located in

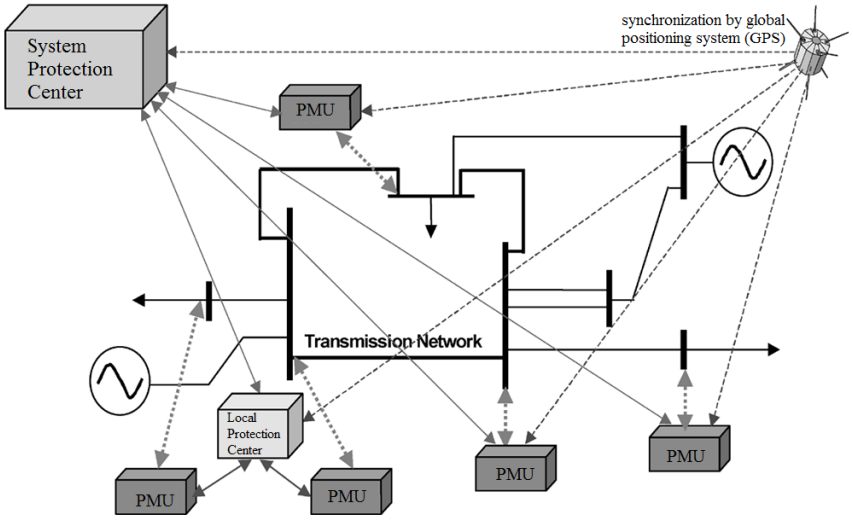

Figure 1.2 Illustration of wide area monitoring system

left from the voltage collapse point, is statically stable, but dynamically unstable [3].

1.3. Definition of Wide Area Monitoring System

In modern power system, the possibility of the disturbance occurrence, which can lead to power interruption, becomes higher since the power system is tend to be operated close to physical limit due to the economic reason. Furthermore, RES integration, which has intermittent characteristic, becomes current trend in response to the sustainability of energy and low environmental impact. On the other hand, the conventional protection devices and the current supervisory control and data acquisition (SCADA) are inappropriate to monitor fast system changing. Moreover, most of the protection devices are uncoordinated due to the decentralized devices. For those reason, the WAMS based on PMU are introduced for monitoring the fast system condition change.

WAMS is defined as measurement systems based on the transmission of analogue and/or digital information using telecommunication systems and enable the synchronization among the measurements using a common time reference [4]. Illustration of WAMS consisting of PMUs, global positioning system (GPS) synchronization, system protection center/ control center and local protection center for monitoring system security is presented in Figure 1.2 [5]. Measurement data among the PMUs are synchronized, and then the data are sent to the control center for the monitoring and controlling purpose. As one of the main component in the

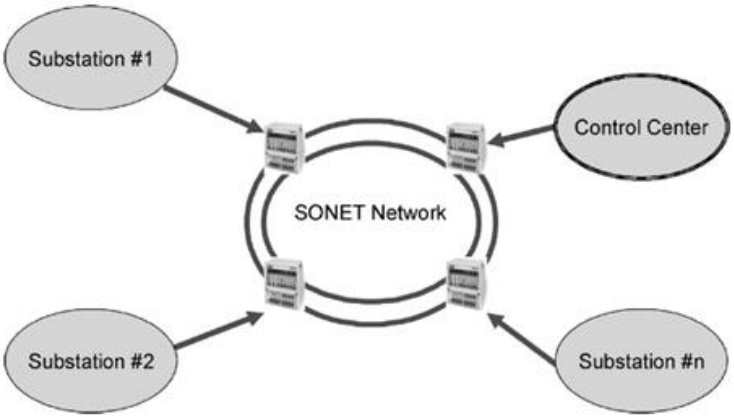

Figure 1.3 Sonet communication system architecture

WAMS, PMU has three advantages comparing to the SCADA conventional measurement; the synchronization process, the fast sampling time and measurement accuracy. Current version of PMU has the sampling time capability up to 20 milliseconds [6] while conventional SCADA has 1 – 10 seconds. From the measurement accuracy perspective, PMU has standard error deviation 10^{-5} while SCADA 10^{-3} as reported in [7]. These capabilities makes WAMS can monitor fast system condition change more accurate than SCADA system so that the effect of the disturbance to the power system reliability can be minimized through some control strategies. Another advantage of PMU installation, the power system condition can be represented more accurate closer to the actual condition which can affect the proper control strategy.

WAMS use the concept that involves the use of system-wide information and the communication of selected local information to a central location [8]. This concept can see all the power system area and can monitor the transmission-lines as unit protection so that disturbance monitoring can be done well [9]. Due to potential loss of communication, the relay of communication system must be designed well to detect failures and tolerate noise. The communication network needs to be designed for fast, robust and reliable operation. For those reason, communication protocol having self-healing capability and ring topology is required. This means that if communication between two nodes is lost, the traffic among them switches over to the protected path of the ring. One of the common communication protocol used in WAMS is Synchronous optical network (Sonet/SDH) which is presented in Figure 1.3 as presented in [5].

1.4. Application of Wide Area Monitoring System

WAMS capability for monitoring fast system change accurately gives advantages to power system utility for developing some applications depend on the needs. Data collected from the PMUs should warrant the system observability, which through the state estimation technique, online power system state variable will be known. Online system state variables are one of the valuable input data for developing application. Practically, applications in WAMS were vary and specific so that the specific algorithm should be developed. Final objective of installing WAMS is to make the power system more powerful by giving real time monitoring information. Algorithm is strictly developed based on the WAMS application that also affects the required variable and the desired output [5].

WAMS control is designed centralized that all data from PMUs are sent to the control center. In the control center, some algorithms related to the anticipation of effect of fast system condition change, such as the fluctuations of RES power output and sudden load changes, can be developed. The algorithm can be applicable for preventive scheme or emergency control and then the results are provided to system operator through an interface system as indicator [6]. Some of the applications are frequency stability assessment, oscillation stability assessment, voltage stability assessment, line temperature monitoring, state estimation correction and parallel application of flexible alternating current transmission system devices as discussed in [6], [10] and [11]. Some of more specific applications are discussed as following section.

1.4.1. Voltage Stability Improvement

WAMS in Southern Sweden was called the special protection system (SPS) [5] for avoiding a voltage collapse after severe fault in a stressed operation situation. WAMS can help the network to increase the voltage stability by increasing the power transfer limit from north Sweden. The system was designed to be in continues operation and independent of system operation condition such as load dispatch, switching state, etc. Some input measurement such as low voltage level, high reactive power generation and generator current limiters hitting limits were used as inputs for the systems and then calculated with specific algorithm to perform the voltage stability assessment, whose the command send to the *Sydkraft* power system.

Local actions were ordered from the *Sydkraft* for performing switching of shunt reactors and shunt capacitors, start of gas turbines, request from neighboring

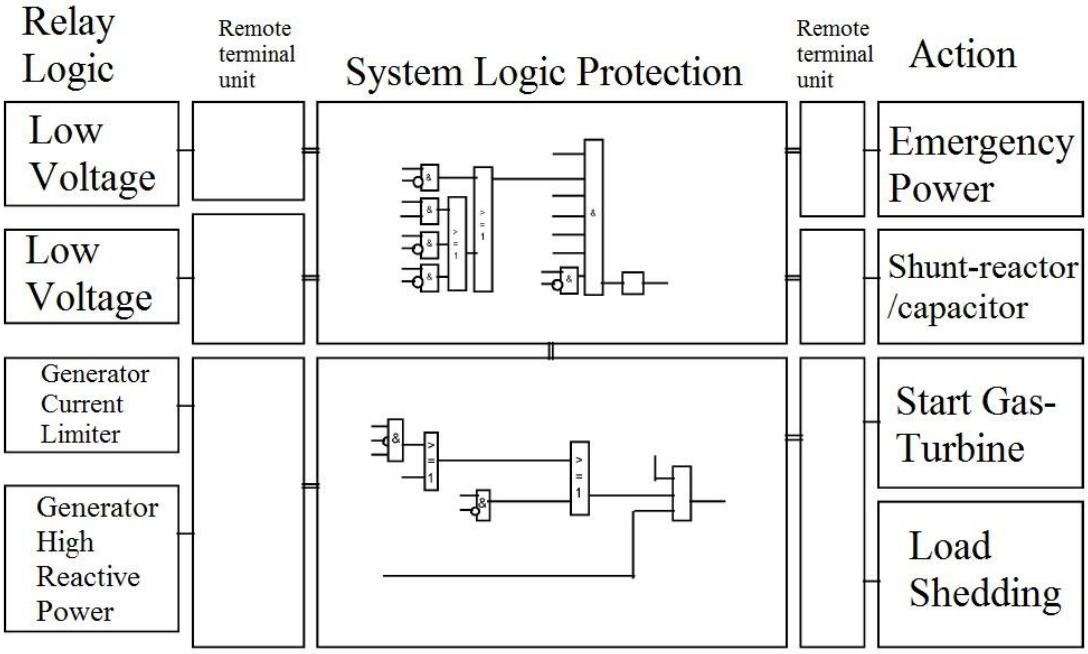

Figure 1.4 Control action logic of Swedish WAMS

areas, disconnecting of low priority load and load shedding, which the logic is shown in Figure 1.4. SPS was designed to have high security and high dependability. Therefore, a number of indicators are used to derive the criteria for each action.

1.4.2. Coordinated Scheme against Losses of Synchronism

Électricité de France (EDF) has applied *Sylopes* for performing coordinated scheme if a loss of synchronism occurs. To get quick and accurate information, angular and frequency difference between two points, the synchronous phasor measurement of the homogeneous group of generator should be recorded. Furthermore, the angle differences among the homogenous areas were compared. More specifically, the function of *Sylopes* are:

- Detection of the loss synchronism
- Tripping of all the lines bordering the homogeneous areas that losses synchronism, and
- Order for load shedding if necessary

Sylopes has been developed for the isolation of two southeastern coherent areas in French system identified as critical toward the loss of synchronism as shown

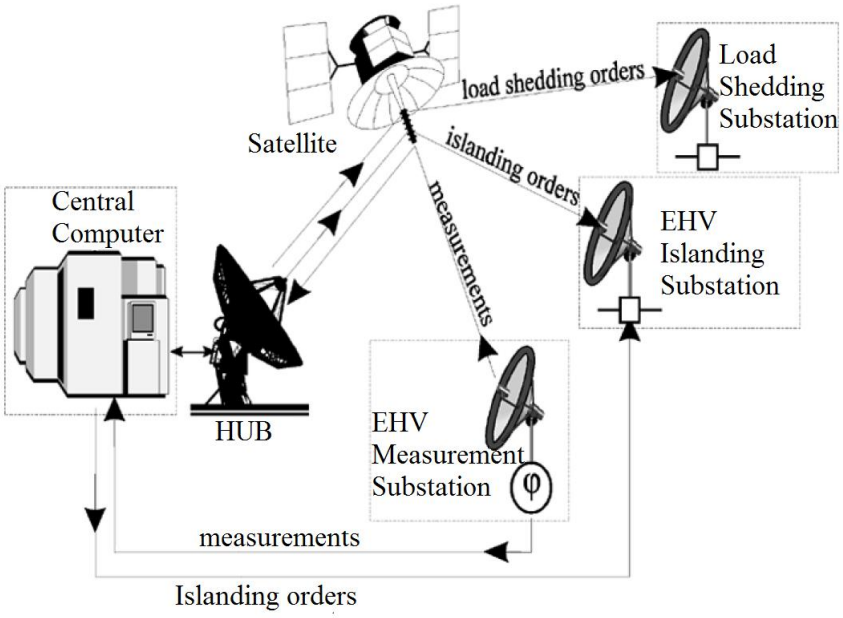

Figure 1.5 Sylopes control scheme illustration

in Figure 1.5. These areas are exporting large amounts of power and need load curtailment to prevent induced loss of synchronism. The *Sylopes* installation gave improvements in the phasor detection accuracy improvement, global processing provided better selectivity and stability improvement after the emergency control.

1.4.3. Remedial Action Scheme against Sudden Contingency

Remedial action scheme (RAS) is also kind of developed SPS, which was developed by Southern California Edison (SCE) as WAMS protection scheme, one of the big power system utility in California, United States [12]. RAS is defined as an automatic protection system designed to detect abnormal or predetermined system conditions and take corrective actions to isolate the faulted component. Each RAS consist of several PMUs as the main measuring devices and some conventional measurements. There is a Central RAS among the installed RAS which enable the communication and data sharing among the RAS. Installing RAS really increase the power system security performance.

One of case occurred during summer 2005, when one of 500kV intertie suffered from outage due to a fire storm, which without any RAS would resulted a significant de-rating and potential generation capacity shortages for several days. Fortunately, using the neighbouring utility's RAS had be able to monitor the intertie remotely and vastly modified the generation amount to save the two lines temporary

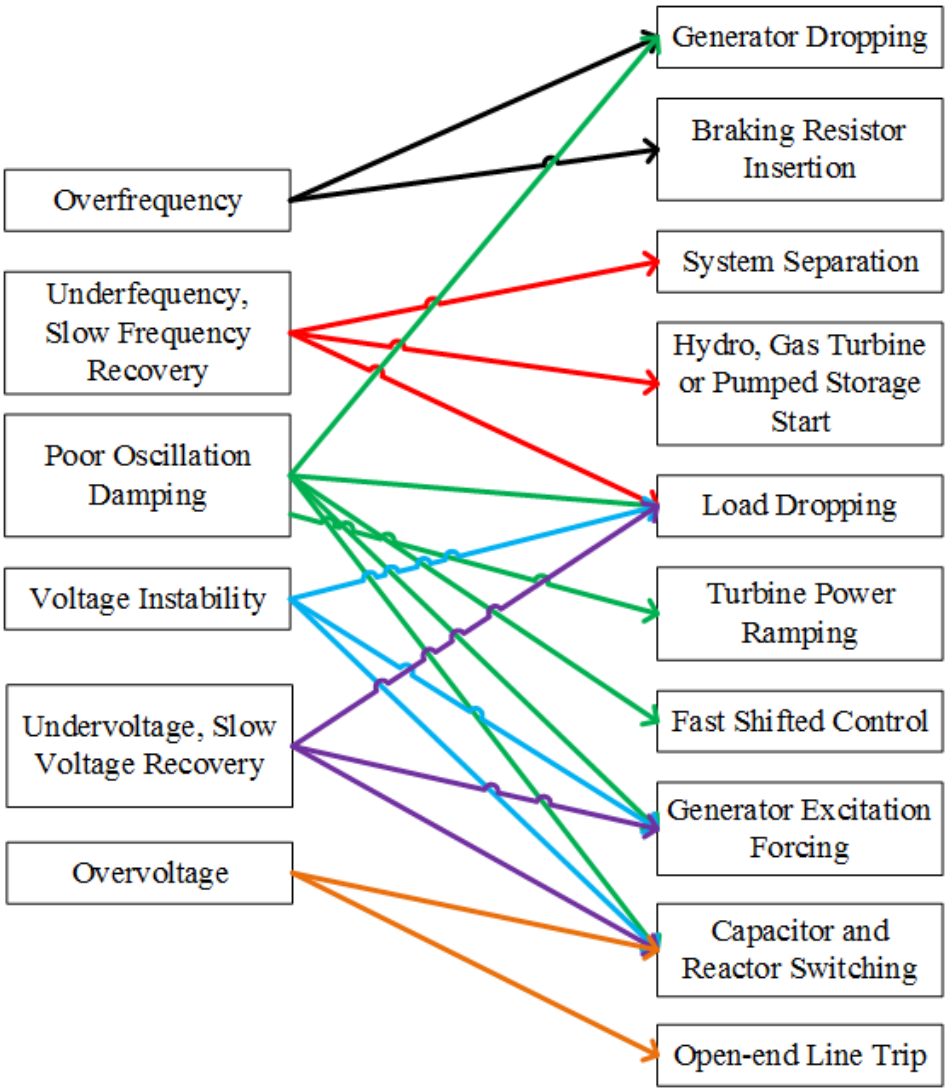

Figure 1.6 WECC RAS emergency control design guideline

operating condition without having to send personnel into the field.

Remedial action in power system has been provided by the Western Electricity Coordination Council (WECC), which should be considered by the power system utility if the unexpected condition happened. Some of the control strategies against the unexpected condition is illustrated in Figure 1.6.

Configuration of wide area monitoring and protection scheme of SCE, which was based on RAS agent scheme, is described in some parts. Existing and forecasted RAS based on April 2012 data were plotted into some Central RASs. Standalone RAS practice required 50 milliseconds (ms) for the monitoring relay to detect line open (2 ms), upwards data transmission (19 ms), controller to process data (4 ms),

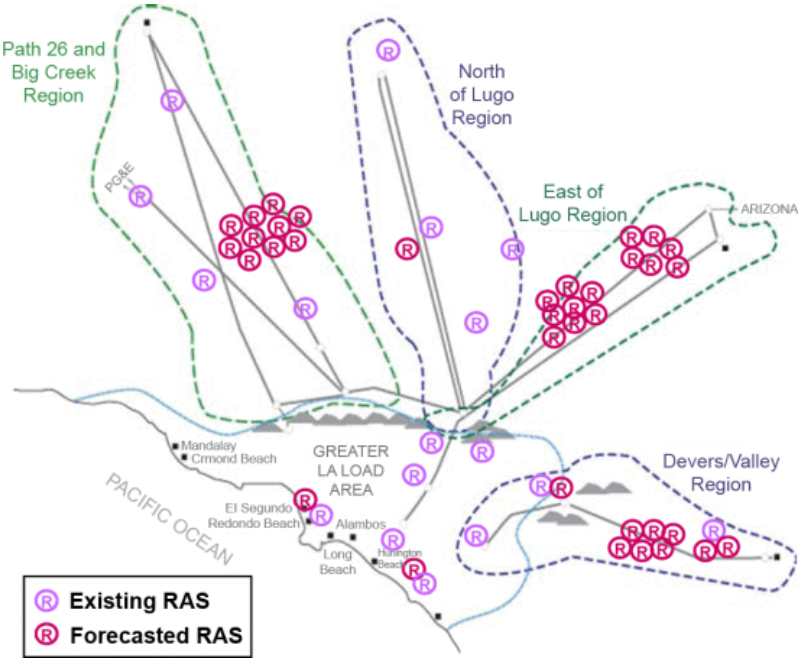

Figure 1.7 SCE service territory with existing and forecasted RASs

downwards data transmission (19 ms), mitigation relay processing (2 ms) and trip contract (4 ms). The detail of SCE service territory are described in Figure 1.7.

1.5. Contribution

The objective of this research is to design of WAMS considering the voltage stability phenomena consisting of the PMUs configuration, state estimation procedures and preventive scheme strategy for securing all scenarios are proposed. The contribution for each process is described as follow:

a. Optimal PMU placement (OPP) technique considering the important busses pertinent to voltage stability and N-1 line contingency criteria is proposed for WAMS having full observability by PMUs.

b. OPP technique considering the important buses pertinent to voltage stability, N-1 line contingency criteria and estimation accuracy improvement is proposed for WAMS – SCADA hybrid system consisting SCADA and PMU measurement.

c. State estimation procedure for minimizing the measurement error effect based on series measurement is proposed for WAMS having full observability by PMUs.

d. State estimation procedure for minimizing the measurement error effect based on weighting factor re-setting is proposed for WAMS – SCADA hybrid system.

e. Multistage preventive scheme strategy for securing voltage stability and security considering RES output and line contingency scenarios is proposed for WAMS, which having high estimation accuracy.

f. Hybrid computation approach for optimal power flow to solve large scale computation problem due to RES output and line contingency scenarios is proposed to realize the application within an acceptable computation time.

1.6. Chapter Organization

This dissertation thesis consists of 7 chapters. Chapter 1 describes the research background related to the uncertainty in power system, voltage stability problem in power system, introduction of WAMS including its application and the contributions of this paper.

Chapter 2 presents the multistage preventive scheme for securing voltage stability and security under uncertainties, including some numerical examples. Voltage stability performance tools, line contingency selection and RES uncertainty modeling are also proposed. In multistage preventive scheme, there are two general stages called preventive scheme having higher hierarchical position and giving single solution of control strategy for all scenario and prepared corrective scheme in lower level solving the solution related to each potential violated scenarios.

Chapter 3 presents some optimization solver for solving optimal power flow in very huge size, including the genetic algorithm and conventional primal dual interior point OPF. In this chapter, the proposed hybrid computational approach for OPF is also described for solving the stochastic SCOPF problem. Some numerical examples are also described.

Chapter 4 presents the extended problem of multistage preventive scheme for a power system which operates the energy storage system (ESS). In this chapter the adjustment of the preventive scheme by optimal re-scheduling active and reactive power of ESS operation is described. Some numerical examples are also described.

Chapter 5 presents the PMU-based WAMS, which all of the measurement are based on PMUs. How PMU should be place in the power system as one of the

importance steps of WAMS design is presented. Furthermore, important buses related to voltage stability are defined. Since measurement error cannot be avoided in practical power system, state estimation technique, which based on series data for minimizing the measurement error effect are proposed. Some numerical examples are also described.

Chapter 6 presents the WAMS hybrid, which decided the number of additional PMUs in the existing SCADA system. By adding the PMUs the overall system state accuracy will improve without make huge major changes in power system. State estimation technique, which based on weighting factor control, is proposed. Some numerical examples to show the merit of the proposed methods are also presented.

Chapter 7 summarizes the results of this research, presents the conclusions and elaborates the prospective future research.

II. SECURING VOLTAGE STABILITY UNDER UNCERTAINTY

2.1. Introduction to Power System Uncertainty

Uncertainty in power system has been existed since several decades. During that period, the sources of the uncertainties were load forecasting, transmission line network, and state estimation error due to network and measurement uncertainty, which are categorized as traditional uncertainty. A lot of research related to them has been conducted to minimize the effect. For example, an N-1 contingency criterion has been widely applied in world-wide power system, of which the power system condition should be secured. Security aspect is related to the voltage regulation, stability, loading of power system component limit, etc. RES generation integration also becomes popular trend in current power system, which gives advantages in reducing new feeder installation [13], saving the generation cost and increasing supply reliability [14]. Considering the current trend of RES integration in power system, fluctuations of RES power output may become another source of uncertainty, which change more frequently comparing to the other uncertainty sources. If the power system utility wants to warrant the power system security for the upcoming time interval, uncertainty should be considered as the decision as the existing controls strategy. Following the common practice to consider the RES fluctuation and N-1 line contingency as the main uncertainty sources, security constrained optimal power flow (SCOPF) problem, which modelled the uncertainty into some scenarios has been applied.

Scenarios for the next upcoming interval are illustrated at Figure 2.1. In that figure, there is two time-slots called T and T+1, which show time interval of power system operation. At time-slot T, it is called the current operation condition, which the operating condition, network parameter status, predicted data of load and RES prediction for the upcoming time interval T+1 are known. Based on those data, the obtained operating condition for T+1 can be estimated. If only conventional analysis of power system is considered, only the main scenario is considered. The main scenario is happened when the power system is on non-contingency and RES power output is the same as predicted. However, there is no guarantee that for T+1 the power system will go into the main scenario. It also has possibility that the power system goes to another direction as illustrated in those figure, in the worst case, it can go to contingency condition and RES power output is different from the predicted data. For the security reason, the control strategy decision for the

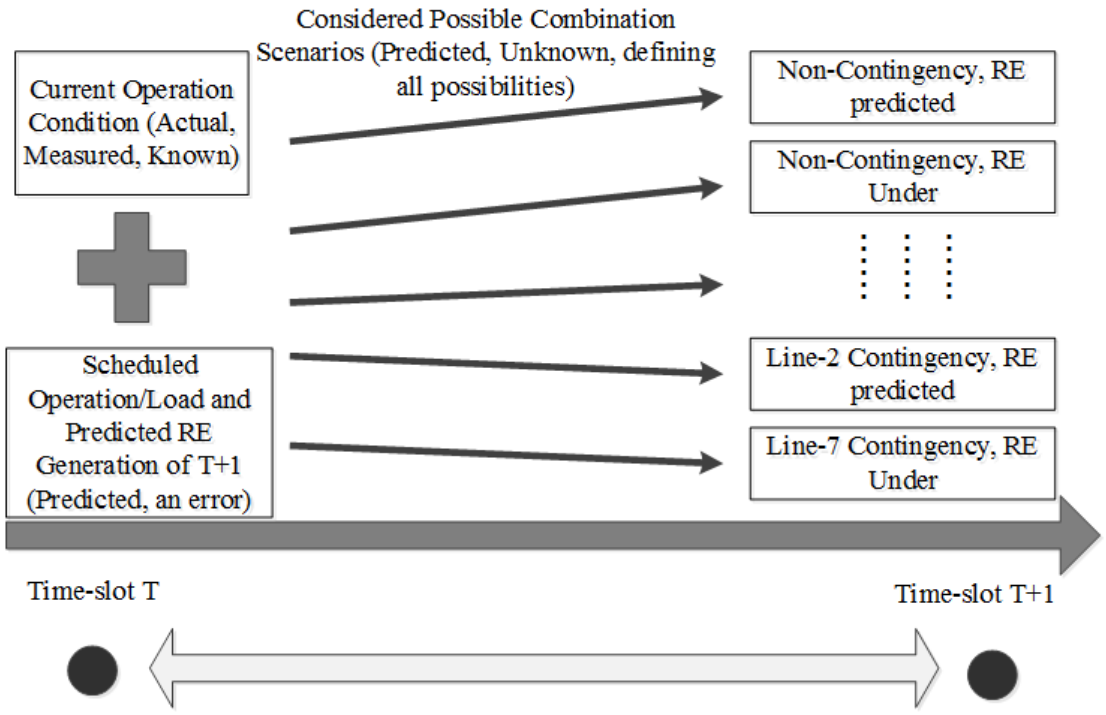

Figure 2.1 Illustration of power system uncertainty

upcoming time-slot should secure all of possible selected scenario in Figure 2.1.

For the sake of power system operation, it will be not rational if all of possible scenario were considered, especially for the large system with high penetration of RES. Selection on important scenario is necessary to be done in the planning process based on the historical data. In this study, two kinds of uncertainties are considered for upcoming time interval's security purposes, which are RES power output fluctuation and line contingency.

2.2. Voltage Stability Performance

In order to secure voltage stability operation of power system, voltage stability performance characteristic should be quantified. The most common tool for assessing the voltage stability performance is PV- curve.

2.2.1. Traditional Simple Analysis

For describing the PV curve characteristic a simple two bus test system is introduced. Voltage stability charactheristic can be described in Figure 2.2. In this figure, there is a simplified two-bus test system. Generator produces active power, which is transferred through a transmission-line to the load. The reactive power capability of generator is sufficient to make the generator terminal voltage V_1 is

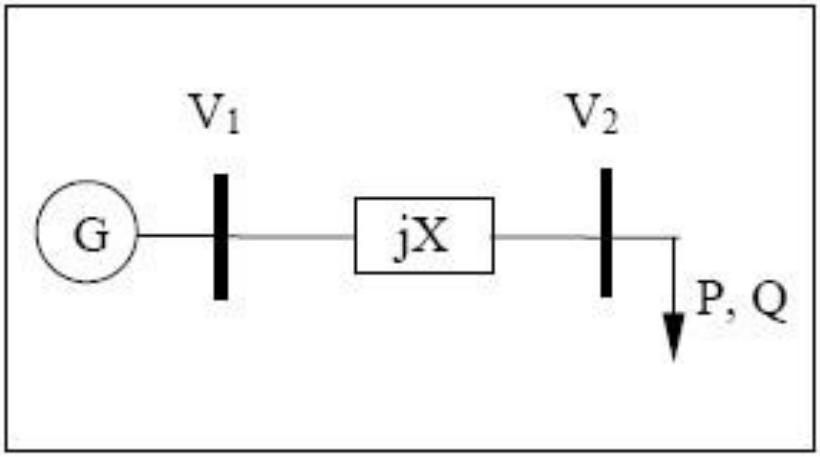

Figure 2.2 Two bus test system

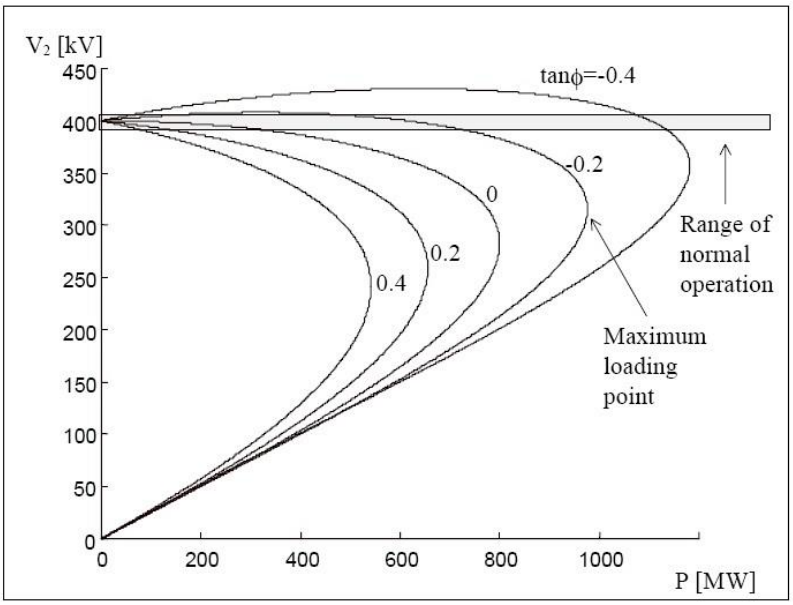

Figure 2.3 P-V curve generated by different operating condition

constant. The transmission-line is shown by the reactance (jX). The load in the receiving bus V_2 is variable, which the load change will affect the voltage of V_2.

The observed bus for voltage stability purpose is bus-2, voltage in bus-2 (V_2) is calculated with the different value of load as presented in equation (2.1)

$$V_2 = \sqrt{\frac{(V_1 - 2QX) \pm \sqrt{V_1^4 - 4QXV_1^2 - 4P^2X^2}}{2}} \tag{2.1}$$

If the active power load (P) is continuously increase with reactive power load increase proportionaly (constant power factor) the PV-curve could be drawn as illustrated in Figure 2.3. In this fashion, the load should be modelled as constant impedance. The PV-curve presents the voltage of the load bus as a function of load or summation of system loads. The solution is stated that it has low current/load will have high voltage and high current will have low voltage. The shape of the P-V curve is strongly depended on the load, each value of the power factor gives different characteristic of the P-V curve, which in those figure is represented in different value of tangen ϕ.

Secure operating condition in power system network is upper the nose of P-V curve that is maintain the bus voltage above the limit. This part of PV-curve is statically and dynamically stable. The nose of the curve is called the maximum loading point, which is the critical point where the solutions unite is the voltage collapse point [1]

Five PV-curves are described in Figure 2.3 for the test system. The test system variables are V_1 = 400 kV and the X = 100Ω. The P-V curves represent different reactive power compensation cases ($\tan\phi$=Q/P), with negative value indexing that reactive power are injected into the system. The smaller value of $\tan\phi$ is beneficial for the power system because of more active power margin to the collapse point or in other word more active power can be loaded. From the different value of $\tan\phi$, it is also reflect that the voltage stability margin is identical to the amount of injected reactive power into the system.

2.2.2. Synchro-phasor Based Real Time Voltage Stability Index

Voltage stability (VSI) can give the quantification of the power system security pertinent to the voltage stability performance. In performing a control strategy in WAMS, fast computation of VSI is needed to give the accurate value of the voltage stability condition in order to make the preventive action in the power system. Synchro-phasor Based Real-Time Voltage Stability Index (SBRTVSI) is one of the VSI that can compute the voltage stability performance of each load bus [15]. In addition, SBRTVSI can calculate voltage stability margin, in form of active load power.

The first step to do the SBRTVSI calculation is to estimate the power in each load bus of the power system. For this purpose, the simplified model of power

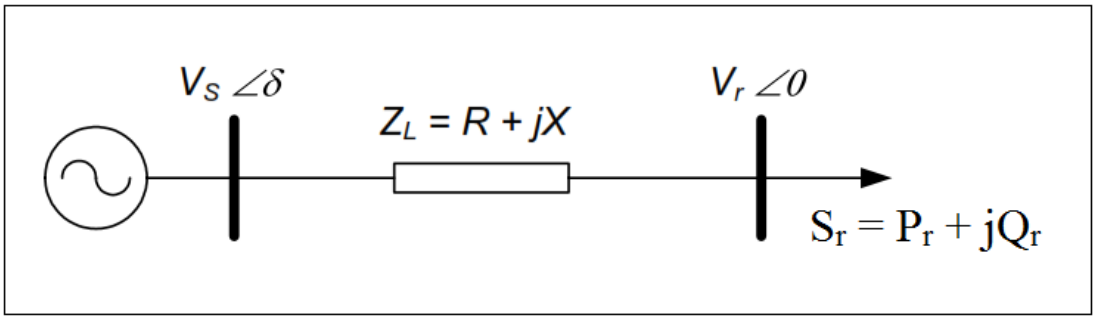

Figure 2.4 Simplified power system model

system is introduced in Figure 2.4.

with V_s, V_r, δ, Z_L, R, X and S_r are voltage magnitude at sending and receiving terminal, voltage angle different between terminals, line impedance, resistant, reactance and apparent power. Then, active (P_r) and reactive power (Q_r) of load bus *r* can be modelled as the function of voltage and impedance as follow:

$$P_r = V_r\left[(V_s cos\delta - V_r)\frac{R}{R^2+X^2} + V_s sin\delta \frac{X}{R^2+X^2}\right] \tag{2.2}$$

$$Q_r = V_r\left[(V_s cos\delta - V_r)\frac{X}{R^2+X^2} + V_s sin\delta \frac{R}{R^2+X^2}\right] \tag{2.3}$$

Arranging equations (2.2) and (2.3), V_r can be represented as the function of load, sending voltage and impedance as follow:

$$V_r = \sqrt{\frac{V_s^2}{2} - (Q_r X + P_r R) \pm \sqrt{\frac{V_s^4}{4} - (Q_r X + P_r R)V_s^2 - (P_r X - Q_r R)^2}} \tag{2.4}$$

Re-write the determinant term of equation (2.4) as new equation for forming the quadratic function of active power:

$$\begin{aligned} A &= \frac{V_s^4}{4} - (Q_r X + P_r R)V_s^2 - (P_r X - Q_r R)^2 \\ &= -(X - Rtan\theta)^2 P_r^2 - V_s^2(Xtan\theta + R)P_r + \frac{V_s^4}{4} \end{aligned} \tag{2.5}$$

Collapse point of the nose curve occurs when the value of determinant A equal to 0, of which the corresponding sending voltage and maximum active power

load can be computed. Assuming the power factor is constant, the corresponding maximum loading point (P_{max}) of sending nodes can be computed as follow:

$$P_{max} = \frac{-V_s^2(Xtan\theta + R) + |Z_L|V_s^2\sqrt{tan^2\theta - 1}}{2(X - Rtan\theta)^2} \tag{2.6}$$

Then for any value of active load under constant power factor, load margin and SBRTVSI can be expressed as follow:

$$P_{margin} = P_{max} - P_r$$
$$SBRTVSI = \frac{P_{margin}}{P_{max}} \tag{2.7}$$

The value of VSI will follow $0 \leq SBRTVSI \leq 1$, with 0 indicates the collapse point.

For the larger power system purpose, network simplification is required for calculating the index. For that reason, network simplification technique based on reference [16] is introduced as shown in Figure 2.5. For each load bus analysis, network is simplified into the associated load bus and equivalent source bus as presented in that figure.

In that figure there is an IEEE 14 buses test system, which represents bus-12 to be a load bus with voltage bus v_l propertiy. On the other hand, the other remaining

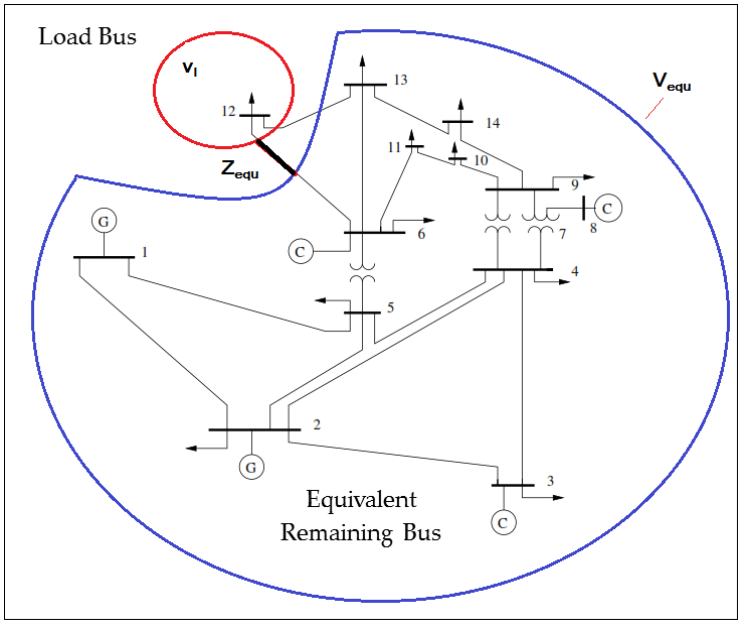

Figure 2.5 Network simplification of power system

busses are formulated to be equivalent bus with voltage v_{equ}. The lines connecting the equivalent circuit is named by Z_{equ}. These three properties have to be considered for performing network simplification.

Then, network simplification can be applied by firstly rearranging the Y_{bus} equation into two groups namely load and generator bus group. The partial Y_{bus} element can be obtained by performing gauss elimination technique as presented in (2.8).

$$\begin{bmatrix} I_L \\ I_G \end{bmatrix} = \begin{bmatrix} Y_{LL} & Y_{LG} \\ Y_{GL} & Y_{GG} \end{bmatrix} \begin{bmatrix} V_L \\ V_G \end{bmatrix}$$
$$\begin{bmatrix} V_L \\ I_G \end{bmatrix} = \begin{bmatrix} Z_{LL} & H_{LG} \\ F_{GL} & Y_{GG} \end{bmatrix} \begin{bmatrix} I_L \\ V_G \end{bmatrix} \tag{2.8}$$

with I_L, I_G, V_L, V_G are load bus, generator bus injected current, load bus and generator bus voltage. Partial matrixes Y_{LL}, Y_{LG}, Y_{GL} and Y_{GG} are belong to Y_{bus}. Furthermore, the component Z_{LL} and H_{LG} are calculated as follow:

$$Z_{LL} = Y_{LL}^{-1}$$
$$H_{LG} = -Z_{LL}Y_{LG} \tag{2.9}$$

The load bus voltage-j (v_{Lj}) can be formulated following the power flow equations.

$$v_{Lj} = Z_{LLjj}\left(\frac{-S_{Lj}}{V_{Lj}}\right)^* + \sum_{i=1, i\neq j}^{N} Z_{LLji}\left(\frac{-S_{Li}}{V_{Li}}\right)^* + \sum_{k=1}^{M} H_{LGjk}V_{Gk} \tag{2.10}$$

Equivalent voltage and impedance are formulated from the simple network in Figure 2.5 and expressed in equation (2.11)

$$\left(\frac{v_{equj} - v_{Lj}}{Z_{equj}}\right)^* v_{Lj} = S_{Lj}$$
$$v_{equj} = \sum_{i=1, i\neq j}^{N} Z_{LLji}\left(\frac{-S_{Li}}{V_{Li}}\right)^* + \sum_{k=1}^{M} H_{LGjk}V_{Gk} \tag{2.11}$$

$$Z_{equj} = Z_{LLjj} \tag{2.12}$$

with v_{Lj}, v_{equj}, Z_{equj}, and S_{Lj} are load bus voltage, equivalent bus voltage, equivalent network impedance connecting buses j and equivalent network and load

bus apparent power, while *i*, *j*, *M* and *N* indexes bus and the number of buses.

Assuming that the power factor is constant during load increment simulation, the maximum loading point is calculated as follow:

$$P_{Ljmax} = \frac{-V_{equj}^2\left(X_{equj}tan\theta_j + R_{equj}\right)\left|Z_{equj}\right|V_{equj}^2\sqrt{tan^2\theta_j - 1}}{2\left(X_{equj} - R_{equj}tan\theta_j\right)^2} \tag{2.13}$$

with P_{Ljmax}, R_{equj}, X_{equj}, and θ_j are maximum predicted active power of load bus, equivalent line resistance and reactance connecting buses *j* and equivalent bus and power angle representing the power factor of bus-*j*.

Load margin, SBRTVSI for each load bus, and the global VSI for the system are presented as follow:

$$P_{Ljmargin} = P_{Ljmax} - P_{Lj} \tag{2.14}$$

$$SBRTVSI_{Lj} = \frac{P_{Ljmargin}}{P_{Ljmax}} \tag{2.15}$$

$$Global\ VSI = min\left(SBRTVSI_{Lj}\right) \tag{2.16}$$

2.3. Line Contingency Scenario

Considering the line contingency uncertainties, the most safety operation condition will be obtained when all of possible line contingencies are considered in the control strategy. However, it is not rational warrant all of possible contingencies, from technically and economically perspectives. Some previous study to select important contingency based on voltage stability performance has been investigated in [17]–[19]. However, those techniques did not consider the importance of occurrence probability, which the lower one can be ignored in the selection process. In this section, the occurrence probability is added as the selection criteria. System operators/planner should select the adequate number of contingencies, considering their occurrence probability [20] and its effect on system voltage stability. The occurrence probability of line contingency can be estimated from the historical data and lifetime of the component using the technique presented in [21]. Effect of a line contingency on voltage stability can be estimated by simulating contingency analysis for all line contingency under a certain operating condition. For a line-*k* contingency, the value of $Global\ VSI_k$ can be calculated.

The proposed contingency selection implements the risk-based N-1 line

contingency selection as an optimization problem formulated as follow

Objective function:

$$Max \sum_{k=1}^{Nk} (A_{csk})^n C_k (1 - VSI_k)^m \tag{2.17}$$

Subject to:

$$\sum_{k=1}^{Nk} A_{csk} C_k + A_{ns} \leq R_{wams} \tag{2.18}$$

with A_{ns} and A_{csk} are the occurrence probabilities of normal scenario, line-k contingency and NK is number of line. C_k specifies whether the line-k contingency is considered (1) or not (0). VSI_k is Global VSI under the line-k contingency. The exponential factors n and m are employed to reflect the system operator's policy in contingency selection. Higher n and m give more significant priority to the line contingency with higher occurrence probability and small stability margin in the most severe bus, respectively. R_{wams} is the desired WAMS reliability level. When higher R_{wams} is applied, more important contingencies would be selected.

2.4. RES Uncertainty Modelling

When RES powers are integrated into the power system, it will cause the

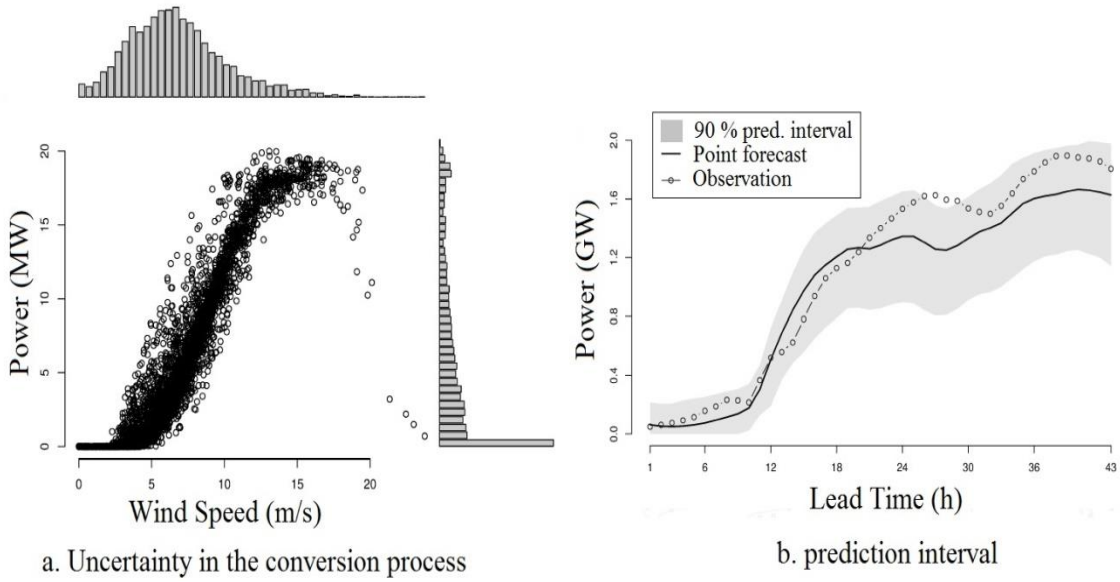

a. Uncertainty in the conversion process

b. prediction interval

Figure 2.6 Example of uncertainty in wind power generation

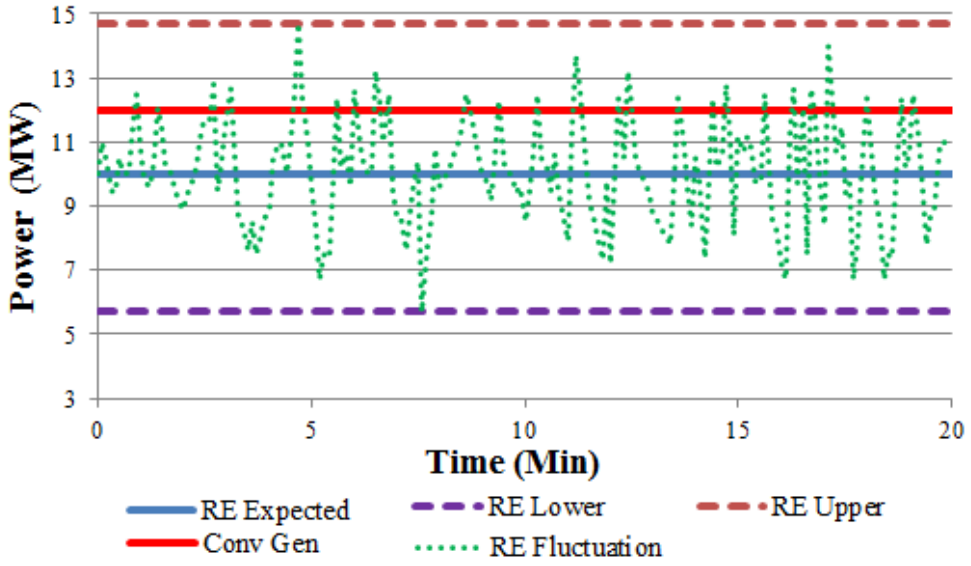

Figure 2.7 Illustration of RES Uncertainty

power fluctuation in the power systems due to its supply uncertainty. The uncertainty occurs mainly due to the difference between forecasted and actual weather condition which is strongly correlated with the actual RES output. One of the examples was illustrated in Denmark system as presented in [22]. Uncertainty also occurs in wind speed forecasted data, which can be modelled as normal distribution. From wind speed distribution data, the output power of wind generation can be estimated, which also follows normal distribution. Finally, the correlation of wind speed and output power is illustrated at Figure 2.6.a. Uncertainty in weather forecast correlated to the prediction of wind power, which there is always a difference from the measured data (after event). For this reason, 90% prediction interval was considered in the prediction data, which illustrated as grey area in Figure 2.6.b.

2.4.1. Single Bus RES Integration

In one operation interval, there will also be a power fluctuation during operation time interval from RES power output as illustrated in Figure 2.7. In those figure, RES is compared to the conventional generator (thermal, hydropower, etc) in term of output fluctuations, which is shown that conventional generator output is relatively not fluctuated represented in red line. For compensating the fluctuations, three scenarios of RES output in one operation interval are proposed. There are RE-Expected, RE-Lower, and RE-Upper for considering the RE fluctuation within one time-slot. RE scenarios have active power and probability properties as defined in Table 2.1, while a conventional generator has only a single scenario. RE-Expected

Table 2.1 RES scenario determination and its propertie

Scenario Number (Name)	**Injected Power P_r^{RE}**	**Probability A_r^{RE}**
1 (RE-Expected)	P_{jP}^{RE}	A_{jP}^{RE}
2 (RE-Upper)	P_{jU}^{RE}	A_{jU}^{RE}
3 (RE-Lower)	P_{jD}^{RE}	A_{jD}^{RE}

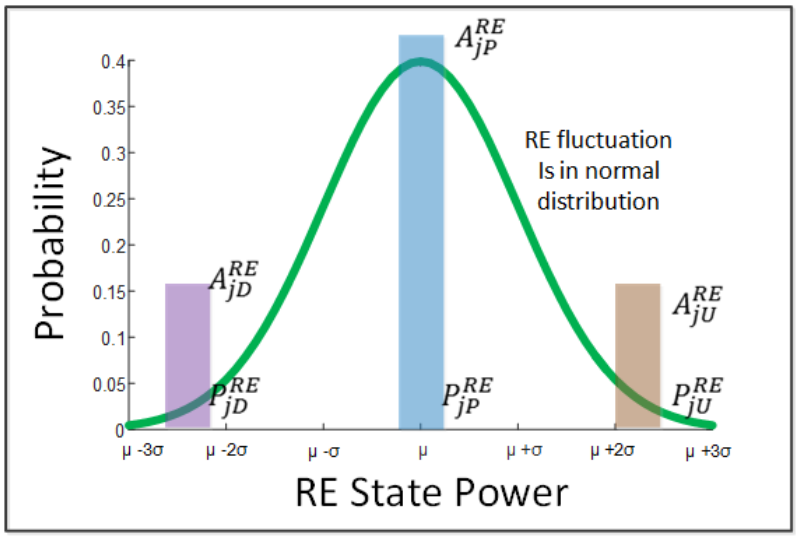

Figure 2.8 RES Fluctuation assumed follow normal distribution

drawn in blue solid line is RE power taken from forecasted data which is sent in every time-slot period, RE-Upper drawn in brown dash line represents the maximum injected power deviation and RE-Lower drawn in purple dash line represents the minimum injected power deviation.

For RES penetrated at single bus-*j*, each scenario-*r* has the associate power and probability, which are indexed by P_{jr}^{RE} and A_{jr}^{RE}, respectively. The number of the RES scenarios are 3 with each possible P_{jr}^{RE} defined as P_{jP}^{RE}, P_{jU}^{RE}, and P_{jD}^{RE} (corresponding to expected, upper and lower scenario, respectively). The generated powers of upper and lower scenarios are defined as $P_{jU}^{RE} = (1 + \varepsilon)P_{jP}^{RE}$ and $P_{jD}^{RE} = (1 - \varepsilon)P_{jP}^{RE}$ with ε is the assumed power deviation. For formulating the value of each power and probability, first, the power fluctuation during operation interval are assumed following normal distribution. Then, discretization associate to the mean and each edge of maximum and minimum RES power output are formulated as presented in Figure 2.8. Each value of A_{jr}^{RE} is defined as A_{jP}^{RE}, A_{jU}^{RE}, or A_{jD}^{RE}, where A_{jP}^{RE} is greater than A_{jU}^{RE} and A_{jD}^{RE} and the sum of these values equal to 1.

Table 2.2 Probability of each scenario for each RES integration

Bus	**Probability of each scenario at bus-*j***		
	A_{jP}^{RE}	A_{jU}^{RE}	A_{jD}^{RE}
Bus-A	0.8	0.1	0.1
Bus-B	0.6	0.2	0.2
Bus-C	0.5	0.3	0.2

2.4.2. Multiple Buses RES Integration

RES source capacities are going to increase in future trend of power system in response to the world word agreement to reduce the CO_2 emission, which in European Union it should be reduced by 30% by 2020 as presented in [23]. Moreover, RES source is more sustainable comparing to the thermal generator, which depends on fossil source. For that reason, power system utility has a roadmap related to RES installation so that the existence of RES will increase and spread all over the transmission network. For anticipating this phenomenon, RES scenario modeling should be adjusted into multiple-bus RES injection.

For power system having RES injected into *n*-buses (station), RES power scenarios become the combination of RE injections, which denotes as P_r^{RE}. Different from single RES integration, it will consist of several P_{jr}^{RE} values, each consisting of P_{jP}^{RE}, P_{jU}^{RE}, or P_{jD}^{RE}. Set of multiple *n*-buses of RES injection buses is defined as $J = \{j1, j2, \dots, jn\}$. The size of the scenario set is equal to $m = 3^n$, with 3 is scenario for each single bus injection. Assumed Ω is m-sets of P_r^{RE}(RES uncertainty scenario), a set of P_r^{RE} for multiple RES injection is defined in (2.19) and the associated scenario probability defined in (2.20). Sets of *m*-scenarios in multiple RES are shown in

Table 2.2, consisted of 3 RES buses in a power system injected at buses A, B and C.

$$P_r^{RE} = \{P_{j1\,r}^{RE}, P_{j2\,r}^{RE}, \cdots, P_{jn\,r}^{RE}\}, \quad P_r^{RE} \in \Omega, \forall r \in R \tag{2.19}$$

$$A_r^{RE} = \prod \{A_{j1\,r}^{RE}, A_{j2\,r}^{RE}, \cdots, A_{jn\,r}^{RE}\} \tag{2.20}$$

For 3 injection buses, the numbers of RES scenario are 27 (3^3). Each

Table 2.3 Top 10 RES scenario on multiple RES integration

RES scenario-*r*	**% RE Power Injection from RE-Expected value**			**RES Scenario Probability** (A_r^{RE})
	Bus-A	**Bus-B**	**Bus-C**	
1	100%	100%	100%	0.24
2	100%	100%	150%	0.144
3	100%	100%	50%	0.096
4	50%	100%	100%	0.08
5	150%	100%	100%	0.08
6	50%	100%	150%	0.048
7	150%	100%	150%	0.048
8	50%	100%	50%	0.032
9	150%	100%	50%	0.032
10	100%	50%	100%	0.03

scenario-r consists of each RES of buses A, B and C, which the scenarios with top-10 probability are presented in Table 2.3.

2.4.3. RES Scenario Selection

More RES injection in power system results in higher number RES scenarios, which increase in quadratic equation. For warranting power system security, all of the uncertainty should be considered. However, there are not rational to consider all of scenario from practical and economic aspects. Moreover, not all RES scenarios are significant because of low occurrence probability. For this reason, low probability scenarios can be ignored in the controlling process of which more number of scenarios require more computation time in any power system application.

RES scenario selection based on the occurrence probability can be selected under selection index called R_{fluct}. Significant RES scenarios under the selection index R_{fluct} are selected by equations (2.21) and (2.22) as follows:

Objective function:

$$Min \sum_{r=1}^{NS} RE_r \tag{2.21}$$

Subject to

$$\sum_{r=1}^{NS} A_r^{RE} RE_r \geq R_{fluct} \tag{2.22}$$

with RE_r is the selection status, 1 if selected and 0 is not. The range of R_{fluct} values is between 0 to 1. When higher R_{fluct} is applied, higher probability RE scenarios are considered. The value of R_{fluct} should be determined in advanced depends on the characteristic of each power system.

2.5. Multistage Preventive Scheme Strategies

For warranting securer operation of a power system, the security for all selected scenario should be considered. For that reason, the preventive strategy for the upcoming time interval is proposed, which warrant the secure operation of all selected scenario.

2.5.1. System Condition Recognition

The preventive scheme evaluates system stability and security for all uncertainty scenarios, associated to line contingency and RES fluctuation. Voltage chart for monitoring purpose is developed based on normal (main scenario) and an the most severe scenario, modified from the reference [24] as shown in Figure 2.9. This tool is useful for recognizing the obtained operating condition, especially in the most severe bus during the most severe scenario. The most severe bus is selected based on the $Global\ VSI$ during main scenario, not including the contingency scenario and RES output is the same as it scheduled. The most severe scenario is selected based on the smallest $Global\ VSI$ among all scenarios *r-k*, except the main scenario.

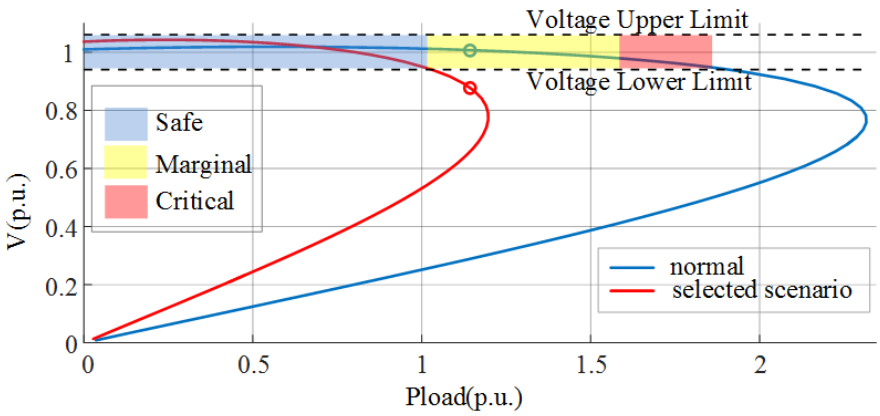

Figure 2.9 Obtained operating point and PV curves for the most severe bus

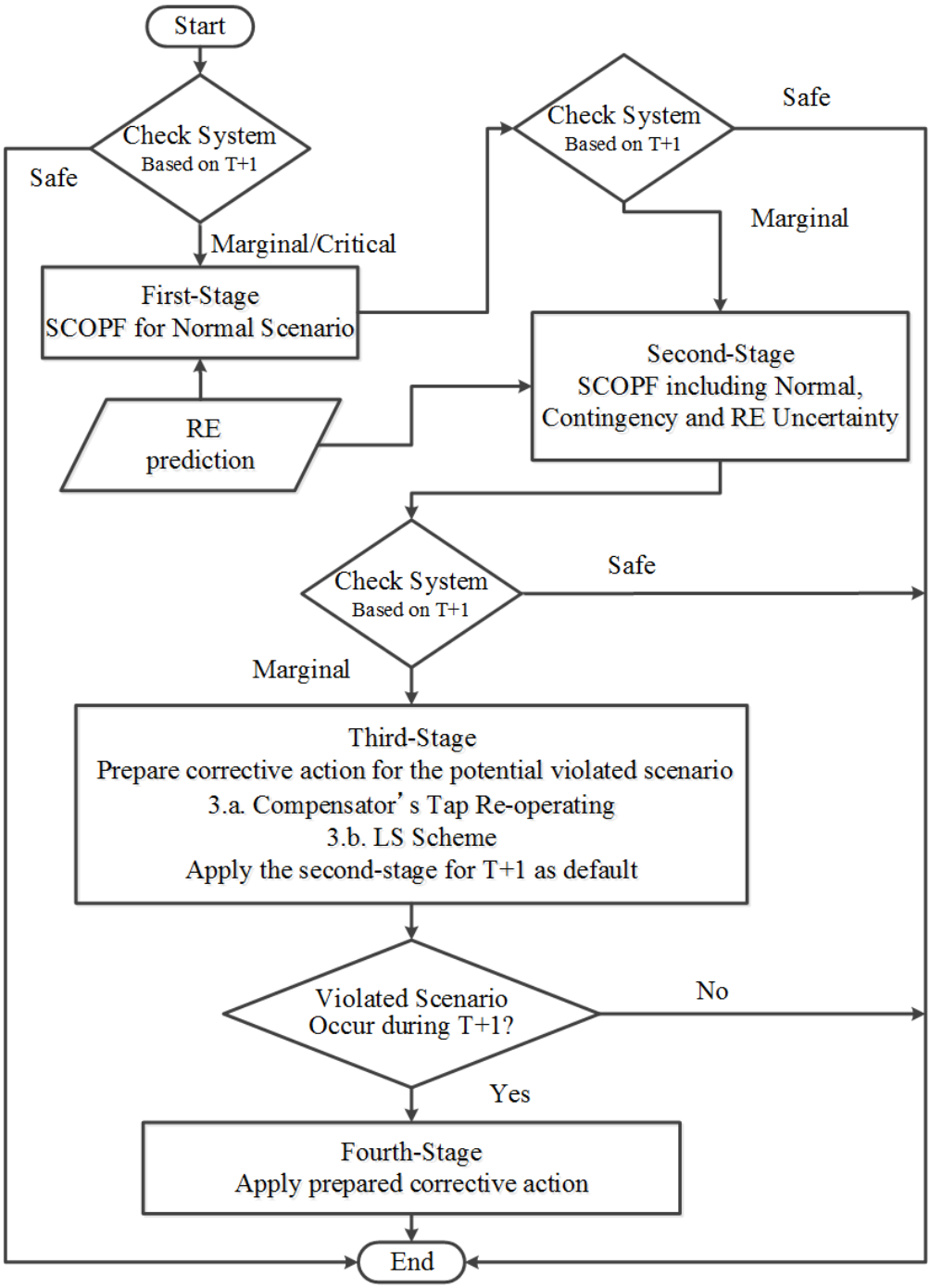

Figure 2.10 Overview of proposed multistage preventive scheme

Based on these PV curves and admissible voltage range, some zones correlated to safe, marginal, or critical situation are created. The safe operation zone (blue-colored area) corresponds to the area where the obtained operating condition is still stable and the voltage stays within an admissible range even the most severe

scenario happens. Then, the marginal zone (yellow-colored area) indicates that the obtained operating condition is safe for the main scenario but not during a severe selected scenario, which the operation condition deviates beyond the admissible range. In the critical zone (red-colored area), the obtained operating condition has a margin less than 5% during the main scenario, which is measured from the edge of main scenario's PV curve.

2.5.2. Hierarchical Control Strategy

Multistage preventive scheme purpose is for preventing the violation caused by the power system uncertainty (line contingency and RES fluctuations). Observation for uncertainty is defined for the next time interval/time-slot T+1, of which the directions of possible scenario are remains unknown but can be predicted as described at Figure 2.10. There are some possible scenarios related to contingency and RES status which might be happened at the next time interval. Without considering the uncertainty, power system may be insecure when any severe scenario happened. Corresponding to the upcoming formulation, RES scenarios are indexed by r and the line contingency scenarios are indexed by k, then the combination scenarios of RES – line contingency is indexed by r-k.

For conducting the observation, data and information at current time-slot T are required, which only consisted of current operating condition, scheduled load and the RES prediction data of T+1. Using those following information, the preventive scheme is calculated between time slot (T to T+1), which practically could be 30 minutes following the conventional generator dispatching interval. The procedures of the preventive scheme for securing all selected scenarios are hierarchically described in Figure 2.10.

The preventive scheme might be executed if marginal/critical operation area for any combination scenarios exists, after the security of all selected scenarios for T+1 were checked. The computation procedures are classified into first, second or third stages based on the severity of the obtained operating conditions. The result of the procedure is applied for the next time interval and kept until the next time interval. The hierarchical steps of each computation procedure are described as follows:

a. First-Stage

First-stage is the one of the computation procedure, of which the calculation output are used for securing all selected scenarios simultaneously.

The procedure is formulated as SCOPF considering only the main scenario correspond to non-contingency (indexed by $k = 0$) and expected RES scenarios of (indexed by $r = 1$). Generator powers, reserve powers, voltages and reactive power compensator's taps are set as the control variable and scheduled for time-slot T+1. The first-stage might be effective for securing all selected scenarios in a time-slot having light system loading condition and low output of RES generation.

b. Second-Stage

Similar to the first-stage procedure, second-stage is also formulated as SCOPF for securing all selected scenarios at T+1 simultaneously, however, all selected scenarios r and k is considered in the computation procedure. The control variables for this stage are also the same as first-stage. Second-stage is applied if there is a (some) scenario(s) stayed within marginal or critical condition (potential violated scenarios) after simulating the first-stage procedure. The second-stage is effective for time-slot having heavy loading condition and high output of RES generation. High output of RES generation will produce large fluctuation as well.

c. Third-Stage

After implementing the second-stage procedure, there is possibility that a (some) potential violated scenario(s) exists. For anticipating this condition, the third-stage is formulated for prepared corrective scheme. The procedure is applied to each violated scenario, individually. The control options of this procedure are rescheduling reactive power compensator's taps and/or load-shedding (LS) scheme, which are calculated hierarchically. The operation of LS scheme is the last possible option of this procedure. For implementation, the output of second-stage is still kept as the main output for time-slot T+1 while the output of third-stage is kept as the secondary output, which is executed for each corresponding violated scenarios.

d. Fourth-Stage

Fourth-Stage is called the implementation stage related to third-stage's output at time-slot T+1. If the power system at T+1 go to the violated scenarios direction, the corresponding prepared corrective scheme is executed.

2.5.3. Stochastic Security-constrained Optimal Power Flow Formulation

The problem is formulated in stochastic SCOPF to minimize the total generation fuel cost, as shown in (2.23), where control variables are reactive power

compensator's tap (discrete), generator power, reserve power, and voltage. Constraints related to the power system operation are required, those are available active and reactive power of generator (2.24) and (2.25), permissible voltage range (2.26), voltage stability limit (2.27) defined by (2.13)-(2.16), compensator tap limit (2.28), reactive power injection from the compensator (2.29), reactive net power (2.30), generator reserve power (2.31), generator and load changes as effects of RE injection in (2.32) and (2.33), power flow in (2.34) and (2.35), and transmission line capacity limit (2.36). Generator reserve power is set to be 10% of system load.

Objective function:

$$Min\ F_T = \frac{\sum_{r=1}^{NS} A_r^{RE} \sum_{i=1}^{NG} (a_i P_{GOir}^2 + b_i P_{GOir} + c_i)}{\sum_{r=1}^{NS} A_r^{RE}} \tag{2.23}$$

Subject to

$$P_{G_{imin}} \leq P_{GOir} + P_{GREVi} \leq P_{G_{imax}} \tag{2.24}$$

$$Q_{G_{imin}} \leq Q_{GOir}^k \leq Q_{G_{imax}} \tag{2.25}$$

$$V_{j_{min}} \leq V_{jr}^k \leq V_{j_{max}} \tag{2.26}$$

$$VSI_{svb\,r}^k > \begin{cases} 0.05, if\ k = 0 \\ 0, if\ k \neq 0 \end{cases} \tag{2.27}$$

$$Tap_{nmin} \leq Tap_n \leq Tap_{nmax} \tag{2.28}$$

$$Q_{Nnr}^k = V_{jr}^{k\,2} Tap_n Q_{Nn}^{base}, \qquad if\ j = n \tag{2.29}$$

$$Q_{Djr}^k = Q_{Nnr}^k + Q'_{Dj}, \qquad if\ j = n \tag{2.30}$$

$$\sum_{i=1}^{NG} P_{GREVi} = 0.1 \sum_{j=1}^{NB} P_{Djr}, for\ r = 1 \tag{2.31}$$

$$P_{Djr} = P'_{Dj} - P_{j\,r}^{RE} \tag{2.32}$$

$$P_{GOir} = P_{GOib} - \alpha_i \left(\sum_{j=1}^{Nre} P_{j\,r}^{RE} \right) \tag{2.33}$$

$$P_{GOjr} - P_{Djr} = V_{jr}^{k} \sum_{m=1}^{NB} V_{mr}^{k} \left(G_{jm}^{k} cos\ \theta_{jmr}^{k} + B_{jm}^{k} sin\ \theta_{jmr}^{k} \right) \quad (2.34)$$

$$Q_{GOjr}^{k} - Q_{Djr} = V_{jr}^{k} \sum_{m=1}^{NB} V_{mr}^{k} \left(G_{jm}^{k} sin\ \theta_{jmr}^{k} - B_{jm}^{k} cos\ \theta_{jmr}^{k} \right) \quad (2.35)$$

$$S_{jmr}^{k} \leq S_{maxjm} \quad (2.36)$$

with some variables are presented as follow:

I is set of buses, $\forall j \in I$.

G is set of generators, $\forall i \in G, G \in I$.

K is set of lines (or line contingencies), $\forall k \in K$.

R is set of multiple RES injection scenarios.

N is set of compensator-injected buses, $\forall n \in N, N \in$ I.

A_r^{RE} is occurrence probability of RE scenario-*r*.

P_{GOir} is generator-*i* active power dispatch.

a_i, b_i , c_i are generation-*i* fuel cost coefficients.

P_{GREVi} is generator-*i* active power reserve.

$P_{G_{imin}}$ and $P_{G_{imax}}$ are lower and upper bounds of generators's active power.

Q_{GOir}^{k} is reactive power of generator-*i*.

$Q_{G_{imin}}$ and $Q_{G_{imax}}$ are lower and upper bounds of generators's reactive power.

V_{jr}^{k} is voltage at bus-*j*.

$V_{j_{min}}$ and $V_{j_{max}}$ are lower and upper bounds of buses's voltage.

$VSI_{svb\,r}^{k}$ is global voltage stability index (at the most severe bus)

Tap_n is tap position at compensator-*n* for first and second stages.

Tap_{nmin} and Tap_{nmax} are lower and upper bounds of compensator's taps.

$Q_{Nn}^{base}$is reactive power of each tap unit of compensator-*n*.

Q_{Nnr}^{k} is reactive power of compensator-*n*.

Q'_{Dj} is reactive power demand at bus-*j*.

Q^k_{Djr} is net reactive power at bus-*j*.

P'_{Dj} is active power demand at bus-*j*.

P_{Djr} is net active power at bus-*j*.

P^{RE}_{jr} is RES power at bus-*j* and scenario-*r*.

P_{GOib} is generator-*i* active power dispatch without being affected by RE injection.

α_i is generator-*i* power reduction coefficient in response to load changes.

G^k_{jm} is conductance between buses *j* and *m*, $\forall m \in I$.

B^k_{jm} is susceptance between buses *j* and *m*.

θ^k_{jmr} is voltage angle difference between buses *j* and *m*.

S^k_{jmr} is apparent power flow in the line connecting buses *j* - *m*.

S_{maxjm} is maximum limit of S^k_{jmr}.

NS is number of considered scenario.

NG is number of generators.

NB is number of buses.

Nre is number of injected RE buses.

$r - k$ is pair of RE scenario-*r* and line-*k* contingency.

j and *m* are also indicating buses.

The stochastic SCOPF is used to execute the first and second-stages of the preventive scheme. In the first-stage, only the main scenario is considered corresponding to RE-Expected ($r = 1$) and non-contingency scenarios ($k = 0$). In the second-stage, the power system is designed to be secure during all selected scenarios represented in a selected combination scenario of *r*-*k* (including $k = 0$). Selection of the credible scenario is determined by selecting the R_{wams} and R_{fluct}.

2.5.4. Reactive Power Compensator's Tap Rescheduling

The first-level of the third-stage is to reschedule the reactive power compensator's tap for the individual violated scenario. Compensator can be capacitive (injecting reactive power) or/and inductive (absorbing reactive power). Rescheduling the compensator's tap by minimizing the tap changes as shown in

(2.37) is formulated for the individual scenario indexed by *r-k*.

Objective function:

$$Min\ F_{Tap} = \sum_{n=1}^{NRCT} |Tap_{nr}^{k} - Tap_{n}| \tag{2.37}$$

Subject to

The constraint in equations (2.25)-(2.27), (2.30), (2.34-(2.35) and (2.38)-(2.39) with the last two equations are modified from (2.28)-(2.29) as follows

$$Tap_{nmin} \leq Tap_{nr}^{k} \leq Tap_{nmax} \tag{2.38}$$

$$Q_{Nnr}^{k} = V_{jr}^{k\,2} Tap_{nr}^{k} Q_{Nn}^{base}, for\ j = n \tag{2.39}$$

with $NRCT$ and Tap_{nr}^{k} are number of reactive power compensators and tap position at compensator-*n* for violated scenario *r–k* at third-stage.

2.5.5. Load-Shedding Schemes

For the second level, LS scheme and rescheduling the compensator's tap should be activated only if the first level failed to recover the violated scenario. The LS scheme is formulated to minimize the amount of load curtailment as shown in (2.40) with the control variables are the load curtailment amount in each bus ($P_{LS_{jmr}}^{k}$) and the rescheduled compensator's tap (Tap_{nr}^{k}).

Objective function:

$$Min\ F_{LS} = \sum_{m=1}^{NL} a_m\, P_{LS_{mr}}^{k\,2} + b_m P_{LS_{mr}}^{k} \tag{2.40}$$

Subject to

The constraint in equations (2.25)-(2.27), (2.30), (2.34)-(2.35) and (2.38)-(2.39) with the additional constraints of permissible load curtailment (2.41), net active power after curtailment (2.42) and generator active power change (2.43) are presented as follows

$$P_{LS_{min}} \leq P_{LSmr}^{k} \leq P_{LS_{max}} \tag{2.41}$$

$$P_{Dmr}^{LSk} = P'_{Dm} - P_{LSmr}^{k} \tag{2.42}$$

$$P_{GOir}^{LSk} = P_{GOir}^{k} - \alpha_i \sum_{m=1}^{NL} P_{LSmr}^{k} \tag{2.43}$$

with P_{LSmr}^{k}, P_{Dmr}^{LSk}, P_{GOir}^{LSk}, $P_{LS_{min}}$ and $P_{LS_{max}}$ are LS amount at bus-m, net active power demand under LS, generator active power dispatch, lower and upper bounds of allowable LS amount. Then, a_m and b_m are respective LS penalty cost coefficients at bus-*m*.

The result of third-stage calculation should be applied in the fourth-stage to anticipate if the power system operates into the corresponding violated scenarios direction.

2.6. Numerical Example

2.6.1. System Condition

A modified IEEE 57-bus test system with additional reactive power compensators at buses 25 and 46 (inductive) and at buses 18 and 34 (capacitive), each with maximum reactive power compensation capacity of 1 Mvar and 10 tap positions is used for demonstrating the benefit of the preventive scheme. The total system load was set at 597 MW. RE power injection penetrated at buses 14, 18, and 56. The $V_{j_{min}}$, $V_{j_{max}}$, Tap_{nmin} and Tap_{nmax} were set at 0.94 p.u., 1.06 p.u., 1 and 10, respectively. Generators were installed at buses 1, 2, 3, 6, 8, 9, and 12 with the $P_{G_{imin}}$ being 0 for all and $P_{G_{imax}}$ set at 576, 100, 140, 100, 550, 100, and 410 MW following the initial value of IEEE 57-bus test system. The preventive scheme is formulated into a stochastic non-convex, non-linear optimization problem. The problem is solved using a genetic algorithm (GA) presented in [25] under the MATLAB environment. Considering all of possible scenarios (corresponding to the combination scenarios of line contingency and RES uncertainty), size of the computation problem becomes very large. Simplification in assuming the load model as constant MVA is required for solving the static power flow equation for all selected scenarios, of which the MATPOWER toolbox [26] is used including the network admittance formulation. The method and numerical results written in this chapter has been published in [27].

Table 2.4 Covered line contingency on different R_{wams}

R_{wams} (%)	Number of Line	Line Number
77	3	3;20;31
80	9	5;8;19;20;30;53;59;60;79
84	18	5;7;8;12;19;20;23;28;30;35;47;53;59;60;65;71;78;79
88	29	2;3;5;7;8;12;14;15;19;20;23;25;27;28;30;35;38;39;47;53;59;60;61;63;64;65;71;78;79
92	40	5;7;8;10;12;14;15;18;19;20;22;23;24;25;27;28;30;33;35;36;38;39;40;46;47;53;56;59;60;61;62;63;64;65;67;68;71;73;78;79
96	75	All, except line 41; 45; 48; 49; 50

Table 2.5 Coverage of RE uncertainty under different R_{fluct}

R_{fluct}(%)	Number of covered scenario	Covered scenario
50	4	1,2,4,5
60	5	1-5
70	7	1-7
75	8	1-6,8,9
80	9	1-9
85	11	1-11
90	14	1-13, 15
95	18	1-15,17-19
100	27	All

2.6.2. Scenario Combination of RES Uncertainty and Line Contingency

For selecting important contingencies, optimization problem in equations (2.17) and (2.18) are solved with the value of *n* and *m* variables are set as 2. Line contingency coverage under various value of R_{wams} are presented in Table 2.4.

In multiple RES integration, the set of RES scenarios is a combination of single RES scenario at each injected bus. In this research, A_{jP}^{RE}, A_{jU}^{RE}, and A_{jD}^{RE} are 0.6, 0.2, and 0.2 at bus 14, 0.8, 0.1, and 0.1 at bus 18, and 0.2, 0.5, and 0.3 at bus 56 similar as presented in Table 2.2 with a deviation level ε of 50%. Then, there are 27 sets of RES scenarios consisting of power and probability as shown in Table 2.3 for the top 10 probabilities, with buses A, B and C becomes buses 14, 18 and 56, respectively. Considering that not all of RES scenarios sets are important, R_{fluct} level is used to select high-probability RES scenarios as shown in Table 2.5. Combination scenarios of RES uncertainty and line contingency depend on the

selected R_{wams} and R_{fluct} chosen by the system operator. The maximum number of combinations is 2025 scenarios (75×27), without non-contingency scenario.

2.6.3. Moderate RES Generation Case

In the moderate case, RES generates the predicted (RE-Expected) net power 5, 7, and 3 MW at buses 14, 18, and 56, respectively. The most severe bus, related to the voltage stability performance, is bus-18. While the worst line contingency which endanger the voltage stability the most, is line-20. The first-stage computationally can only successfully satisfy the main scenario. If all possible scenarios *r-k* on the maximum possible R_{wams} and R_{fluct} were considered using the first-stage output, 99 out of 2025 scenarios will violate the overvoltage and/or undervoltage limits with the most severe scenario is scenario 10-20 (RES power 5, 3.5 as RE-Lower and 3 MW at buses 14, 18 and 56) as illustrated in Figure 2.11.a.

When the second-stage was applied under the maximum possible R_{wams} and R_{fluct}, no violated scenarios is remained after this control stage. Obtained operating condition at bus-18 for scenario 10–20 (RES scenario 10 and line-20 contingency) is in safe zone as shown in Figure 2.11.b. It is improved comparing to the first-stage performance. The improvement can also be observed in the voltage stability index and the maximum predicted loading point, expressed by VSI_{svb} and $P_{L\,svb}^{Max}$. Under the first-stage control, $VSI_{svb\,10}^{20}$ is 0.1325, and $P_{L\,svb\,10}^{Max\,20}$ is 1.177528. After the

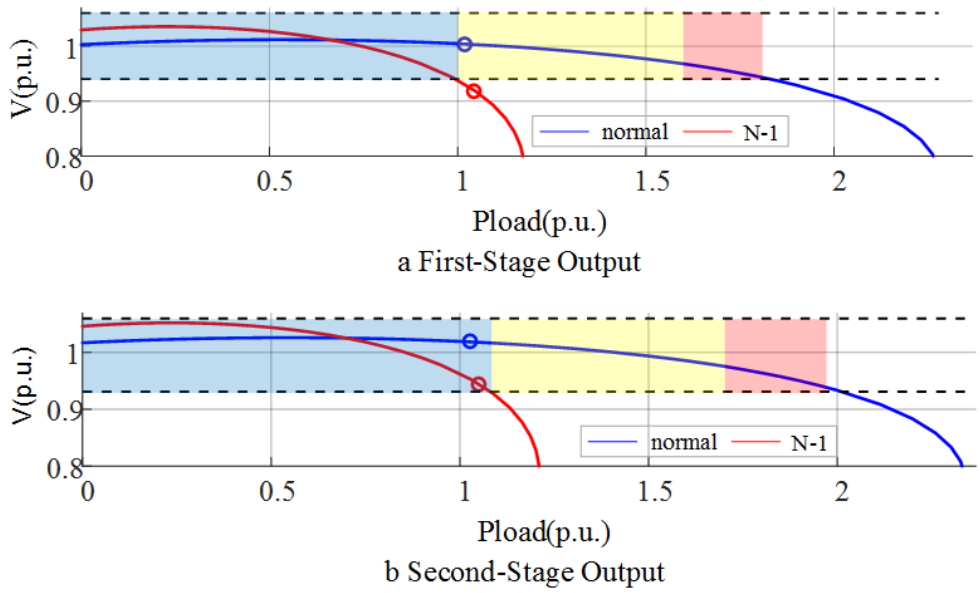

Figure 2.11 Obtained operating condition at moderate RES case

second-stage control, $VSI^{20}_{svb\ 10}$ and $P^{Max\ 20}_{L\ svb\ 10}$ increases to 0.1742 and to 1.211235, respectively.

The proposed preventive scheme has more benefit comparing to the preliminary work reported in [24], which did not consider RES uncertainty. In this comparison case, only scenarios correspond to the RE-Expected can be considered in method [24]. If the method in[24] is applied to deal with the RES fluctuation, 63 violated scenario are potentially remained. For comparison, the obtained operating point at bus-18 of scenario 10-20 is presented at Figure 2.12.a showing that RES fluctuation scenarios cannot be secured. From that figure, It is presented that method in [24] fail in securing RE-Lower scenarios, which represent the RES fluctuation. On the other hand, the proposed preventive scheme can correct the method [24], since no potential violation remains after RES scenario is simulated. For confirmation, the obtained operating point at bus-18, illustrated the uncertainty scenario, is presented at Figure 2.12.b which is identical to the Figure 2.11.b.

2.6.4. Heavy RES Generation Case

In heavy RES generation case, deviation level is set the same as moderate case. RESs generate active power 9, 12, and 7 MW at buses 14, 18, and 56, respectively. Consequently, heavier RES output result in larger RES fluctuation when the magnitude between moderate and heavy case are compared. As the result, the

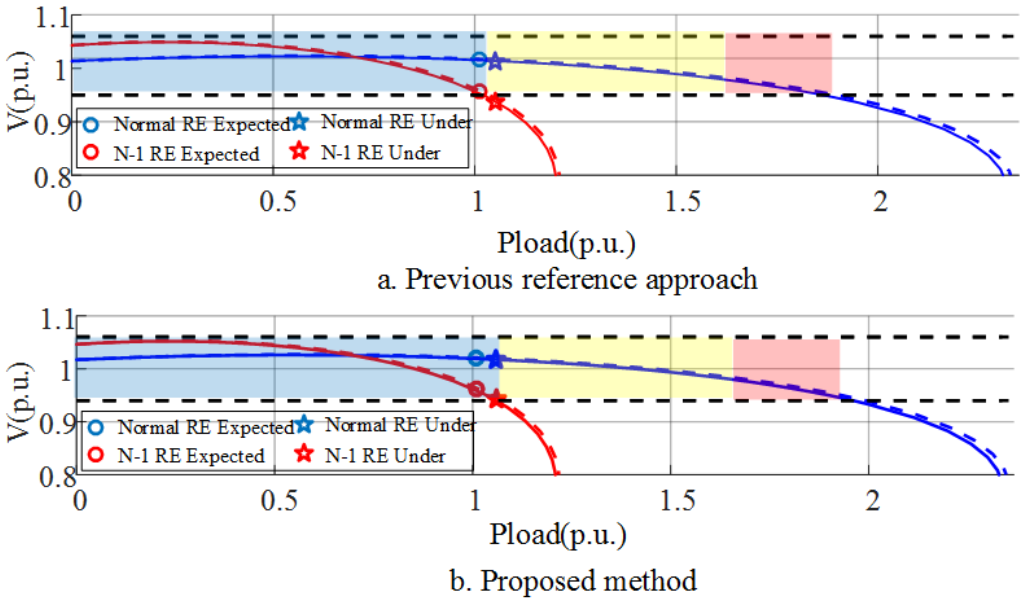

Figure 2.12 Obtained operating condition at moderate RES case using method [24]

first-stage control also fail in securing selected scenarios (under maximum R_{wams} and R_{fluct}), resulting in 219 violated scenarios. After second-stage control, one potential violated scenario is remained. It is scenario 24–40, when RES injected 4.5, 6, and 3.5 MW at buses 14, 18, and 56, respectively, of which, the obtained operating condition is presented in Figure 2.13.

The violated scenario corresponds to undervoltage condition, occurs at bus-28, while the most severe bus is still safely operated during this scenario. Comparison related to the line contingency endanger voltage stability the most is necessary, which is line-20. The comparison in voltage stability is shown in Figure 2.13.a. From the VSI value, it is also confirmed that $VSI_{svb\ 24}^{20}$ is smaller than $VSI_{svb\ 24}^{40}$ (0.2185 compared to 0.5955). Even result in lower VSI, the scenario 24–20 was still safely operate, as shown in Figure 2.13.b. Based on this observation, the violated scenario 24–40 is categorized as undervoltage problems (not voltage stability problem). In this situation, the first level of third-stage, which do compensator's tap rescheduling should be prepared, which changes the capacitive compensator tap at bus-34 from 0.3 to 0.5 p.u. for compensating the undervoltage.

Selecting lower R_{wams} and R_{fluct} result in smaller number of selected scenario, which has more chance to ensure the system security computationally.

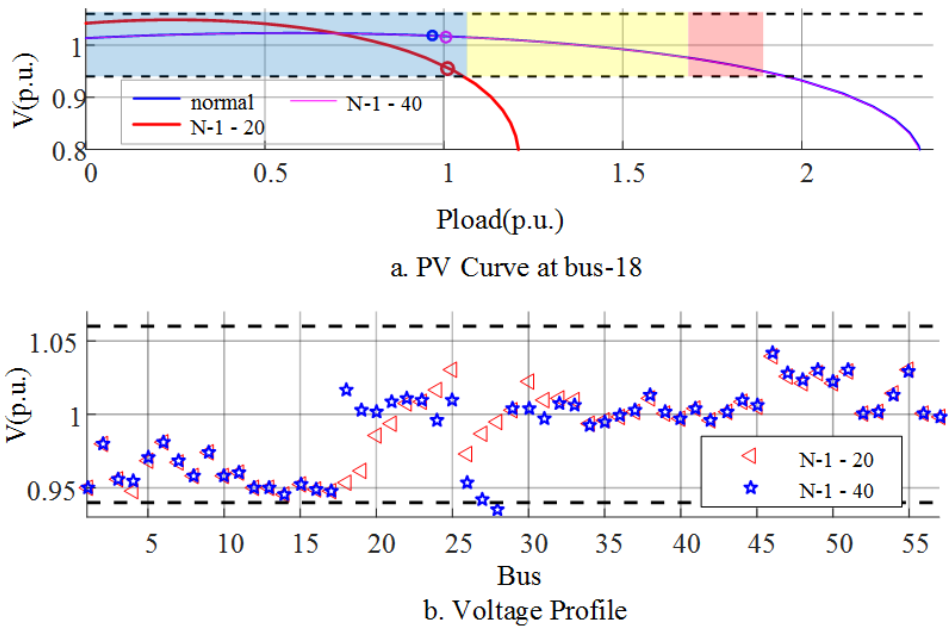

Figure 2.13 Obtained operating condition after second-stage at heavy RES case

Selecting R_{wams} at the maximum value and R_{fluct} equal to 90%, which covers 14 RES scenarios (1050 of 2025 combined scenarios), ensures the security of selected scenario (1050 scenarios). In this selection, 13 RES scenarios, including scenario-24, are excluded.

2.6.5. Stressed System Loading Case

For stressed system loading case, system load is intentionally increased so that loads at bus-18 increases by 7% from the base-case. RES generates power similar to the moderate case. After implementing the second-stage control, 10 out of 2025 scenarios remained violated into marginal zone category, which two of them are scenarios 10–20 and 24–40.

Scenario 10–20 has $VSI^{20}_{svb\,10}$ of 0.0861, having close distance to voltage stability limit, and voltage at bus-18 drops to 0.9171 p.u. with the other bus still operate within admissible range, as illustrated in Figure 2.14. After the third-stage control, rescheduling of compensator's tap & LS are needed for compensating the violation. For recovering the voltage at 0.941 p.u., the LS curtailment of 0.010 p.u. at bus-18 is needed. Only rescheduled the compensator's tap, the voltage becomes 0.9316 p.u. (still violated). The correction is also confirmed from $VSI^{20}_{svb\,10}$, which increased to 0.1159. The improvement after applying third-stage control is presented

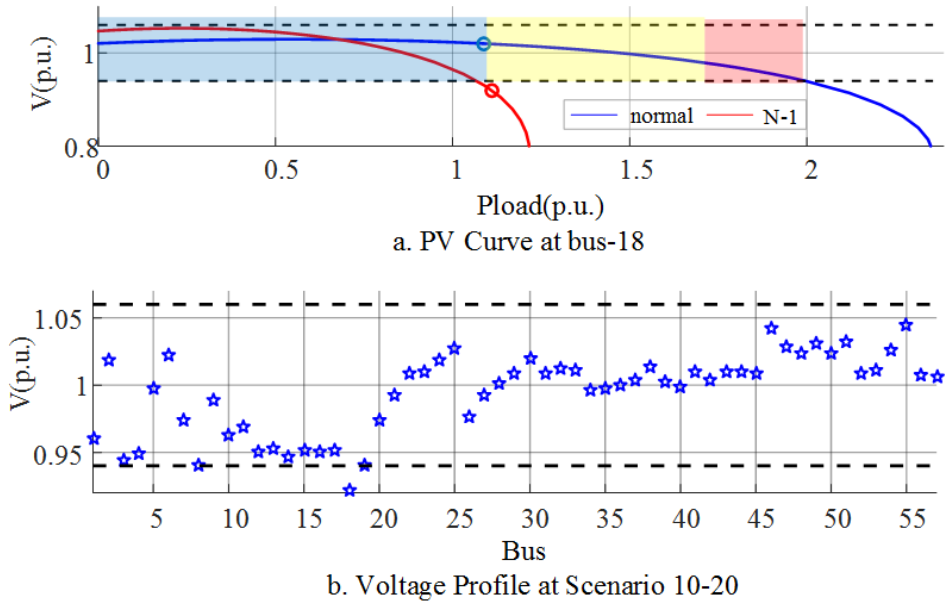

Figure 2.14 Obtained operating condition at stressed load after second-stage

in Figure 2.15.

Violation if scenario 24–40 occurs is categorized as undervoltage problem, which cause the voltage at bus-28 drop to 0.937 p.u. This violated scenario is not correlated to the most severe bus, so observation on the voltage stability is not necessary. For this scenario, rescheduling the compensator's tap is sufficient for recovering the bus voltage within the admissible range, as shown in Figure 2.16. Reactive compensator tap at bus-34 changes from 0.6 to 0.7 p.u. Similar process should be prepared for 8 remaining violated scenarios.

2.6.6. Scenario Selection and Cost Comparison

Determining R_{wams} and R_{fluct} is an important step before implementing the proposed preventive scheme. If higher values are selected, the system security is

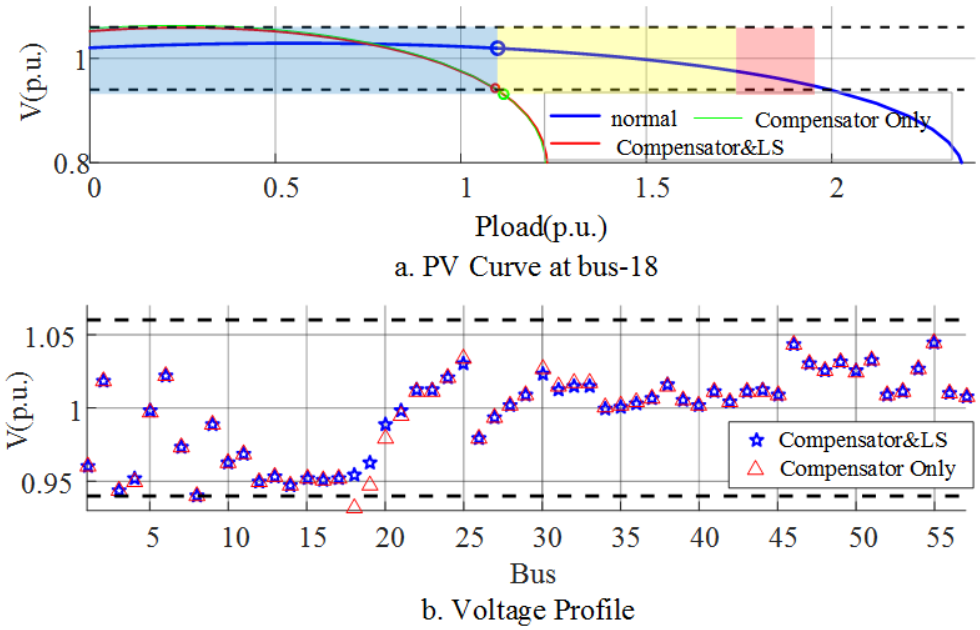

Figure 2.15 Obtained operating condition at stressed load at different stages

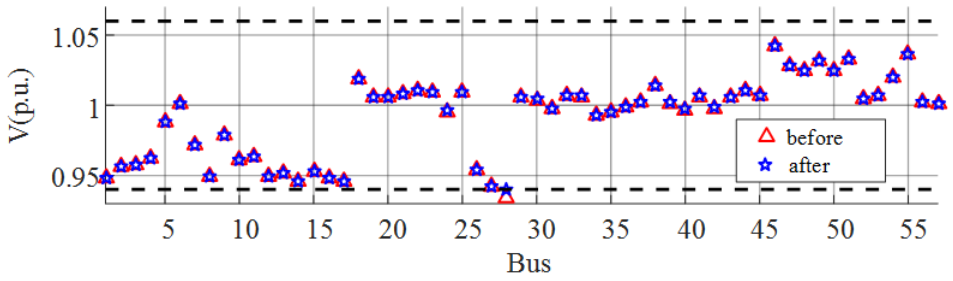

Figure 2.16 Obtained operating condition at stressed load at different stages

Table 2.6 Generation cost and violation on moderate case at various R_{fluct}

R_{fluct}(%)	50	70	80	90	95	100
Generation Cost (Unit Cost)	15756	15883	15773	15857	16189	16401
The Number of Violation case*	8	3	3	2	1	0
Violated scenarios*	3-40 8–40 13-42 14–40 16-40 23-42 24–40 26–40	8–40 14–40 24–40	14–40 23–42 24–40	14–40 24–40	24–40	–

Table 2.7 Generation cost and violation on moderate case various R_{wams}

R_{wams}(%)	77	80	84	88	92	96
Generation Cost (Unit Cost)	15704	15720	15736	15769	16251	16401
The Number of Violation case*	54	41	37	30	27	0

* Violation cases based on maximum level of R_{wams} and R_{fluct}.

securer, since more scenarios are computationally secured. On the other hand, more selected scenario will also result in more expensive generation (fuel) cost after second-stage control. Obtained total generation cost and potential remained violated scenarios in moderate cases under different number of selected scenario is presented in Table 2.6, which illustrated the effect on different value of R_{fluct}. More specifically, total generation cost increases from 15756 to 16401 unit cost for different R_{fluct} from 50% to 100% while in the first-stage the cost is 15470 unit cost. For different values of R_{wams}, it is confirmed that higher values of R_{wams} secure more scenarios but require higher generation cost.

On the other hand on selecting higher value of R_{wams} under constant value of R_{fluct} will also ensure securer power system operation and higher generation cost. Prove on this is presented under the maximum R_{fluct} and varies value of R_{wams} variable as presented in Table 2.7.

Table 2.8 Generation cost and violation on heavy case at various R_{fluct}

R_{fluct}(%)	50	70	80	90	95	100**
Generation Cost (Unit Cost)	15469	15490	15862	15987	16308	16484
The Number of Violation case*	11	8	6	5	1	1
Violated scenarios*	3–75 8–40 9–75 10–75 14–40 14–75 16–75 18–75 24–40 24–75 26–75	8–40 14–40 14–75 18–75 23–60 24–40 24–75 26–75	14–75 23–32 24-40 24–75 18-75 26–75	14–75 23–32 24-40 24–75 26–75	24–40	24–40

* Violation cases based on maximum level of R_{wams} and R_{fluct}.

** Infeasible solution for the selected and R_{fluct}level

Heavy RES generation generates heavier fluctuation, which cause more uncertainty in the system. Heavier RES generation case at different values of R_{fluct} and maximum level of R_{wams} is presented in Table 2.8. It is also presented that selecting higher R_{fluct} ensure system security and require more expensive generation cost. Comparing to moderate case, considering the combination *r-k* scenario in heavy RES penetration requires higher generation cost for R_{fluct} = 90 and 95%. It seems that the second-stage control cannot satisfy the maximum number of selected scenario, since scenario 24–40 is still remained violated. From the security aspect, the number of violated scenarios after second-stage control also increases compared to the moderate case.

Comparison on heavy and moderate RES generation cases were done in the generation cost (fitness value) and the number of violated scenario. More RES generation generally gives more reliability to the power system and reduces the generation cost generated from non-RES. However, RES uncertainty affect the conventional generator in generating more expensive cost as illustrated in Table 2.8 and Table 2.7 at R_{fluct}> 80%. On the other hand, if less RES scenario is selected (in

Table 2.9 Generation cost and violation on stressed case at various R_{fluct}

R_{fluct}(%)	50	70	80	90**	95**	100**
Fuel Cost (Unit Cost)	16530	16810	17415	17509	17662	17676
The Number of Violation case*	15	12	10	10	10	10

* Violation cases based on maximum level of R_{wams} and R_{fluct}.

** Infeasible solution for the selected and R_{fluct}level

example at R_{fluct} 50 and 70%), less expensive generation cost is required. From the security aspect, it can be concluded form both tables which more RES generations increases the possibility of the number of violated scenario occurrence. This comparison also shows the benefit of the proposed preventive scheme comparing to the preliminary work presented in [24]. If the RES uncertainty is neglected in the problem formulation, the system will have more risk suffering from grid violation, which can be under voltage, over voltage or even voltage stability

In stressed system loading condition case, the generation fuel cost increment pattern is presented in Table 2.9. From the security aspect, it becomes more difficult for securing more scenarios simultaneously. Furthermore, the second-stage control can only computationally satisfy the selected scenarios up to R_{fluct} = 80% under the maximum level of R_{wams}. For R_{fluct} = 90, 95, and 100%, there are still some violated scenarios remained after the second-stage control, so third-stage control is required.

2.6.7. Computation Time

Problem is simulated using 64-bit PC with 3.0 GHz CPU and 32 GB memory. GA is used for solving all of the stages procedures. For the first and second stages, population and iteration are set 100 and 200, while for the third-stage are set 30 and 50, respectively. The longest computation time is on the second-stage procedure, which required 1 to 40 minutes for each simulation cases depending on the number of selected scenario. Computation time for another stages are relatively fast, which could be completed within 1 minute. For the practical implementation purpose, all of the computation processed should be finished within 30 minutes. In the current computation tools specification, It can only satisfy up to R_{wams}= 92%. However, PC up to 128 GB memory is available in the market. The total required computation

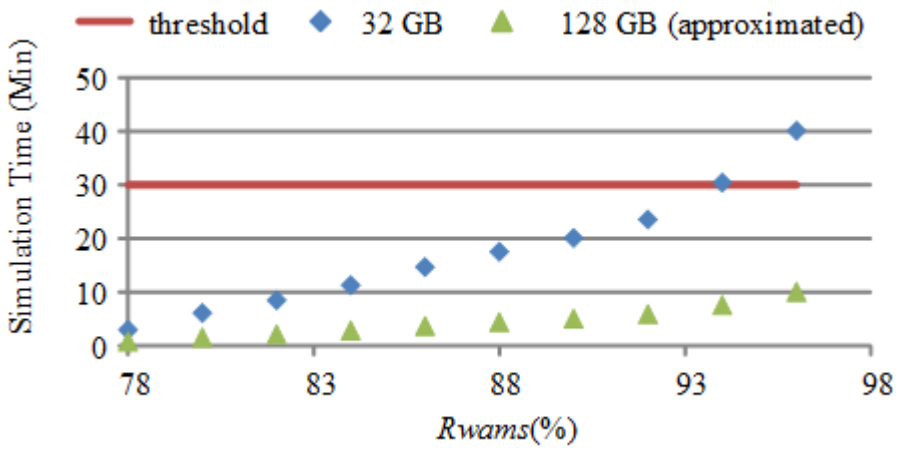

Figure 2.17 Required simulation time at the various R_{wams}

times on the maximum R_{fluct} under various R_{wams} is shown in Figure 2.17. Approximation of computation times using that high speed PC is also presented in this figure, which will make the computation time acceptable for any selected scenario.

Even though the first and second-stages are subject to the same problem and the control variables are also similar, the function of these stages is different. The first-stage of is more beneficial to deal with time-slot having light system loading whit low RES generation. In a light loading condition and moderate RES case, there is an computational experience that first-stage can secure the system when R_{wams} and R_{fluct} are set 80% covers 9 line contingencies and 9 RES scenarios. Compared to second-stage, the first-stage has smaller problem size since only consider the main scenario.

III. SOLVING LARGE SCALE OPTIMUM POWER FLOW

3.1. Stochastic Large Scale OPF

The multistage preventive scheme strategies presented in the previous chapter consist of some optimization problems, which were solved using the genetic algorithm (GA) technique. GA was selected because the problem is non-linear and non-convex, which is one of the advantage this technique. Moreover, the problem size is dramatically increased due to the existence of combinational scenario, which causes the computational burden. Second-stage of the preventive scheme is the most time-consuming part among another stage. It is necessary to develop the computational solver for solving the large scale OPF.

Related to the proposed method solution, some previous work in solving the OPF including the uncertainty and voltage stability has been investigated. Preventive scheme strategy against voltage stability in the considering some credible line contingencies has been proposed in [28]. It solves the OPF problem consisted of economic load dispatch (ELD) and voltage collapse proximity indicator minimization with necessary load curtailment action as corrective control. Risked based for improving voltage security and stability considering line contingency using multistage preventive scheme based on ELD and load curtailment was proposed in [24]. Moreover, controlling reactive power injection/absorption by managing generator or synchronous condenser can help to improve voltage stability as has been discussed in [29]. Various technique of SCOPF analysis has been widely applied for securing the power system against the selected contingencies as presented in [30]–[32]. However, heavy computation burden and poor accuracy are still remained as the weaknesses so that algorithm related to SCOPF is still developing. Furthermore, most of those techniques are insufficient to handle the intermittency of RES scenario.

Iterative SCOPF with compression on the network topology was proposed in [33] to distinguish between dominant and non-dominant contingency and provide proper corrective action for the uncovered contingency. Technique for narrowing the generator limit and combining to corrective scheme in rescheduling generator power for SCOPF was proposed in [34]. Penetration of RES in the power system requires special generation schedule formulated in dynamic ELD, which should be solved using dynamic programming [35], quadratic programming [36], simulated annealing [37], hybrid differential evolution [38] and high speed dynamic ELD [39]. However,

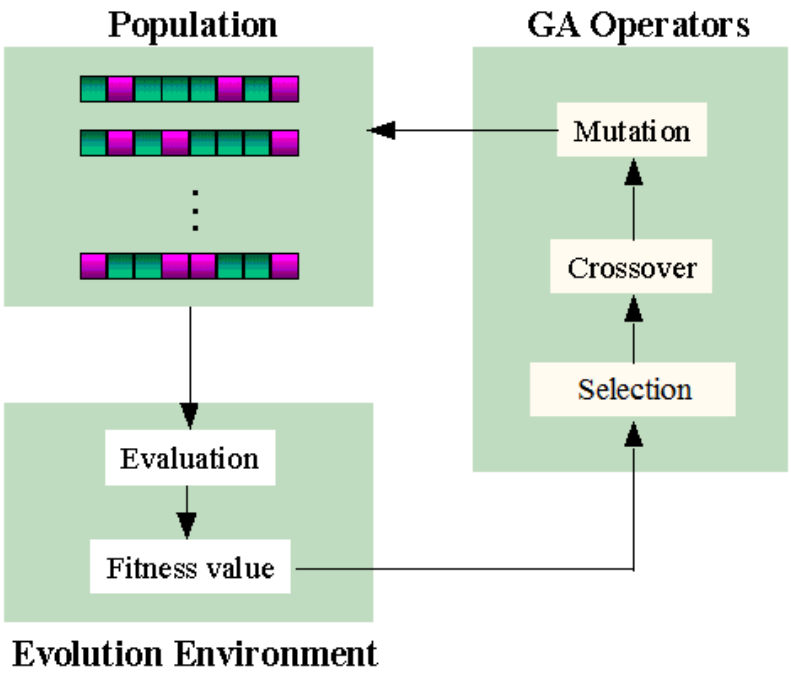

Figure 3.1 Evolution flow of genetic algorithm

those algorithms are not effective for solving the multistage preventive scheme strategy. In this chapter, a novel computation technique based on genetic algorithm heuristic method and primal dual interior point algorithm is proposed to handle large computation space within reasonable computation time.

3.2. Overview of Genetic Algorithm

GA has been introduced in some previous research as presented in [25], [40]–[44] , including its application for OPF. GA algorithm simulates the most optimum solution of a defined problem among (fitness value) individuals over some generations. In each generation, there is existed a population consist of some characters which is similar to the chromosome in the human body. Each individual consists of string, which is representing genes in a chromosome. Some generations are required for completing the GA process represents the evolutionary process. Briefly the GA process can be summarized in Figure 3.1, which the major part are explained in the following subsection.

3.2.1. Individual Generation

For the first generation, n-number of individual consisted of strings is generated as shown in Figure 3.2. Define the fitness function/ objective function as

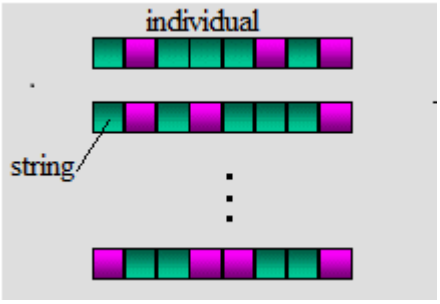

Figure 3.2 Individuals generation in population

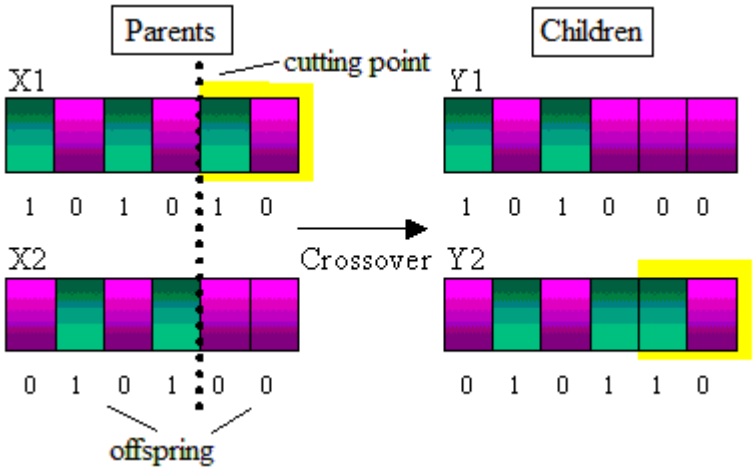

Figure 3.3 Illustration of Crossover between two individuals

f(x), x is the decision variable and the length of x is n, each individual will consist of n strings. The generated string in each individual are randomly decided within each permissible range of variables x.

3.2.2. Selection/Elitism

For each individual, the fitness value f(x) is calculated, and then some elite individual are selected based on the finesses. Those individual will be remained for the next generation and will have more possibility to be a parents. The parent will be selected through the roulette wheel selection scheme.

3.2.3. Crossover

Each individual can be divided into two parts by cutting point, the two separation parts ware called offspring. The offspring between parents are switched to generate new individual for the next generation as illustrated in Figure 3.3

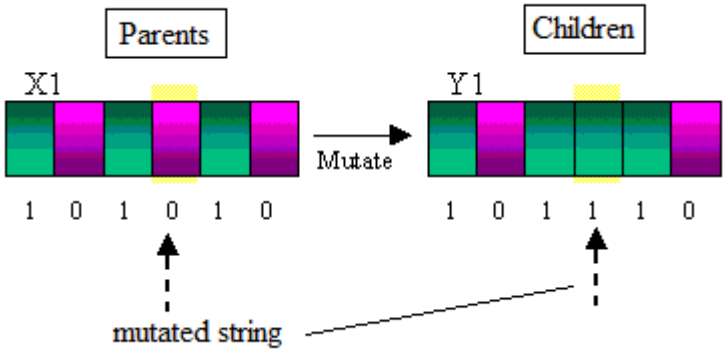

Figure 3.4 Illustration of mutation process

3.2.4. Mutation

Mutation consists of reversing a randomly chosen bit. For example, assume that the individuals are represented as binary strings. In bit complement, once a bit is selected to mutate that bit will be flipped to be the complement of the original bit value. For example, let the parents x1=101010 and suppose that the mutational bit is bits 4 (where the bits are numbered from left to right starting at 1). Then the child is y1=101110. Figure 3.4 demonstrates this example. This mutation adds a white noise to the gene selected for mutation.

3.3. Conventional OPF with Primal Dual Interior Point Algorithm

The primal-dual interior point method (PDIPM) has been popular worldwide in its capability to solve various OPF problems as reported in those following reference [45]–[51]. The OPF based on PDIPM then developed into the optimization solver based on various software environments such as MATLAB [52], GNU Octave [53], GUROBI [54] or PSS/E RAW [55], etc, which called as the interior point solver (IPS) as presented in [26].

Briefly the PDIPM based on the equation (2.23)-(2.26), (2.28)-(2.36) for solving the second-stage equation on main scenario are formulated as follows:

$$\begin{aligned} &Min\ f(X) \\ &\text{Subject to:} \\ &H(X) = 0 \\ &G(X) \leq 0 \end{aligned} \tag{3.1}$$

Those equations represent the objective function, equality constraints and inequality constraint of the main scenario of the problem in those equations. Equation related to the voltage stability index (2.27) cannot be solved in the PDIPM solver because another complex formulation in (2.13)-(2.16) should be computed in advanced.

The problem then converted into a sequence of unconstrained optimization problems in the form of Lagrangian equation, which should be solved iteratively.

$$L^{\gamma}(X,Z,\lambda,\mu) \equiv f(X) + \lambda^{T}H(X) + \mu^{T}(G(X)+Z) - \gamma\sum_{m=1}^{ni} ln(Z_m) \tag{3.2}$$

with X is vector of the decision variable, Z is vector of positive slack variable with the length ni, λ and μ are the lagrange multipliers, and γ is a positive scalar vector. The first-order Karush-Kuhn-Tucker (KKT) condition then derives as follow:

$$\begin{gathered} \nabla_X L^{\gamma}(X,Z,\lambda,\mu) = 0 \\ H(X) = 0 \\ G(X) + Z = 0 \\ [\mu]Z - \gamma e = 0 \\ Z > 0, \mu > 0 \end{gathered} \tag{3.3}$$

with e is the unitary vector and $[\cdots]$ is operator for diagonal command. Newton's method can be used to solve the equation (3.3) which further described as follow.

$$\begin{bmatrix} \nabla^2_{xx}L^{\gamma}(X,Z,\lambda,\mu) & 0 & \nabla H(X) & \nabla G(X) \\ 0 & \left[\frac{\mu}{Z}\right] & 0 & I \\ \nabla H(X)^T & 0 & 0 & 0 \\ \nabla G(X)^T & I & 0 & 0 \end{bmatrix} \begin{bmatrix} \Delta X \\ \Delta Z \\ \Delta\lambda \\ \Delta\mu \end{bmatrix} = \begin{bmatrix} -\nabla_X L^{\gamma}(X,Z,\lambda,\mu) \\ -(\mu - \gamma[Z]^{-1}e) \\ -H(X) \\ -G(X) - Z \end{bmatrix} \tag{3.4}$$

Equation (3.4), then can be reduced as equation (3.5) as follow:

$$\begin{gathered} \Delta Z = -G(X) - Z - \nabla G(X)^T \Delta X \\ \Delta\mu = -\mu + [Z]^{-1}(\gamma e - [\mu]\Delta Z) \\ \begin{bmatrix} M & \nabla H(X) \\ \nabla H(X)^T & 0 \end{bmatrix} \begin{bmatrix} \Delta X \\ \Delta\lambda \end{bmatrix} = \begin{bmatrix} -N \\ -H(X) \end{bmatrix} \\ M = \nabla^2_{xx}L^{\gamma}(X,Z,\lambda,\mu) + \nabla G(X)[Z]^{-1}[\mu]\nabla G(X)^T \\ N = \nabla_X L^{\gamma}(X,Z,\lambda,\mu) + \nabla G(X)[Z]^{-1}([\mu]G(X) + \gamma e) \end{gathered} \tag{3.5}$$

The PDIPM maintains the strict feasibility of the solution by shorten the Newton step as follow:

$$\begin{aligned} \alpha_p &= min\left(\xi min_{\Delta Z_m<0}(-Z_m/\Delta Z_m), 1\right) \\ \alpha_d &= min\left(\xi min_{\Delta \mu_m<0}(-\mu_m/\Delta \mu_m), 1\right) \\ X &= X + \alpha_p \Delta X \\ Z &= Z + \alpha_p \Delta Z \\ \lambda &= \lambda + \alpha_d \Delta \lambda \\ \mu &= \mu + \alpha_d \Delta \mu \end{aligned} \tag{3.6}$$

with ξ is a constant scalar marginally less than one. In PDIPM γ is called the parameter of perturbation and must converge to zero during the Newton-like iterations. How to update the value of γ can be different case by case depend on the application. However, in the IPS in [26] use the following rule to update the γ in each iteration, after updating Z and μ:

$$\gamma = \sigma \frac{Z^T \mu}{n_i} \tag{3.7}$$

with the value of σ should be between 0 and 1. In IPS, it was set 0.1.

3.4. Hybrid Computational Approach for Solving Optimum Power Flow

A novel hybrid computational approach for solving optimum power flow (HC-OPF) combines the heuristic and numerical method of optimization solution. HC-OPF basically based on GA to find the optimal value of discrete variable and in each individuals/chromosome, while the optimal value of continuous variables is solved using numerical method in each individual. The procedures of HCOPF are briefly summarized in Figure 3.5, which each block is explained in another subsection.

3.4.1. Population Generation

In HC-OPF, the decision variables are the same as original GA process (compensator tap position, generator power, reserve power, and voltage) with the pseudo generator limit becomes the additional variable. Different from original GA process in the previous chapter, which decides all of decision variables, GA process in HC-OPF only decides the compensator tap position and pseudo generator limit, while the other variables are solved using numerical method.

Pseudo generator limit purpose is to limit the output of generator having low contribution to the preventive scheme. The value of the pseudo generator limit and

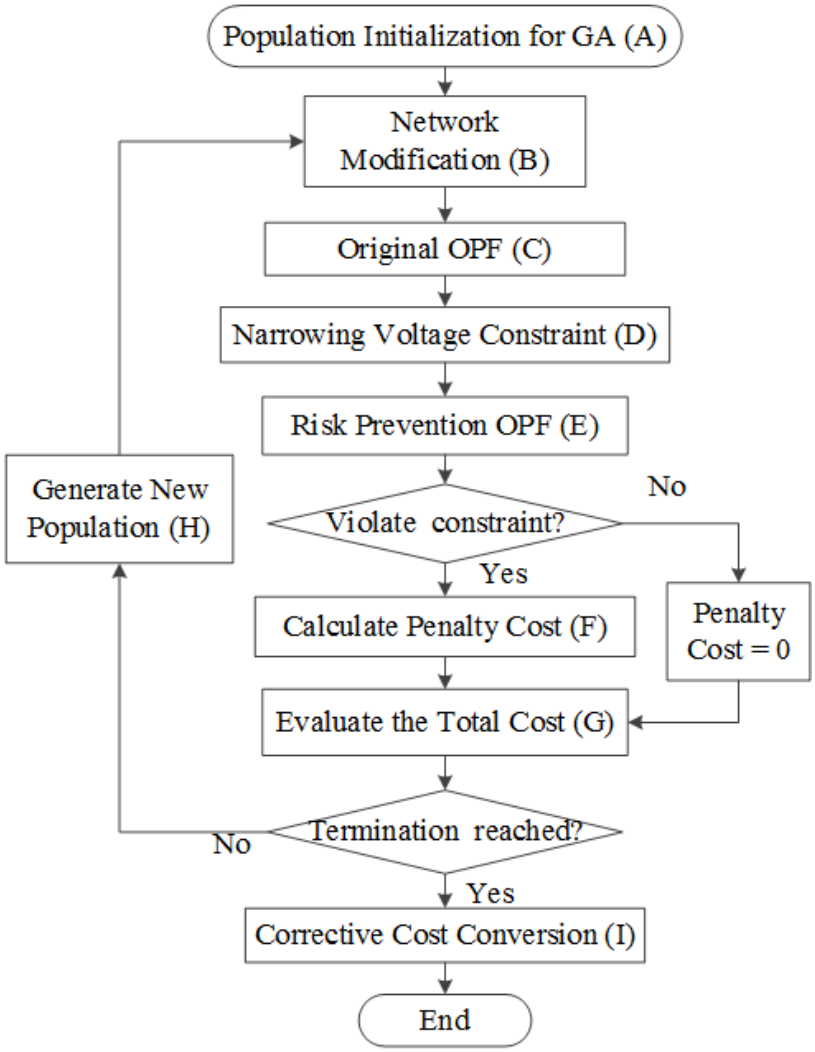

Figure 3.5 Proposed hybrid computation approach for solving opf

the generator output in (2.24) are rewritten as follow.

$$\widehat{P_{G_{imax}}} \leq P_{G_{imax}}$$
$$P_{G_{imin}} \leq P_{GOir} + P_{GREVi} \leq \widehat{P_{G_{imax}}} \tag{3.8}$$

with $\widehat{P_{G_{imax}}}$ is the pseudo generator limit. For each individual, considerable random number within each admissible range is generated for those two variables.

3.4.2. Network Modification

Power system network is modeled using bus admitance matrix showing the connection among the buses. Tap_n are randomly generated in each

individual/population so that the power system network need to be updated in each generation as described in block B.

3.4.3. Original OPF

A non-linear numerical OPF based on PDIPM, which has been built in [26] are used to execute single main scenario as represented in block C. The main scenario is corresponding to the expected value of RE generation (r=1) and at non-contingency state (k = 0). The solver is called original OPF, which solves equations (2.23)-(2.26), (2.28-(2.36). Output of the computation is only feasible for the main scenario and will be used as initialization for the next step.

3.4.4. Narrowing Voltage Constraint

Using the result of original OPF, the operating conditions for another selected scenario *r-k* can be estimated, including the buses voltage. Obtained buses voltage of some scenarios may violate the original voltage constraints. The uncertainties caused by another scenario are observed in buses voltage variation. Those voltage variations affect the bus voltage limit, which becomes the new additional variable called as pseudo voltage limit. Pseudo voltage limit can be calculated as follow:

$$\begin{aligned} \widehat{V}_{J_{min}} &= V_{j_{min}} * max\left\{\frac{V_{j1}^{0}}{V_{jr}^{k}}\right\}, if\ max\left\{\frac{V_{j1}^{0}}{V_{jr}^{k}}\right\} > V_{j_{max}} \\ \widehat{V}_{J_{max}} &= V_{j_{max}} * min\left\{\frac{V_{j1}^{0}}{V_{jr}^{k}}\right\}, if\ min\left\{\frac{V_{j1}^{0}}{V_{jr}^{k}}\right\} < V_{j_{min}} \end{aligned} \tag{3.9}$$

with $\widehat{V}_{J_{min}}$ and $\widehat{V}_{J_{max}}$ are minimum and maximum pseudo voltage limit. The value of pseudo voltage limit must be in the range of original admissible voltage range. It assumed that only maximum and minimum fluctuation of RES generation associate to the security border of the power system. For this reason, only 2 out of n^3 RE states are considered in this step.

3.4.5. Risk-based Preventive OPF

This part is associated to block E, which once against solves numerical OPF [26] for the main scenario. The difference from block C, the voltage constraint of the optimization problem is updated using the pseudo voltage constraints. For that reason, equation (2.26) is updated as follows:

$$\widehat{V}_{J_{max}} \leq V_{jr}^{k} \leq \widehat{V}_{J_{min}} \tag{3.10}$$

By narrowing the voltage constraint, the new control variable may change from the original problem (from block C) and relax the operating condition from the constraint.

3.4.6. Calculating Penalty Cost

Even if, the feasible solution of risk-based preventive OPF (RBOPF) can be obtained, there is no guarantee that the optimization result in block E can secure all selected scenario, especially for voltage stability constraint, which is non-linear. For this purpose, a penalty cost calculation (block F) is formulated. Penalty cost should be associated to the corrective scheme strategy (third-stage). The penalty cost consists of some parts related to voltage constraint, voltage stability and line loading violations. In HC-OPF, penalty cost is linearized for obtaining the acceptable computation speed. In addition, power flow and continuation power flow analysis corresponding to each scenario are calculated. The penalty cost corresponds to RES scenario and formulated as follow:

$$\begin{aligned} Pcost_r = Cof * \Bigg(& \sum_{k=1,k\neq 0}^{NC} \left(-VSI_{svb\,r}^{k}\right) * ksvb_{rk} \\ & + \sum_{k=1}^{NC} \sum_{j=1}^{NLB} \left(V_{j_{min}} - V_{jr}^{k}\right) * kmin_{jrk} \\ & + \sum_{k=1}^{NC} \sum_{j=1}^{NB} \left(V_{jr}^{k} - V_{j_{max}}\right) * kmax_{jrk} \\ & + (0.05 - VSI_{svb\,r}^{0}) * ksvb_{t0} \\ & + \sum_{jm}^{NK} \left(S_{jmr}^{k} - S_{max\,jm}\right) * kS_{jmrk} \Bigg) \end{aligned} \tag{3.11}$$

In total cost evaluation procedure (block G), the set of individual in a generation having lower costs is selected. The termination criteria are reached if the iteration finished or the convergence is obtained. In each iteration, the new populations of Tap_n and $\widehat{P_{G_{imax}}}$ in block H are re-generated within GA procedure. In the final solution, if the penalty cost is not zero, it will be converted to the

corrective cost action by executing third-stage each violated scenario.

3.5. Numerical Example

3.5.1. System Condition

The same system condition as the previous chapter are used as the test system with heavy RES generation at buses 14, 18 and 56, each with 9, 12 and 7 MW, respectively with deviation level 40%. For the scenario selection, various line contingency selections determined by R_{wams} are considered as the line contingency scenario. On the other hand, all of RES scenario is considered which 27 scenarios are. Performance of HC-OPF is compared to the GA-OPF, which has been presented in the previous section and [27]. The methods and the numerical result of this chapter have been published in the following reference [56].

3.5.2. Effect on Second-Stage of Preventive Scheme

HC-OPF computation result for the second-stage can be directly evaluated by the voltage stability performance. It can be compared to genetic algorithm method (GA-OPF) used in the previous section. Lines 5, 19, 20 and 53, correspond to R_{wams} = 78%, are considered while the net active power for the main scenario in the most severe bus is 0.96 p.u. From Figure 3.6, it can be observed that the obtained operating condition from HC-OPF result can also satisfy problem formulation as the

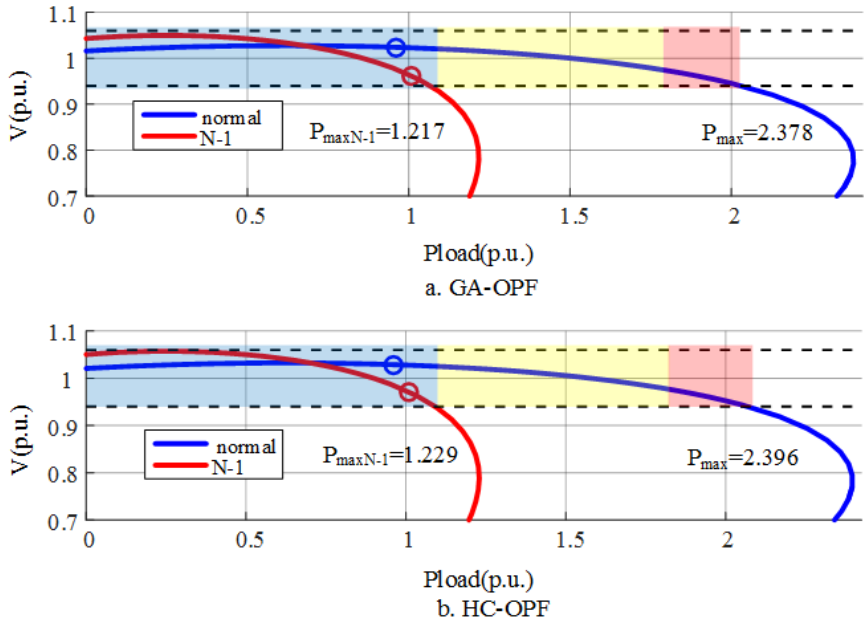

Figure 3.6 Obtained operating condition under different techniques

GA-OPF did. The most severe bus is bus-18, Scenario 10-20 (RES scenario correspond to RE-Upper and line-20 contingency) is used to show the effectiveness of the second-stage of preventive scheme.

Furthermore, the voltage stability indexes are still far greater than the operating point which are $VSI_{svb\ 10}^{20} = 0.1717$ (GA-OPF) and 0.1798 (HC-OPF). From those figure, it can be seen that both of the computation solver have the ability for solving the second-stage. In scenario 10-20, the operating point lies on $P_{L\ svb\ 10}^{Max\ 20}$= 1.008 p.u. with the voltage 0.962 p.u. (GA-OPF) and 0.968 p.u. (HC-OPF), which is within the voltage

3.5.3. Effect on Fitness Value

More scenarios considered in the problem requires more expensive generation cost for both GA and HC-OPF as presented in [24] and Table 3.1. For comparison, Normal-OPF considering only the main scenario (only for *k*=0 and *t*=1) requires 15228 unit costs. The generation cost increase linearly with the increment of the number of scenario for both GA-OPF and HC-OPF. Both techniques show linear correlation between numbers of scenarios and generation cost. HC-OPF method gives more optimum result than GA-OPF. However, for complete scenarios determined by R_{wams} = 96%, HC-OPF fails to secure all scenario. For this result, the fitness value result in 20443 unit costs, which consist of 15749 as the generation cost and 4694 as penalty cost with Cof is 10^7. In addition, pseudo variables can prevent the violated scenario. In the Normal-OPF, the uncertainty effect from the other scenario is not considered and the original generator limit and voltage constraint are still used in the HC-OPF procedure. The Normal-OPF is used as comparison tools to show the effectiveness of HC-OPF.

The example of the pseudo variable's usage is shown for R_{wams} = 88% in

Table 3.1 Generation cost at various of R_{wams} using GA-OPF and HC-OPF

R_{wams} (%)	Number of line contingencies	Generation Cost (Unit Cost)	
		GA-OPF	HC-OPF
78	5	15312	15238
80	10	15360	15242
82	14	15397	15242
84	18	15413	15242
86	25	15390	15298
88	30	15549	15340
90	35	15595	15372
92	41	15793	15489
94	54	15910	15966
96	76	16464	20443*

* including penalty cost

Table 3.2 Effect of pseudo variable on R_{wams} = 88% and non-contingency

Pseudo Variable		**Obtained Variable after the Optimization**		
Variable name	**Searched**	**Variable name**	**HC-OPF**	**Normal - OPF**
$\widehat{P_{G_{1max}}}$	405.10	$P_{G1\,1}$	98.94	83.31
$\widehat{P_{G_{8max}}}$	408.13	$P_{G8\,1}$	294.18	249.05
$\widehat{P_{G_{12max}}}$	142.46	$P_{G12\,1}$	135.34	199.25
$\widehat{V_{25_{max}}}$	1.051	$max\{V_{25r}^{k}\}$	1.048	1.050
$\widehat{V_{30_{max}}}$	1.041	$max\{V_{30r}^{k}\}$	1.040	1.044
$\widehat{V_{46_{max}}}$	1.044	$max\{V_{46r}^{k}\}$	1.0598	**1.076**
$\widehat{V_{47_{max}}}$	1.042	$max\{V_{47r}^{k}\}$	1.049	**1.065**
$\widehat{V_{48_{max}}}$	1.036	$max\{V_{48r}^{k}\}$	1.042	1.058
$\widehat{V_{49_{max}}}$	1.042	$max\{V_{49r}^{k}\}$	1.041	1.057

* Active power unit on MW and voltage in p.u.

Table 3.3 Calculation time comparison between GA-OPF and HC-OPF

R_{wams} (%)	Number of constraints	Computation Time(Second)	
		GA-OPF	**HC-OPF**
78	2399	178.33	27.58
80	4807	367.71	40.68
82	6588	507.20	50.65
84	8622	675.63	62.71
86	12172	880.39	78.51
88	14710	1049.91	89.82
90	17254	1203.82	100.95
92	20300	1409.91	111.05
94	26888	1823.12	147.10
96	38032	2603.86	208.72

Table 3.2, of which the maximum constraints are lower than the maximum original constraint. After optimization process, the obtained operating condition for all possible scenarios is presented in that table. For the selected R_{wams} = 88%, HC-OPF can secure all selected scenarios as the evidence no-violated voltage in any scenario. However, using the Normal-OPF there are some violations as the evidence there are voltages violations at buses 46 and 47.

3.5.4. Computation Time

The computation time of HC-OPF is still correlated to the problem size, which consist of equality and inequalities' number. Problems are simulated in MATLAB environment using 64-bit PC with 3.00 GHz CPU and 32 GB memory. Comparison of the computation time is presented in Table 3.3. For solving numerical OPF as part of HC-OPF, modified MATPOWER 4.1 toolbox [26] is used. For GA-OPF, the number of control variable is set as 25, which consist of generator power (7 variables), voltage (7), reserve (7) and controllable reactive power compensator (4) and the number of population is set to be 100 and the iteration is 200. For HC-OPF,

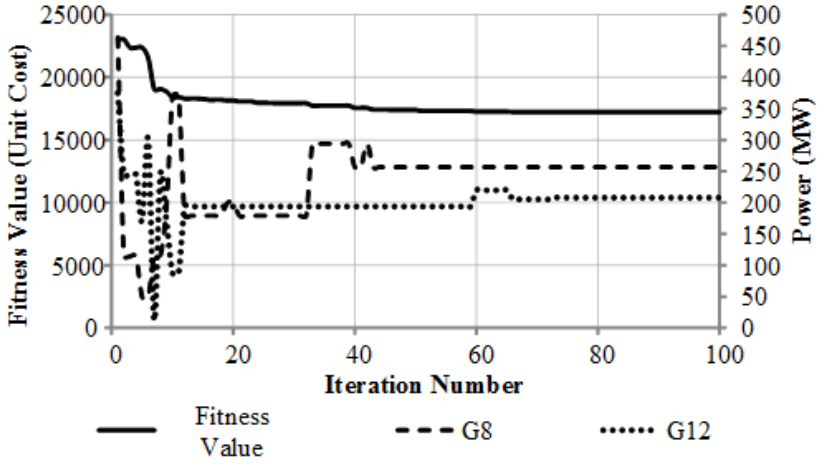

Figure 3.7 Convergence curve of GA-OPF

the number of discrete control variable is set as 11 which are controllable reactive power compensator (4) and pseudo generator limit (7) while the others variable is determine by numerical OPF. For equality purpose to GA-OPF, the number of population in HC-OPF is set to be 50 and the number of iteration is 20. Generally, HC-OPF gives 6-13 times faster than GA-OPF.

Having faster calculation time, HC-OPF will give more flexibility for handling the power system uncertainty, especially for power system analysis purpose without requiring higher computation hardware. Even if for some selection criteria there will be no feasible solution, most of the selection criteria values still obtained the feasible solution. The non–feasible solution will happened if all selected scenario were chosen. Moreover, there will be irrational if all scenarios are considered.

3.5.5. Solution Convergence

For evaluating the global optimum solution of a computation solver, the convergence speed is used as the criteria, of which for GA-OPF as presented in Figure 3.7 and for HC-OPF in Figure 3.8. HC-OPF gives faster convergence than GA-OPF. For R_{wams} = 80%, the convergence can be seen in the generation cost (objective value), generator power at buses 8 (G8) and 12 (G12). GA-OPF requires up to 60 iterations for obtaining the optimum value while HC-OPF only requires 4 iterations. In addition, more fluctuations are occurred in the iterations process before the convergence in GA-OPF as appeared on G8 and G12. Especially at G12, even after 50 iterations, the fluctuation is not stopping. It is the effect of threating some control variables as discrete value, of which the small change in the evolutionary

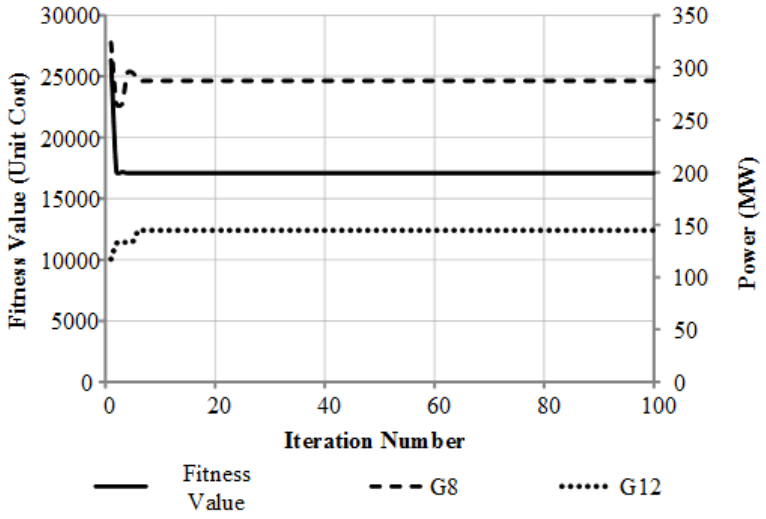

Figure 3.8 Convergence curve of HC-OPF

process affects the solution. On the other hand, generator output's convergence in HC-OPF follows the fitness value's convergence, which becomes the advantage of HC-OPF. Based on the convergence analysis, the iteration number for general case in HC-OPF (and also GA-OPF) can be approximated, which for this case was set to be 20 for HC-OPF (and 200 for GA-OPF).

3.5.6. Solution Consistency

For measuring the consistency of each solution, several sets of simulation are intentionally conducted for the similar environment criteria (same number of scenario, loading condition and proportional number of population). The consistency is important for practical power system usage. Moreover, consistency in the solution is one of the important criteria for measuring the effectiveness of the optimization solver.

In the similar environment, 8 sets simulations under the scenarios selected at R_{wams} = 88% are simulated for GA-OPF and HC-OPF. The consistency is observed in the generator output and reactive power compensator's tap. The generator outputs for 8 simulations for GA and HC-OPF are shown in Figure 3.9. From that figure, it is shown that the fluctuation of the GA-OPF result is greater than HC-OPF. On contrary, in compensator's tap setting both GA and HC-OPF have large fluctuations as shown in Figure 3.10. From those figure, it was implied that the control variable threated as continuous variable tend to have better consistency than those threated as discrete variable. From this aspect, once again, the HC-OPF shows the beneficial for

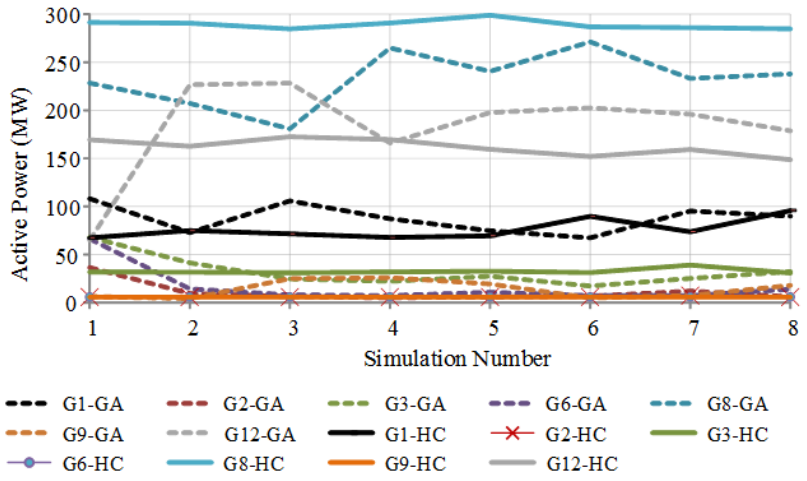

Figure 3.9 Consistency on generator power output

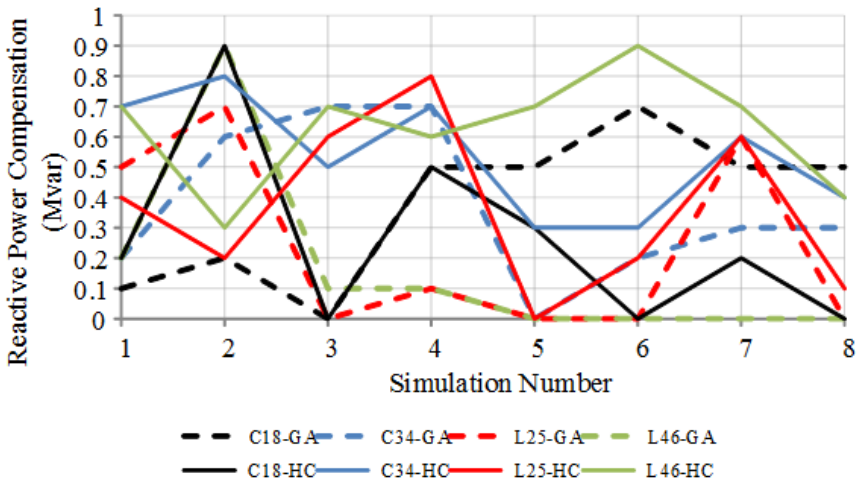

Figure 3.10 Consistency on compensator's tap

practical power system use.

IV. PREVENTIVE SCHEME STRATEGY FOR ESS SYSTEM

4.1. Role of Energy Storage System in Power System

Energy storage systems (ESS) such as batteries, flywheels, pumped hydro and compressed air energy storage have played important roles to provide the grid flexibility in power system [57]. Major purposes of ESS integrated in a large power system have been contributed on peak shaving, energy management and/or power regulation/dispatch as presented in [58]. Furthermore, application of ESS for ancillary services such as frequency support and contingency reserve are also presented in [59]. On the other hand, as the progress of RES generations integration in power systems having great uncertainties, necessity for ESS installation is growing rapidly. ESS installation could enhance the flexibility of power system operation, and as a result, the amount of RES curtailment would be minimized as presented in [60] and [61]. ESS would become one of the flexibility sources alongside the dispatchable conventional generator, RES generation and LS strategy.

Optimal operation of isolated power systems including ESS and large amount of intermittent RES were studied in [62], [63]. OPF strategy considering ESS together with optimal location and sizing of RES was discussed in [64]–[66]. Moreover, some demonstration of ESS operation are, or have been, conducted in actual power systems. For example, Tohoku Electric Power Company in Japan has installed 40 MW Li-Ion battery system in 2015 at Nishi-Sendai substation [67]. ESS is also applicable for voltage regulation (related to ancillary service) as reported in many literatures [68]–[71], which should be suitable to face the effect of the RES generation uncertainty.

In this section, the preventive scheme strategy for securing uncertainty in the power system with ESS. The preventive action strategy proposed in chapter 2 and in [27] is adjusted. The preventive strategy is modelled as SCOPF, in which operation of reactive power compensator, rescheduling of ESS operation and LS strategy are considered. Case studies in this paper reveal that the proper ESS rescheduling strategy proves the network flexibility improvement against the uncertainties, especially in heavy loading condition.

4.2. ESS Model and Role

Considering the ESS, this paper assumes battery-type inverter interfaced storage systems shown in Figure 4.1, which are capable of reactive power support.

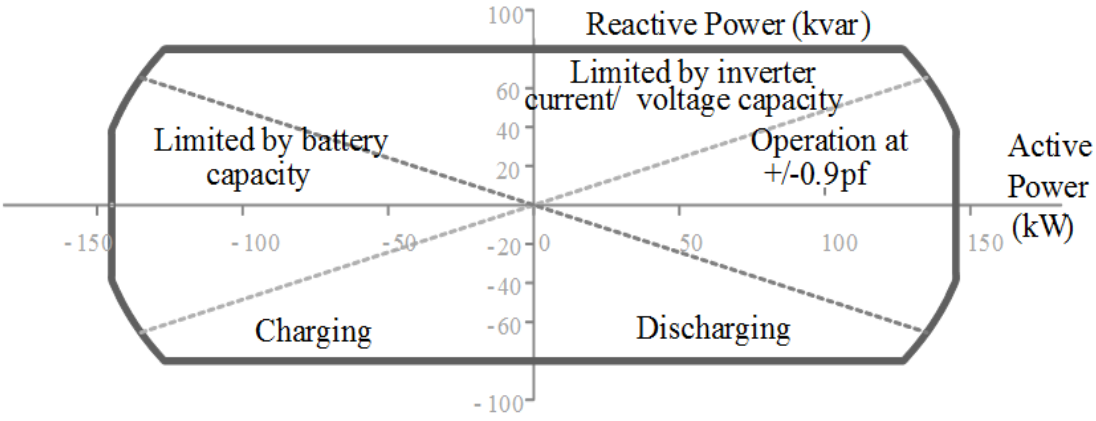

Figure 4.1 Inverter capability curve of ESS with inverter

That is, both of active and reactive powers of ESS are controllable for both directions; which can be as injection and absorption.

The optimum ESS rescheduling strategy provides more reserve active and reactive power for an existing power system. Wider operation control range for voltage and voltage stability purpose is expected having the capability for handling wider possible scenario's operating condition. Based on this control option, the flexibility of the power system operation can be increased.

4.3. Adjustment in Multistage Preventive Scheme Strategy

If the power system equipped with ESS, rescheduling of the ESS operation can be included in the preventive action scheme. For that purpose, the flow of Multistage Preventive Scheme is re-formulate as described in Figure 4.2, with the major revision is the enhancement considering the active and reactive power rescheduling of the ESS operation.

In first and second stages, generator power, reserve power and voltages, rescheduled reactive power compensator and ESS reactive power operation are decided. In these stages, the system operators are only permitted to reschedule the reactive power of the ESS operation for additional control and the active powers of the ESS are maintained as that they have been scheduled in the day-ahead unit commitment (UC) process, ELD control or other preceding controls/operations.

In second-stage process, there is a loop existed in the process since there is no guarantee that HC-OPF always has feasible solution for securing all scenario. Different from GA solver, which some solutions can still be used whether it were

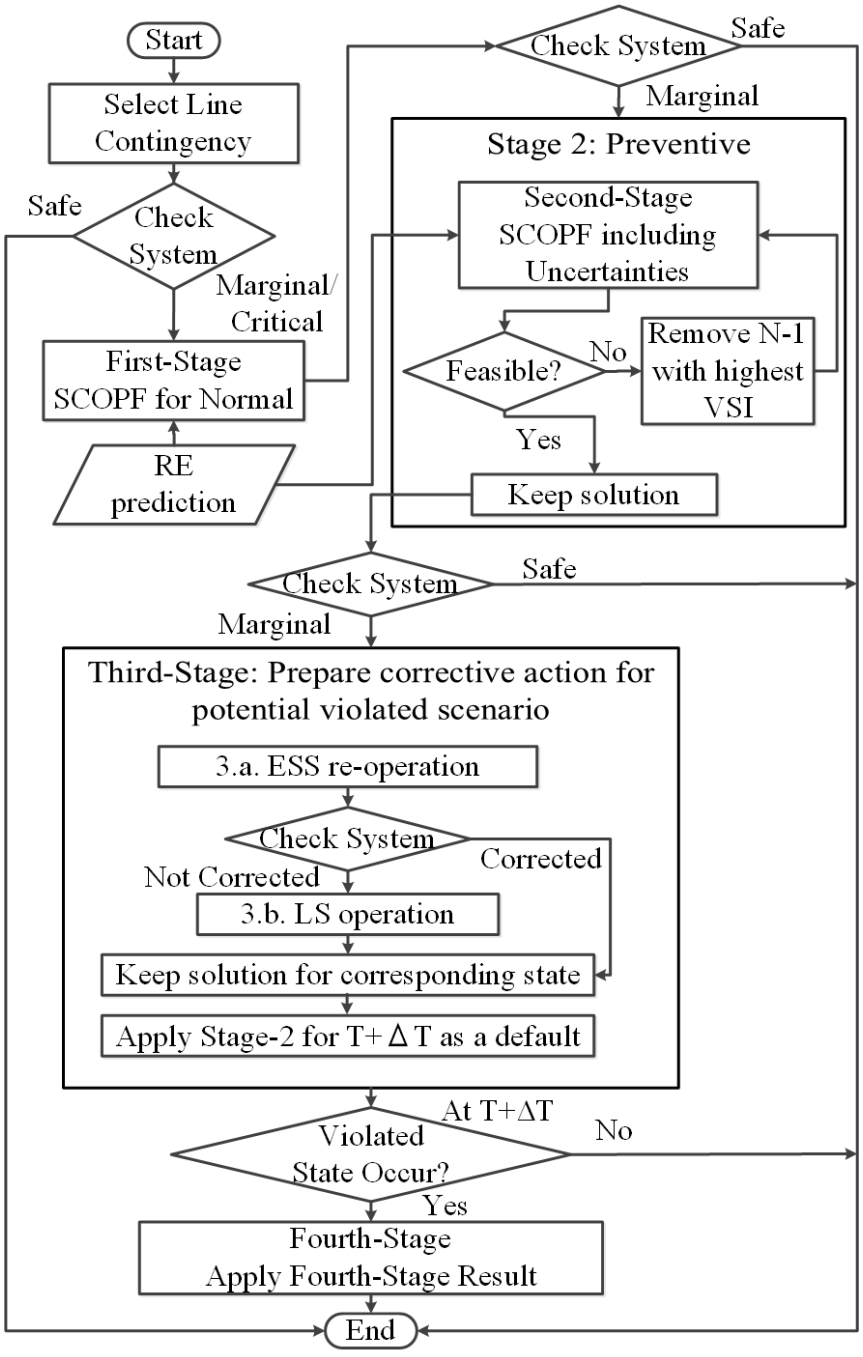

Figure 4.2 Adjustment of preventive scheme with ESS operation

infeasible, most of infeasible HC-OPF solution cannot be used. For this reason, if there is infeasible solution under specific given contingencies, a line contingency with the highest VSI will be removed for the next iterations.

Third-stage consists of two different steps. Stage-3A focuses on the

rescheduling of ESS active power operation while Stage-3B focuses on LS operation for securing the potential violated scenarios. The LS operation is set as the last control option considering the power system control option priority. The adjustments on each stage are presented in the following subsections.

4.3.1. Stochastic Security-constrained Optimal Power Flow

Basically, the Stochastic SCOPF is based on equations (2.23)-(2.36), which minimizes the generations cost considering all selected scenario. However, some modifications are required. Equations (2.30) and (2.32) are modified into equations (4.1) and (4.2), respectively.

$$Q_{Djr}^{k} = Q_{Nnr}^{k} + Q'_{Dj} - Q_{z}^{inv}, \ \ if \begin{cases} j \neq n, Q_{Nnr}^{k} = 0 \\ j \neq z, Q_{z}^{inv} = 0 \end{cases} \tag{4.1}$$

$$P_{Djr} = P'_{Dj} - P_{jr}^{RE} + C_{z0} - D_{z0}, \ for\ j = z \tag{4.2}$$

with Q_{z}^{inv}, C_{z0} and D_{z0} are ESS' reactive power, the initial charging and discharging rates of ESS's active power in bus-z. Other constraints related to the ESS operation are reactive power limit (4.3), inverter capacity limit (4.4) and grid power factor limit (4.5).

$$Q_{z,\,min}^{inv} \leq Q_{z}^{inv} \leq Q_{z,\,max}^{inv} \tag{4.3}$$

$$0 \leq \sqrt{(C_{z0} - D_{z0})^2 + Q_{z}^{inv\,2}} \leq S_{z\ max}^{inv} \tag{4.4}$$

$$PF_{z\,min} \leq PF_{z\,r}^{k} \leq PF_{z\,max} \tag{4.5}$$

with PF_{zr}^{k} is the grid power factor with $Q_{z\,min}^{inv}$, $Q_{z\,max}^{inv}$, $S_{z\,max}^{inv}$, $PF_{z\,min}$ and $PF_{z\,max}$.are the admissible limit related to ESS's reactive power, inverter and grid power factor.

4.3.2. Rescheduling of ESS Active Power Operation

Rescheduling of ESS's active power operation in stage-3A control option is used for preparing the compensation of the potential violated scenario(s). The rescheduling of active power (F_{bat}) operation should be minimized for considering the ESS' lifecycle. Rescheduling of reactive power compensator is also decided in this stage including the ESS's reactive power operation. The related formulation is described as follow.

Objective Function:

$$F_{bat} = \sum_{z=1}^{NE} |C_z - C_{z0}| + |D_z - D_{z0}| \tag{4.6}$$

Subject to:

Equations (2.25)-(2.27), (2.34)-(2.36), (2.38)-(2.39), (4.1), (4.3) and (4.5) with the additional constraints:

$$0 \leq \sqrt{(C_z - D_z)^2 + Q_z^{inv^2}} \leq S_{z\,max}^{inv} \tag{4.7}$$

$$P_{Djr} = P'_{Dj} - P_{jr}^{RE} + C_z - D_z,\ for\ j = z \tag{4.8}$$

$$SOC_z = SOC_{z0} + (\eta_z^c (C_z - C_{z0}) - (D_z - D_{z0})/\eta_z^d)\Delta T \tag{4.9}$$

$$0 \leq SOC_z \leq SOC_{z\,max} \tag{4.10}$$

with equations (4.9) and (4.10) are the equations related to the battery state of charge (SOC) and C_z, D_z, SOC_z, SOC_{z0}, η_z^c, η_z^d, ΔT, $SOC_{z\,max}$ are rescheduled charging and discharging rate, rescheduled and initial battery SOC, charging and discharging efficiency, time interval and maximum battery capacity.

4.3.3. Load Shedding Strategy

LS operation is set as the very last option with the main objective of third-stage 3B is for minimizing the total load curtailment (F_{LS}), other control variables controlled in this formulation like rescheduled ESS active and reactive power operation and reactive power of compensator tap. By this, the load curtailment amount can really be minimized as follows:

Objective Function:

$$Min\ F_{LS} = \sum_{m=1}^{NL} P_{LS_{mr}}^{k} \tag{4.11}$$

Subject to:

Equations (2.25)-(2.27), (2.34)-(2.36), (2.38), (2.39), (2.42), (2.43) (4.1), (4.3), (4.5), (4.7), (4.9) and (4.10) with the additional constraints:

$$P_{Djr} = P'_{Dj} - P_{LSmr}^{k} - P_{jr}^{RE} + C_z - D_z,\ for\ j = z \tag{4.12}$$

Table 4.1 Specification of installed ESS and grid limit

Battery	**Capacity (MWh)**	**Charging/ Discharging rate (-/+MW)**	**Penalty Cost Coef. (f_z)**	**Reactive Power Limit (+/-MVar)**	**Grid PF Limit**
20	300	30	200	10	0.85
34	200	20	200	10	0.85
57	250	25	200	10	0.85

4.4. Numerical Result

4.4.1. System Condition

Similar system condition as the previous chapter are used as the test system with heavy RES injection at buses 14, 18 and 56, each with 9, 12 and 7 MW (RE Expected), respectively with deviation level 40%. ESSs are installed at buses 20, 34 and 57, at where the loading condition is heavy or high capacity of RES is integrated. Charging/discharging efficiency is assumed very near to 1 and the inverter's capacity is capable to handle the maximum charging/discharging rate of active power and reactive power limit simultaneously. The battery capacity, charging/discharging rate, penalty cost coefficient, reactive power limit and grid power factor (PF) limit are presented in Table 4.1. The initial battery's SOCs are assumed at 100 MWh each for the corresponding time-slot. The initial discharging/charging rates of ESS are 5, 3 and 10 MW with "+" indicating discharging while the ESS's reactive powers are 0. LS should be avoided in the power system operation as much as possible. For this purpose, the penalty cost of the LS is determined 5 times more expensive than the penalty cost of ESS active power operation rescheduling.

Heavy loading condition is intentionally used as the basic case to show the merit of the ESS operation effect. For comparison, the control strategy at chapter 2, which is renamed as C1 control, is used as comparison with the ESS system is assumed at unity power factor and the rescheduling of ESS operation is unavailable as a control option. At buses injected with ESS, the net active power is calculated by considering the ESS active power injection with equation (2.32) is replaced by (4.2). The system with ESS power rescheduling control option is called as C2. Four case studies are considered for demonstrating the effectiveness of ESS cooperation for the security relief considering 4 lines contingency at lines 5, 19, 20 and 53 under R_{wams}= 78% selection is considered.

- Case-1 represents control capability limit of C1 with heavy loading condition which load at bus-18 becoming 114% and 117% of base case in chapter 2 and

reference [27].

- Case-2 represents the operation of Stage-3A with heavier loading condition, which load at bus-18 becoming 120% of base case. Case-2 shows the advantage of the ESS's reactive power operation.
- Case-3 represents the operation of Stage-3B with extremely heavy loading condition with load at bus-18 becoming 130% of base case. Case-3 shows the advantage of rescheduling of ESS's active power operation.
- Finally, Case-4 presents the calculation time of the proposed method by comparing the different number of line contingency condition on C2.

The methods and the numerical result of this chapter have been published in reference [72].

4.4.2. Control Capability Limit without ESS operation

The loading profiles of the test system are increased so that the load at bus-18 becoming 114% and 117%, respectively. In 114%, both methods can secure against the selected scenarios under the second-stage. Generation costs for conventional generator are 16404 and 15185 unit cost, respectively. It seems that C2 has advantage in ESS's reactive power operation, the participation of ESS's reactive power is shown in the system losses reduction comparing from C1 solution so that the obtained generation cost is cheaper. In C1 control, the main scenario (non-contingency and RE Expected) results in 13.735 MW and 80.31 Mvar system losses while in C2 7.168 MW and 51.82 Mvar. This advantage is realized from the additional reactive power support from the ESS.

In 117%, only C2 can secure all combination states. C1 still remains 9 violated scenarios which one of them is presented at Figure 4.3.a. having under voltage violation. This scenario will occur when line-20 is tripped and RES produces less power than expected, which is also called as scenario 24-20. In voltage stability index (VSI_{N-1}) perspective, it is shown that C2 obtains higher VSI_{N-1} as shown in Figure 4.3.b, 0.0790 compare to 0.0769 (C1). This higher index confirms the merit of the C2 in securing voltage stability. Generation costs of C1 and C2 for the main scenario (after implementing the second-stage) are 16540 and 17476 unit cost, respectively. Higher generation cost is required by C2 for performing the effectiveness of the multi stage preventive scheme. Even if the generation cost of C1 is lower, if the violated scenario occurs, some penalty cost related to the third stage will be required. So, higher generation cost at C2 for this case can be considered as

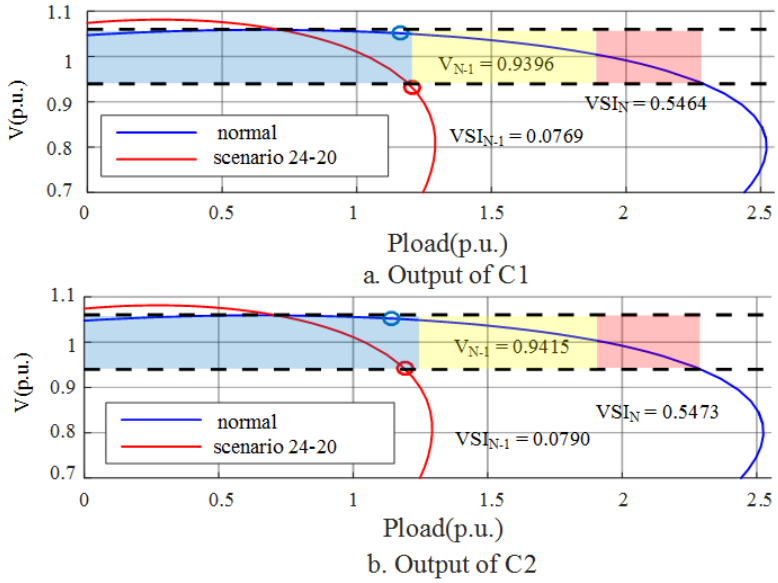

Figure 4.3 Obtained operating condition at 117% loading after second-stage

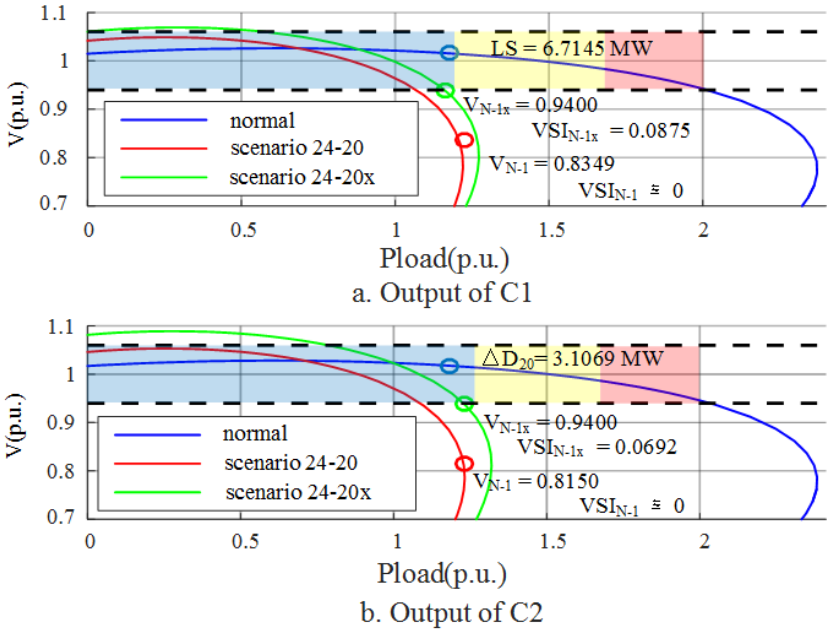

Figure 4.4 Obtained operating condition at 120% loading

the price for securing the uncertainties. Simulation result in this loading level show the limitation of C1 compared to C2 in 117% loading condition.

4.4.3. Operation of ESS's Active Power

In this section, the performance of the third-stage 3A of C2 is compared to the

third-stage 3B of C1 under the load level of bus-18 is 120%. The system load is intentionally increased so that none of C1 or C2 can secure the selected scenario under second-stage, so the third-stage should be executed for securing the potential violated scenarios. At this loading condition, stage-3A of C1 is not sufficient for securing the most severe violated scenario, while stage-3A of C2 is capable. For this purpose, the performance of C1's third-stage 3B, which do rescheduling of reactive power compensator and LS, is compared to C2's third-stage 3A, which do rescheduling of reactive power compensator and ESS's reactive power operation. The generation costs after second-stage are 15410 and 15408 unit cost for C1 and C2, respectively, and 26 violated scenarios are still remained in marginal zone.

In this load level, compensation of operating ESS's active power is needed for securing some violated scenarios in third-stage 3A of C2. One of the violated scenarios is the same as the previous subsection (4.4.3). Both C1 and C2 can secure the corresponding scenario as shown in Figure 4.4 with N-1x indexing the system obtained operating condition after corrective control of third-stage. In C1, 6.7145 MW load curtailment at bus-18 is required for securing the violated scenario. More specifically, the reactive power compensators at buses 18, 25, 34 and 46 become 0.9 (0), -0.9(-0.6), 0(0.5) and -0.3(-0.8) Mvar, respectively. Values inside brackets represent the previous values before rescheduling, with '-' indicates reactors and values represented in 1 p.u. of bus voltage. In C2, active power compensation is realized by the rescheduled ESS's active power operation with the active power change of ΔD_{20}, ΔD_{34} and ΔD_{56} become 3.1069, 0 and 0 MW, respectively. More specifically, the ESS reactive powers of Q_{20}^{inv}, Q_{34}^{inv} and Q_{56}^{inv} become 10(2.0956), 5.8267(1.6356) and -10 (-2.3649) Mvar, while reactive power compensator at buses 18, 25, 34 and 46 become 0.9 (0), -0.5(-0.9), 0 (0.2) and -0.9(-0.6) Mvar, respectively. Calculating the penalty cost for corresponding control strategy, C1 requires 6714.5 while C2 only requires 621.38 unit cost.

4.4.4. Operation of LS Strategy

In this case the overall system loading is intentionally increased so that the load level at bus-18 becomes 130%, which makes the LS strategy of third-stage from both controls should be operated as shown in Figure 4.5. The generation costs after second-stage are 15771 and 15758 unit cost while 26 and 27 violated scenarios are still remained in marginal zone for C1 and C2, respectively.

One of the violated scenarios is the same as the previous subsections (4.4.2) and (4.4.3). Both stage 3B of C1 and C2 can secure the corresponding scenario as

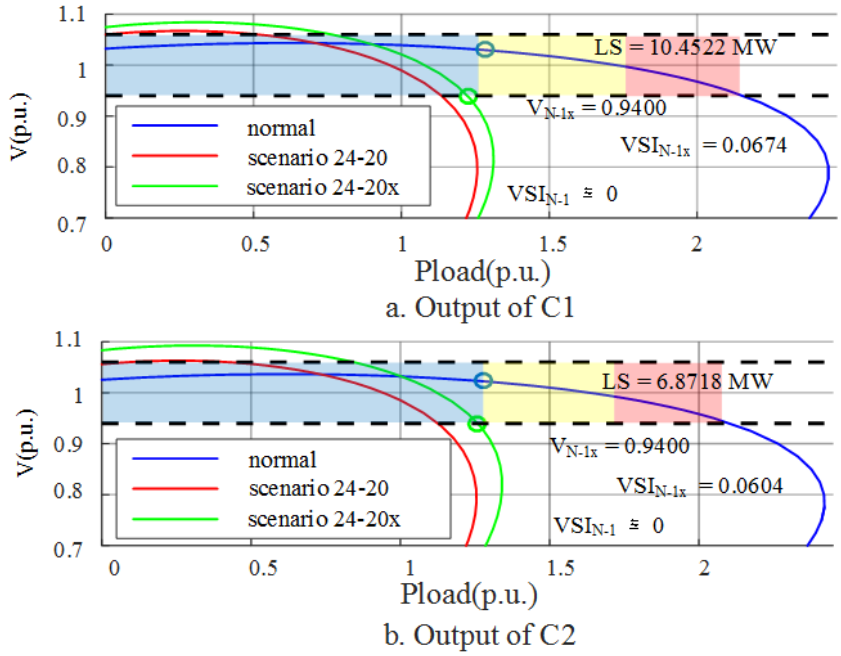

Figure 4.5 Obtained operating condition at bus-18 at 130% loading

shown in Figure 4.5 by activating the LS strategy. In C1, 10.4522 MW load curtailment at bus-18 is required for securing that scenario. More specifically, the reactive power compensators at buses 18, 25, 34 and 46 become 0.9 (0), -0.6(-0.9), 0 (0.5) and -0.3(-0.8) Mvar, respectively. In C2, active power compensation is done by 6.8718 load curtailment at bus-18 and the rescheduled ESS active power operation with the active power changes of ΔD_{20}, ΔD_{34} and ΔD_{56} become 5.2729, 0 and 0 MW, respectively. More specifically, the ESS's reactive powers of Q_{20}^{inv}, Q_{34}^{inv} and Q_{56}^{inv} become 10(4.1379), 7.774(-0.7698) and 5.893 (-3.7531) Mvar, while reactive power compensator at buses 18, 25, 34 and 46 become 0.8 (0), -0.6(-0.5), 0.9 (0.9) and -0.2(-0.2), respectively. Calculating the penalty cost, C1 requires 10152.2 while C2 only requires 7926.4 unit cost. Even if both load curtailment is required, C2 control strategy requires less load curtailment than C1 that reflects the main advantage of C2

4.4.5. Required Computation Time

HC-OPF proposed in chapter 3 and [56] is used for solving the second-stage computation problem, considered all selected scenarios, which makes the computation size larger. In the second-stage, 50 populations and 20 iterations are used.

HC-OPF, which can handle the discrete variable, is also modified for solving

Table 4.2 Required computation time

Case	Stage Number	C1 (second)	C2 (second)
Case-1	second	26.017 (83.92)	27.13 (85.92)
Cases 2 and 3	second	46.64 (156.16)	51.8 (157.95)
	third	3.82 (3B)	2.49(3A) / 3.11 (3B)

* for the computation time inside the bracket is related to $Rwams$ = 88%

the third-stage, related to rescheduling of ESS (Stage-3A) or LS strategy (Stage-3B). For the third-stage computation, 10 populations and 10 iterations are used. Simulation is conducted in MATLAB environment using 64-bit PC with 3.00 GHz CPU and 32 GB memory. MATPOWER 4.1 toolbox [26] is modified for solving the load flow analysis calculation.

Computation time comparisons are observed for C1 and C2. For further comparison more line contingency scenarios under R_{wams} = 88%, which covers 29 lines (2, 3, 5, 7, 8, 12, 14, 15, 19, 20, 23, 24, 25, 27, 30, 35, 38, 39, 47, 53, 59, 60, 61, 63, 64, 65, 71, 78, and 79), are also considered. For overall, C2 has more control variable than C1. Additional control variables are came from the ESS, active and reactive powers. Different number of line contingency scenarios, R_{wams}= 78% (5 line contingency scenarios, including non-contingency and R_{wams}= 88% (30), affect the required computation time as shown in Table 4.2.

Second-stage requires longer computation time than third-stage because of more complex problem formulation as also summarized in Table 4.2. C2 has slightly longer computation time than C1 because C2 has more number of control variables. Third-stage cannot be directly compared since the severity level of each violated scenario is different. It is also depend on the previous result of the corresponding second-stage. Generally, more severe violated scenarios will require longer computation time. Moreover, more expensive generation cost is obtained by R_{wams}= 88% which requires 16404 unit cost in second-stage compare to 15408 for R_{wams}= 78%. Considering the number of scenarios, more number of scenarios are more difficult to be solved and requires longer computation time and generation cost (in second-stage) similar to the result in reference [56]. Generally, in both R_{wams} levels, the computation times are still acceptable. Each operation interval practically was defined 30 minutes (1800 seconds) to get the most update data of RES generation. If the control strategy can be prepared within operation time-slot, multistage preventive scheme strategy can support the system.

V. DESIGN OF PMU-BASED WIDE AREA MONITORING SYSTEM

5.1. Important Aspects in PMU-based WAMS Design

A PMU has the benefit in measuring the magnitudes and phase angles of voltage and current at the same common reference. PMU records the bus voltage and line current phasors then send those data to the control center, which estimates the system state based on those data. PMUs are popular measurement device to be installed in WAMS as the measurement devices, which can realize frequency monitoring, inter area oscillation monitoring, voltage stability monitoring, etc.[5], [6], [8]–[10], and [73]. In this chapter, PMU placement method for PMU-based WAMS is discussed. Moreover, state estimation technique to increase the estimation accuracy considering measurement error is also proposed.

PMU-based WAMS is a system which completely used PMU as measurement devices neglecting the conventional measurement. For PMU-based WAMS's reliable, the system observability by PMUs should be ensured. From the economic consideration, locations and number of PMUs used in WAMS should be optimized. Various methods for determining the sufficient number of PMU for a specific power system have been investigated such as Genetic Algorithm (GA) [74], Particle Swarm Optimization (PSO) [75], Adaptive Clonal Algorithm [76], Differential Evolution [77] and Immunity Genetic Algorithm in [78]. Moreover, various numerical methods for realizing considerable computation time and accuracy have also been investigated. PMU placement technique using Integer Linear Programming method considering bus connectivity via bus incident matrix, supported by conventional measurement and zero injection buses (ZIB) effect has been investigated in [79]. PMU placement problem considering incomplete observability which admits partial non-observability at less important buses has been investigated in [80], [81]. The number of required redundant measurement for N-1 criterion considering single-line contingencies was presented in [82], [83], which warrant the system observability even if the contingency occurs. Consideration of all N-1 line contingencies requires more PMUs which affect in cost increase, therefore, references [20], [84], [85] recommended for choosing a partial of N-1 line contingencies to be considered in PMU placement problem using the occurrence probability as weighting factor. The accumulation of occurrence probability from considered line contingencies reflects the system reliability, that is, higher reliability level covers more line contingencies. The concept weighting factor can also be applied for power systems bused, which

represents the importance of bus. This concept was introduced in [86] which consider the voltage stability performance to define the importance. PMU placement which considers islanding operation as sub problem was also developed in [87].

State estimation of the PMU data is one of the important aspects in WAMS design and it has different characteristic from the conventional measurements. Some state estimation technique for PMU data has been proposed in some previous researches, which some of them has anticipated the measurement error possibility. In PMU-based WAMS which completely observable by PMU, the system state can be linearized by WLS technique as presented in [7]. Measurement may consist of errors which possibly come from noises in recording or data transmitting process. The measurement errors have risk to bias the estimation result. For anticipating the measurement error effect, bad data processing method is implemented by applying the largest normalized residual test, which cost expensive computation time [88]–[92] and modification of measurement weight [91]–[94]. Further bad data processing using two separate WLS estimations based on the conventional measurement or PMU data, which can determine the bias measurement and allow data replacements on those was proposed in [95]. Related to the limitations from the previous technique, LAV estimator technique as presented in [96], which is rearranged in linear programming problem, was developed to minimize the estimation error. In power system dynamic state, the state variables for the next time slot is estimated using the current system state and PMU data as presented in [97]. However, high estimation error still comes up as the main problem. Voltage stability margin can be estimated using the knowledge base generation and regression tree technique by offline training procedure as presented in [98]. Even the concept is simple, the estimation computation time and the estimation errors are still appeared as the problem.

In this chapter novel Optimal PMU placement (OPP) and state estimation procedure for PMU-based WAMS are proposed. A new PMU placement algorithm, which can minimize the number of PMU, considering network connectivity, ZIB, N-1 line contingency, system reliability and voltage stability level is proposed. By introducing the concept of system reliability, the proposed method can effectively reduce the number of PMU while ensuring the observability for major contingencies. Furthermore, state estimation technique considering measurement errors to increase the estimation accuracy based on time-series PMU data - LAV estimator is proposed. Proposed state estimation method can minimize the estimation error which has been proven in fast system condition, voltage instability and preventive scheme strategy

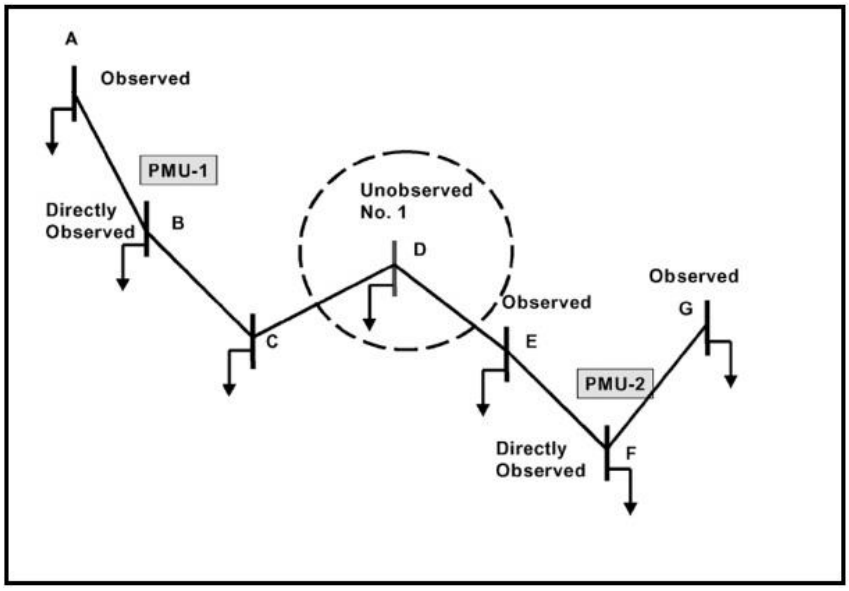

Figure 5.1 Illustration of observable and unobservable of PMU

cases.

5.2. Optimum PMU Placement Procedure

5.2.1. Concept of Network Observability

The sufficient number of the PMU should be calculated to warrant the observability of the entire power system network. The concept of observability means the location of station is observable in the power system. This concept is called with the topologically observable [99].

There are three kinds of condition of a bus/station that are directly observed, observed and unobserved. These three criteria are defined by the topological of the bus in the power system. Bus is called directly observe when the PMU is installed on that bus and the bus is called PMU bus. However, bus is called observed when the bus is stand next to the PMU bus. Bus stands next to the PMU bus is often called by immediately adjacent bus or calculated bus. The other bus condition is on the unobservable. The bus is unobservable when the bus is immediately adjacent to the PMU bus and the PMU bus as shown in Figure 5.1.

PMU placement method based on several considerations are summarized in this sub-chapter, including the proposed method which combining some considerations.

5.2.2. Network Connectivity Concept

Primary concept of PMU-based WAMS placement, which only considers network connectivity, is formulated as follow:

Objective function:

$$Minimize = \sum_{j \in I}^{NB} x_j \tag{5.1}$$

Subject to:

$$f_i = \sum\nolimits_{j \in I} a_{ij} x_j \geq 1 \tag{5.2}$$

Objective function (5.1) is total number of installed PMU. Equation (5.2) ensures the observability at all nodes with f_i is called as observability function. Variable x_j is binary variable specifying PMU installation at power system buses, 1 if PMU is installed, and otherwise 0. Variable a_{ij} is element of bus incident matrix, taking binary values 1 if buses *i* and *j* are directly connected by transmission line, otherwise 0. Note that a PMU can monitor the voltage at the installed node and current(s) flowing at the associated lines and can estimate the neighboring nodes' condition.

5.2.3. Zero Injection Bus Consideration

Existence of ZIB could realize one of the adjacent buses observable if the other remaining adjacent buses are observable as presented in [100] via the concept of Kirchhoff Current and Voltage Laws. Consideration of ZIB existence in OPP with the observability function is updated as follow.

$$\begin{gathered} f_i = \textstyle\sum_{j \in I} a_{ij} x_j + \sum_{j \in I} a_{ij} z_j y_{ij} \geq 1 \\ \sum\nolimits_{i \in I} a_{ij} y_{ij} = z_j \end{gathered} \tag{5.3}$$

The value of z_j is equal to 1 if bus-*j* is a ZIB, y_{ij} is an element of auxiliary variable matrix, and is equal to 1 if bus-*j* is a ZIB and used for ensuring the observability of bus *j*. ZIB can be connected to more than one buses. Equations (5.3) would ensure that one ZIB could only have one auxiliary variable which is decided among buses connected to each ZIB. The process has been illustrated in Figure 5.2, which shows buses 1 and 2 are indirectly observable by ZIBs 4 and 8.

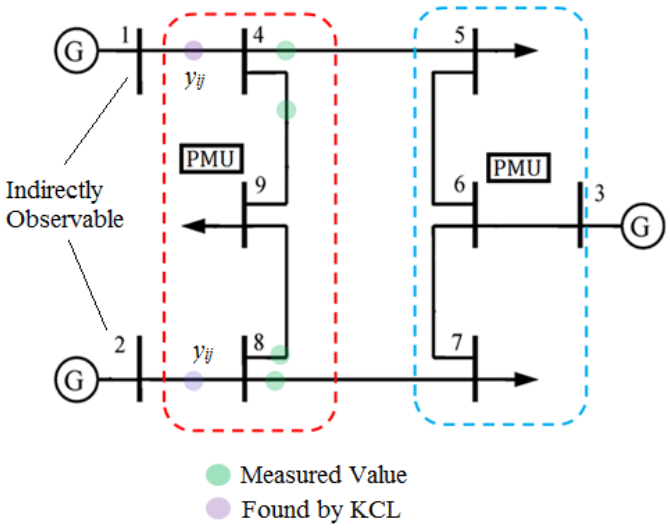

Figure 5.2 Illustration of zero injection bus existence

5.2.4. N-1 Line Contingency Consideration

For ensuring the observability of bus-*j* during the line-*k* contingency, the following equations, which add-*k* index in the formulation should be added as constraints. Equation (5.4) revises equation (5.3), with *k* indexes line-contingency and *k*=0 representing normal condition.

$$f_i^k = \sum_{j \in I} a_{ij}^k x_j + \sum_{j \in I} a_{ij}^k z_j y_{ij}^k \geq 1$$
$$\sum_{i \in I} a_{ij}^k y_{ij}^k = z_j \tag{5.4}$$

Considering all N-1 contingencies into the problem formulation requires large number of PMUs. For this reason, it would be more economical for considering high occurrence probability line contingency. The occurrence probability of contingency is included into the optimization problem by adding the equation (5.5) to the original objective function in (5.1).

$$-\sum_{k \in K}^{NL} A_{cs_k} C_k \tag{5.5}$$

with variable C_k is binary decision variable and equals to 1 if the contingency of line-*k* is still covered by the WAMS.

Furthermore, equations (5.6), should be added as constraint to ensure the observability of all buses, including buses connected by line-*k* and another bus adjacent to those buses, relating to the line-*k* occurrence.

$$\begin{aligned} f_{sb}^{k} &= \sum_{j\in\Omega sb} x_j + \sum_{j\in sb} y_{ij}^{k} - C_k \geq 0, k \neq 0 \\ f_{rb}^{k} &= \sum_{j\in\Omega rb} x_j + \sum_{j\in rb} y_{ij}^{k} - C_k \geq 0\,, k \neq 0 \end{aligned} \tag{5.6}$$

If the system operator determines a reliability level based on the historical data of occurrence probability, R_{cov} the following equation (5.7) should be added as a constraint.

$$\sum_{k=1}^{NL} A_{cs_k} C_k + A_{ns} \geq R_{cov} \tag{5.7}$$

5.2.5. Voltage Stability Performance Consideration

Since the occurrence probability of N-1 line contingency is relatively lower than the normal condition, load buses which have lower SBRTVSI are considered, which is also presented in chapter 2. During peak load period, those buses must be observable during line contingency occurrence. Bus observability during contingencies is defined as b_{VSIi}, as presented in (5.8) in which the value of $VSI_{threshold}$ is specified by power system operator.

$$b_{VSIi} = \begin{cases} 1, if\ SBRTVSI_i < VSI_{threshold}\ or\ k = 0 \\ 0, otherwise \end{cases} \tag{5.8}$$

Considering the voltage stability level, constraint (5.4) should be modified as follow:

$$f_i^k = \sum_{j\in I} a_{ij}^k x_j + \sum_{j\in I} a_{ij}^k\, z_j y_{ij}^k \geq b_{VSIi} \tag{5.9}$$

5.2.6. Proposed Optimal PMU Placement

The proposed OPP considers network connectivity, ZIB, N-1 line contingency occurrence, power system reliability and voltage stability performance is finally summarized as follows:

Objective Function:

$$\text{Minimize } \sum_{j\in I}^{NB} x_j - \sum_{k\in K}^{NL} Acs_k C_k \tag{5.10}$$

Subject to:

Equations (5.5)-(5.8). with two additional constraints are presented as follow:

$$f_i^k = \sum\nolimits_{j\in I} a_{ij} x_j + \sum\nolimits_{j\in I} a_{ij}\, z_j y_{ij}^k \geq b_{VSIi} \tag{5.11}$$

$$\sum\nolimits_{i\in I} a_{ij} y_{ij}^k = z_j \tag{5.12}$$

Note that the network connectivity variable a_{ij}^k in (5.9) and (5.4) is replaced with the normal state value as shown in (5.11) and (5.12) since the contingency coverage is a binary decision variable.

5.3. State Estimation Procedure

5.3.1. Least Absolute Value

If PMU data is used, the measurement function can be linearized. For that purpose, LAV has been proposed in [96] for power system based on PMU data. LAV has also been proven having better estimation accuracy than traditional WLS, especially in its robustness against measurement error.

The LAV estimation is basically formulated by minimizing the residual in eq. (5.13) with the decision variable are vector y consisting of bus voltage $\bar{x}$ and residual $\bar{r}$:

$$\begin{gathered} \min c^T y \\ s.t.\ My = \bar{z} \\ y \geq 0 \end{gathered} \tag{5.13}$$

with $\bar{x}$ and $\bar{r}$ are defined in eq.(4) with Z_n is 1 x $4n$ zero vector, O_m is 1 x $4m$ ones vector, X_a^T and X_b^T are 1 x $2n$vectors, U and V are 1 x $2m$vectors, and I_{2m} is identity matrix sized $2m$ x $2m$:

$$\begin{gathered} c^T = [Z_n \quad O_m] \\ y = [X_a \quad X_b \quad U \quad V]^T \\ M = [H \quad -H \quad I_{2m} \quad -I_{2m}] \\ \bar{x} = X_a^T - X_b^T \\ \bar{r} = U^T - V^T \end{gathered} \tag{5.14}$$

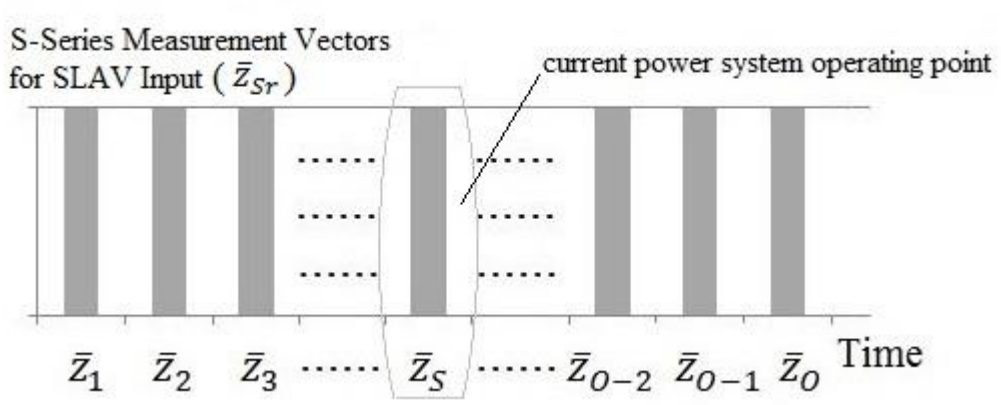

Figure 5.3 Series set PMUs data in 1 second measurement

Location \ Series		Measurement Data of time slot r					
		$\bar{z}_1$	$\bar{z}_2$	$\bar{z}_3$	.....	$\bar{z}_{R-1}$	$\bar{z}_R$
Element of Measurement Data at time slot r	z_{1r}^{re}	X	X	△	....	△	△
	z_{2r}^{re}	△	△	X	....	X	△
	⋮	⋮	⋮	⋮	⋮	⋮	⋮
	$z_{m-1\,r}^{re}$	X	△	△	⋮	X	△
	z_{mr}^{re}	△	△	X		△	△
	z_{1r}^{im}	X	X	△		△	△
	z_{2r}^{im}	△	△	X		X	△
	⋮	⋮	⋮	⋮	⋮	⋮	⋮
	$z_{m-1\,r}^{im}$	X	△	△	....	X	X
	z_{mr}^{im}	△	△	X	....	△	X

△ : Healthy Measurement
X : Error Measurement

Figure 5.4 Different location of measurement error

5.3.2. Consideration of Series PMU Data

Considering the series time-slot of PMU data, some modification are needed in LAV technique for realizing the proposed state estimation procedure. Different from the conventional LAV in [96], series set of PMU data shown in Figure 5.3 is considered for increasing the number of redundant measurement. In state estimation procedure, redundant measurement has benefit in enriching the measurement data to increase the estimation accuracy. Measurement errors may exist in the different location of measurement in each time-slot as illustrated in Figure 5.4. Measurement function for considering the series time-slot is expressed in (5.15).

$$\bar{z}_S = H_S \bar{x} + \bar{r}_S y \tag{5.15}$$

with $\bar{z}_S$, $H_S, \bar{x}$ and $\bar{r}_S$ are the series data of PMU measurement represented in grey area of Figure 5.3, Jacobian matrix, state variable and measurement residual, respectively. State variable is modeled as real and imaginary part of node voltage. Furthermore, the $\bar{z}_S$ and $\bar{x}$ elements are described in (5.16).

$$\begin{gathered} \bar{z}_S{}^T = [\bar{z}_1^T \ \bar{z}_2^T \ \dots \ \bar{z}_R^T], \in \mathbb{R}^{1x2mR} \\ \bar{z}_r^T = \left[z_{1r}^{re} \ z_{2r}^{re} \ \dots \ z_{mr}^{re} \ z_{1r}^{im} \ z_{2r}^{im} \ \dots \ z_{mr}^{im}\right], \in \mathbb{R}^{1x2m}, \bar{z}_r \in \bar{z}_S \\ \bar{x}^T = \left[x_1^{re} \ x_2^{re} \ \dots \ x_n^{re} \ x_1^{im} \ x_2^{im} \ \dots \ x_n^{im}\right] \in \mathbb{R}^{1x2n} \end{gathered} \tag{5.16}$$

with $\bar{z}_r^T$ represents the measurement data of time-slot r with r, R, m and n are indexing the time-slot number, total number of time-slot in a series data, length of PMU measurement in one time-slot and number of state variables. PMU sampling rate is represented as B per second. When R series data length of PMU is considered, $R < B$ and R also denotes the current power system operating condition.

5.3.3. Series LAV Formulation

Series leverage average value (SLAV), for R series time-slot by minimizing the measurement residual is formulated in (5.17).

$$\begin{gathered} min \ \bar{c}_S{}^T \bar{y}_S \\ \text{s.t. } M_S \bar{y}_S = \bar{z}_S \\ \bar{y}_S \geq 0 \end{gathered} \tag{5.17}$$

Under PMU-based WAMS, equation (5.17) is linear and the additional variables are further described in (5.18).

$$\begin{gathered} \bar{c}_S{}^T = [Z_n \quad w_1 x O_m \quad \cdots \quad w_R x O_m], \in \mathbb{R}^{1x(4n+4mR)} \\ \bar{y}_S = [X_a \quad X_b \quad U_S \quad V_S]^T, \in \mathbb{R}^{(4n+4mR)x1} \\ M_{Sr} = [H_S \quad -H_S \quad I_{2mR} \quad -I_{2mR}], \in \mathbb{R}^{\,2mR\ x\ (4n+4mR)} \\ \bar{x} = X_a^T - X_b^T, \in \mathbb{R}^{2nx1} \\ \bar{r}_S = U_S{}^T - V_S{}^T, \in \mathbb{R}^{2mRx1} \end{gathered} \tag{5.18}$$

With Z_n is $1\,x\,4n$ zeros vector, w_r is scalar weighting factor with $w_R > w_{R-1} > \cdots > w_2 > w_1$, O_m is $1 \text{ x } 4m$ vector, U_S and V_S are $1 \text{ x } 2mR$ vectors, and I_{2mR} is $2mR \text{ x } 2mR$ identity matrix.

5.3.4. Power Injection Estimation

The estimated bus voltage in phasor form ($\bar{x}$) can be expressed in rectangular form as $\hat{V}^T = [x_1^{re} + jx_1^{im} \quad \cdots \quad x_n^{re} + jx_n^{im}]$. Modelling the network using the admittance matrix (Y_{Bus}) with $n \text{ x } n$ size, injected bus current ($\hat{I}$)and apparent power ($\hat{S}$) are estimated as shown in (5.19).

$$\begin{aligned} \hat{I} &= Y_{Bus}\hat{V} \\ \hat{S}_i^* &= \hat{V}_i^* \hat{I}_i \ , \forall \hat{S}_i \in \hat{S}, \forall \hat{I}_i \in \hat{I}, \forall \hat{V}_i \in \hat{V} \end{aligned} \tag{5.19}$$

Generation information (S_{Gi}) is needed for calculating the injected load. It

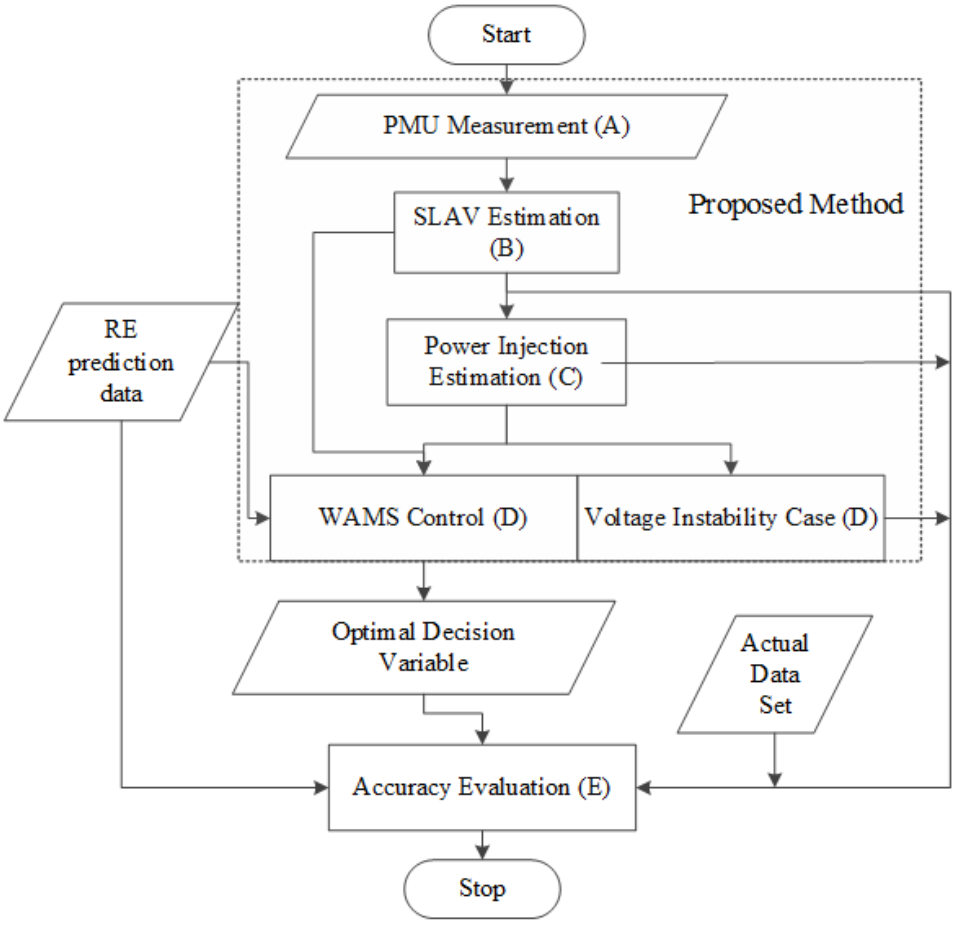

Figure 5.5 State estimation procedure for WAMS voltage stability

should be known since it was important for every power system, then the load of each bus ($\hat{S}_{Di}$) can be calculated by $\hat{S}_{Di} = \hat{S}_i - S_{Gi}$.

5.3.5. Preventive Scheme for WAMS Application

PMU-based WAMS with preventive control scheme presented in [27] was applied to show the effectiveness of the estimation method. Preventive control for securing system's voltage stability and security against uncertainties were proposed. One of procedures is second-stage scheme which is also called RBOPF, which considers line contingency and RES fluctuation as the uncertainty source. The whole state estimation procedure considering the preventive scheme is shown in Figure 5.5

The RBOPF is applied as the part of the state estimation procedure as shown in Block D, with the control variables are generator power, reserve, voltage and compensator tap while network branch (Y_{Bus}) and load information ($\hat{S}_{Di}$) are needed for input. The RBOPF is executed using the state estimation result with RES generation data prediction updated every time-slot. In addition, the voltage instability case is also considered for showing the state estimation accuracy.

5.4. Numerical Example

5.4.1. System Condition

Modified IEEE 57-bus test system, equipped with the RE generation and compensator data (the detail in chapter 2) is used to demonstrate the proposed PMU placement and SLAV. The general system condition is described in [27]. Transmission line reliability index follows the given data in [84] with the estimated occurrence probability of non-contingency scenario (A_{ns}) is 68.14% and the summation of occurrence probabilities of all N-1 line contingencies is 26.21%. Therefore, the R_{cov} should be determined within 68.14% and 94.35% (calculated from 68.14+26.21). PMU placement for different value of R_{cov} and $VSI_{threshold}$ are analyzed to show the flexibility of the placement method. In addition, prior result from reference [20] is also compared to the proposed OPP. Furthermore, the result about OPP has been published in [101].

Related to state estimation procedure, 4 line contingencies at lines 5, 19, 20 and 53 are considered. RES are installed at buses 14, 18 and 56 with each generates active powers 5, 7 and 3 MW (RE Expected), respectively with 40% of fluctuation level. From that consideration, the RBOPF should secure the system operation of 135 scenarios. The power system is completely observable by PMU-based WAMS, which the number is also determined in this section.

Three scenarios are simulated in state estimation procedure, which considers the existence of measurement error. In the first scenario, the SLAV performance is compared to the existing traditional LAV and WLS (modification in block B) in the estimation accuracy and security on RBOPF result accuracy. In second scenario, the series data length effect on the estimation accuracy is investigated. Finally, in the third scenario the SLAV performance is observed during incremental load changes (voltage instability situation). Furthermore, The result related to the PMU-based WAMS state estimation procedure has been published in [102].

The simulation is conducted under MATLAB environment using 64-bit PC with 3.4 GHz CPU and 8 GB memory. The CPLEX toolbox [103] is employed for solving the optimization problem and MATPOWER toolbox [26] is employed for solving power flow analysis.

5.4.2. Optimal PMU Placement

Table 5.1 shows the PMU location by proposed method at VSI level 1 which all buses should be observable. The solutions found by the algorithm developed in [20], which neglecting ZIB, require 27, 22, 18 and 17 PMU when the R_{cov} are 94%, 90%, 85% and 84.57%. The solutions obtained by the proposed method require less PMUs, for the same reliability level. This advantage comes up by introducing the

Table 5.1 PMU placement considering the reliability level

R_{cov}	**Number of PMU**	**Location of PMU**	**Number of Covered Contingencies**
94.35%	17	1, 4, 6, 9, 15, 20, 24, 28, 31, 32, 36, 38, 39, 41, 47, 51, 53	80
92.5%	16	1, 6, 12, 14, 15, 19, 25, 28, 31, 33, 38, 41, 51, 52, 54, 56	76
91.5%	15	1, 6, 12, 15, 19, 27, 30, 32, 38, 41, 46, 51, 52, 54, 56	75
89.5%	14	1, 6, 12, 15, 19, 27, 30, 32, 38, 41, 50, 52, 54, 56	71
88%	13	1, 6,9,15,19, 25,28, 32, 38, 41, 50, 53, 56	65
87.5%	12	1, 6, 9, 15, 19, 25, 28, 32, 38, 50, 53, 56	61
86%	11	1, 6, 9, 15, 19, 25, 28, 32, 38, 50, 56	61

Table 5.2 Priority bus based on VSI level

Level of VSI	**Number of Priority Bus**	**Priority Bus (VSI based)**
0.95	27	16, 17, 18, 19, 20, 23, 25, 27,29, 30, 31, 32, 33, 35, 38, 41, 42, 44, 47,49, 50, 51, 52, 53, 54, 56, 57
0.9	17	16, 17, 18, 19, 25, 27, 30, 31, 32 33, 35, 42, 47, 50, 53, 56, 57
0.85	11	18, 25, 30, 31, 33, 42, 47, 50, 53, 56, 57
0.8	8	18, 25, 30, 31, 33, 42, 53, 57
0.7	2	31 and 53
0.6	1	31

Table 5.3 PMU placement result under different VSI level

Level of VSI	**Number of PMU**	**Location of PMU**	**Unobservable bus**
0.95	16	1, 6, 10, 12, 19, 27, 30, 32, 33, 38, 41, 46, 50, 52, 54, 56	3, 21, 24, 36, 39, 45
0.9	15	1, 6, 9, 12, 19, 25, 28, 31, 33, 42, 44, 47, 50, 53, 56	3, 14, 23, 26, 34, 36, 39, 43
0.85	14	1, 4, 9, 19, 25, 28, 31, 33, 42, 44, 46, 50, 53, 57	23, 35, 40, 43, 48
0.75	13	1, 4, 9, 19, 25, 28, 31, 33, 44, 46, 50, 53, 56	23, 35, 43
0.7	12	1, 4, 9, 20, 28, 30, 32, 45, 46, 50, 53, 56	23, 35, 38, 43
0.6	11	1, 4, 13, 20, 25, 29, 32, 38, 41, 51, 54	8, 23, 27, 35, 47, 57

formulation of ZIB. Similar to the method in [20], the required number of PMUs can be reduced if the index R_{cov} is set small, since some line contingencies are neglected.

Related to VSI level effect in the calculation, different level of VSI is investigated on the proposed method. Priority buses are determined by the VSI level, which the calculation result during peak load time period is shown in Table 5.2. Number of priority bus decreases if the VSI level decreases. Priority buses, which have VSI below the determined VSI level, should be observable during non-contingency and contingency.

Table 5.3 shows the simulation result at the R_{cov} value 94.35%, which consider all of possible contingency under different VSI level. Solutions for smaller

VSI level require lesser number of PMU as shown in that table. On the other hand, there are some unobservable buses remained, which are unobservable during contingency scenario.

Practically, applying lower VSI level can also decrease the number of PMU, but there will be unobservable buses during covered contingency. Smaller value of R_{cov}, 91.5%, require smaller number of PMU by ignoring some minor contingencies, which requires 12 PMUs for VSI level 0.95 and 0.9, then 11 PMUs for VSI level 0.85, 0.8, 0.7 and 0.6, respectively. However, there are not clear correlations between the number of unobservable buses and the VSI level.

When only considers the non-contingency scenario and ZIB, the required number of PMU is 11 and located at busses 1, 4, 13, 20, 25, 29, 32, 38, 51, 54 and 56 as presented in [82]. This number is the same number as proposed method for reliability level of 91.5 % and VSI is 0.8, 0.7 and 0.6. With the minimum number of PMU in non-contingency scenario, it can also cover contingencies with some limitation by reconfiguring the PMU location. For state estimation procedure simulation, 17 PMUs installed on buses 1, 4, 6, 9, 15, 20, 24, 28, 31, 32, 36, 38, 39, 41, 47, 51 and 53 at the VSI level 1 and R_{cov}= 94.35% are assumed installed in PMU-based WAMS.

5.4.3. Comparison of WLS, LAV and SLAV in Estimation Accuracy

Even the measurement error of PMU is warranted very small (less than 1%) as presented in [104], the measurement error can still come from communication congestion including communication network error. The measurement error existence cannot be ignored since reliable WAMS not only required the high speed data transmission and calculation but also precise estimation accuracy.

At first scenario of state estimation procedure, the measurement errors are intentionally applied in 5 different random current line measurement locations within 6 time slots of a data ($R = 6$) while the voltage phasor measurement is assumed correct. PMU data reference ($\bar{z}_{ref}$), which has measurement error at line $I_{9\text{-}8,}$ $I_{1\text{-}15}$, $I_{6\text{-}8}$, $I_{15\text{-}1}$, $I_{6\text{-}4}$, is determined for comparison purpose to traditional LAV and WLS (which only requires 1 time-slot data. The $\bar{z}_{ref}$ is also intentionally set as a part of the series data. The measurement errors for another 5 time-slots are different from $\bar{z}_{ref}$. The measurement error is set to be 20% for representing extreme error magnitude. The weighting factor w_1, w_2, …, w_6 are 1 to 6, respectively. The mean square error (MSE) is used to measure the error between estimated and actual value is

presented in (5.20) with i is indexing the state variable and k is the number of state variable.

$$MSE = \sqrt{\frac{1}{k}\sum_{i=1}^{k}(x_i^{est} - x_i^{true})^2} \tag{5.20}$$

The effectiveness of the SLAV can be observed on voltage magnitude (Vm), angle (Va), active (P) and reactive powers (Q), which the MSEs for traditional WLS, LAV and SLAV are presented in Table 5.4. SLAV results in the lowest MSE value for every estimated variable, which becoming one of the merit of the estimation procedure.

SLAV also improving the performance of traditional LAV, of which the demerit of applying only traditional LAV is investigated compare to WLS. Even though the number of state variable error is less than WLS, some error magnitudes for several state variables are higher. Presented in Figure 5.6, some of bus voltage magnitude errors of LAV are higher than WLS, for example in buses 1, 2, 8 and 17. Similar outcomes are also happened in voltage angle, active and reactive powers estimation.

In RBOPF, the estimated variables are used as input. Considering that it may

Table 5.4 MSE comparison of WLS, LAV and SLAV

Variable	WLS	LAV	SLAV
Vm (p.u.)	0.00234	0.00229	0.00061
Va (rad)	0.00719	0.00468	0.00016
P (p.u.)	0.14761	0.14104	0.00075
Q (p.u.)	0.04796	0.05335	0.01163

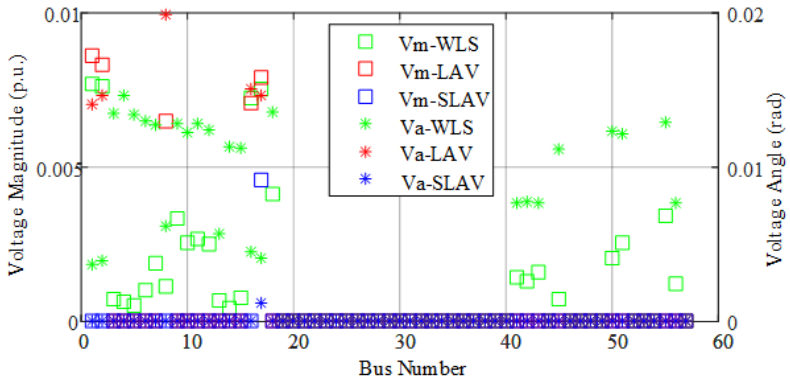

Figure 5.6 Voltage estimation error comparison

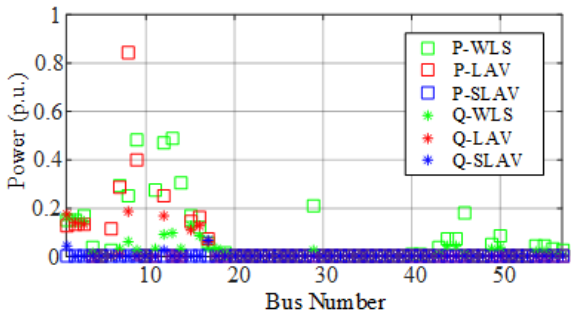

Figure 5.7 Active and reactive power estimation error

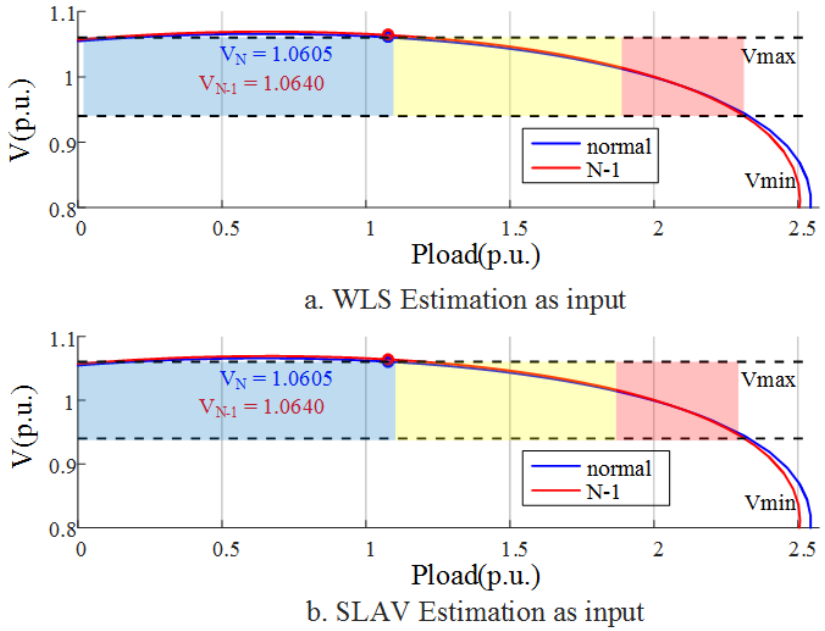

Figure 5.8 Estimation error effect in the obtained operating condition of RBOPF

consist of some error, the RBOPF control output may also be inaccurate. However, the control output should secure the actual operation condition, including the consider scenario. Using WLS, the control output cannot secure all of the scenario, 32 scenarios out of 135 will remain in violations. The violation happened at bus-18 having the voltage magnitude 1.0605 (non-contingency) and 1.0640 p.u (line-53 contingency) shown in the blue and red dot of Figure 5.8.a. On the other hand, applying LAV estimation technique, 40 violations will be remained after RBOPF calculation. The violated scenario is happened because of the measurement error, which will affect the estimation accuracy.

SLAV can deal with this matter, which can secure all scenarios after the RBOPF control, with the correction for the most severe violated scenario of WLS is

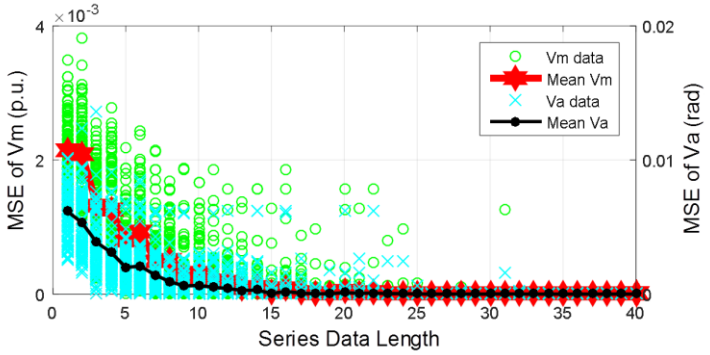

Figure 5.9 MSE of voltage magnitude and angle in various data length

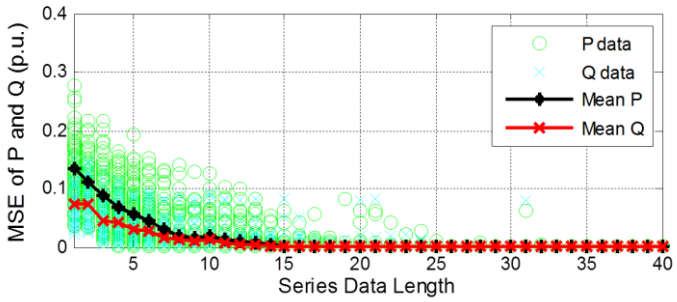

Figure 5.10 MSE of active and reactive power in various data lengths

shown in Figure 5.8 with the voltage magnitude become 1.0555 (non-contingency) and 1.0586 p.u. (line-53 contingency). SLAV can diminish the measurement error effect so that the control output difference based on estimated and real data becomes minor.

Inaccurate estimation for RBOPF input caused inaccurate control result which can result violated scenarios. Estimation accuracy improvement by SLAV has confirmed the accurate control output of RBOPF. Even the computation time for state estimation will increase due to the series data. However, for practical use, the computation time should not be a major problem because of the capability of high speed computer with memory up to 128 GB.

5.4.4. Effect of Series Data Length

Effect of series data length is investigated in the second scenario. For this purpose, measurement error is set randomly in 25 different current lines measurement locations for each time-slot. Data lengths (R) are investigated within 1 to 40 length in steady state system operation. For each data length, simulations are conducted 100 times for obtaining consistency. MSE for voltage magnitude and angle are shown in Figure 5.9, which is decreased as data length increment. Similar results are obtained in active and reactive powers MSE as shown in Figure 5.10.

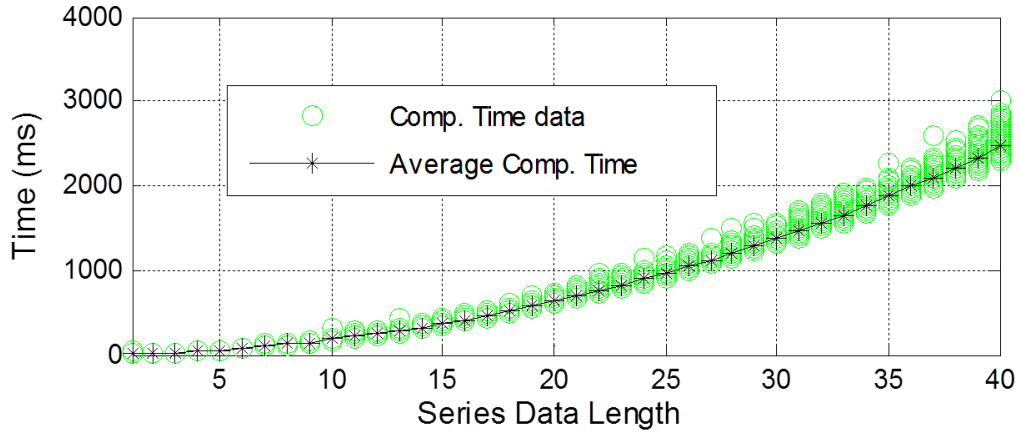

Figure 5.11 Required computation time in various data lengths

The computation time increases as data length increment as shown in Figure 5.11 following the represented problem size expressed in (5.17) and (5.18). MSE is convergence after 10-13 lengths, which requires 178.57 – 282.77 ms for completing SLAV based on the further observation in Figure 5.9 and Figure 5.10. For comparison, 1, 2, 20 and 40 series data lengths require 7.02, 13.66, 631.10 and 2483.6 ms, respectively, for completing the SLAV.

Rational series data length is necessary to be decided for realizing the estimation accuracy within considerable computation time. The exact number of series data length is not decided in this study. However, based on the observation in this sub-chapter, the MSE will convergence in a data length, which makes choosing So long series data is not necessary. The MSE convergence is also affected by measurement error number and magnitude, which practically can be analyzed from system historical data. If the measurement error level is known (or can be assumed in a certain range), the series data length for a power system can be decided using the similar analysis, which for this case requires 10-13 series data length for 20% error in randomly 25 different measurement locations.

5.4.5. Voltage Stability Monitoring Performance

SLAV capability for WAMS instability monitoring is investigated in third scenario. For this purpose, simulation is also performed under 25 randomly different current lines measurement error locations within 10 series data length with the weighting factor vector $[w_1, w_2, \cdots, w_{10}]$ is set to be 1 to 10, respectively. Load at bus-21 is intentionally increased from 0 to 1.53 p.u within 30 and 600 second,

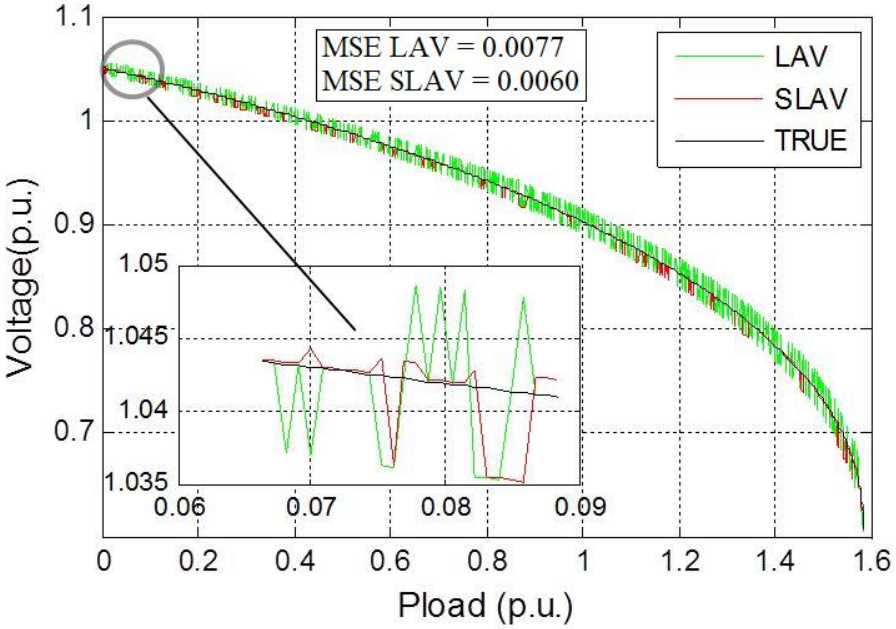

Figure 5.12 Obtained operating point for fast case

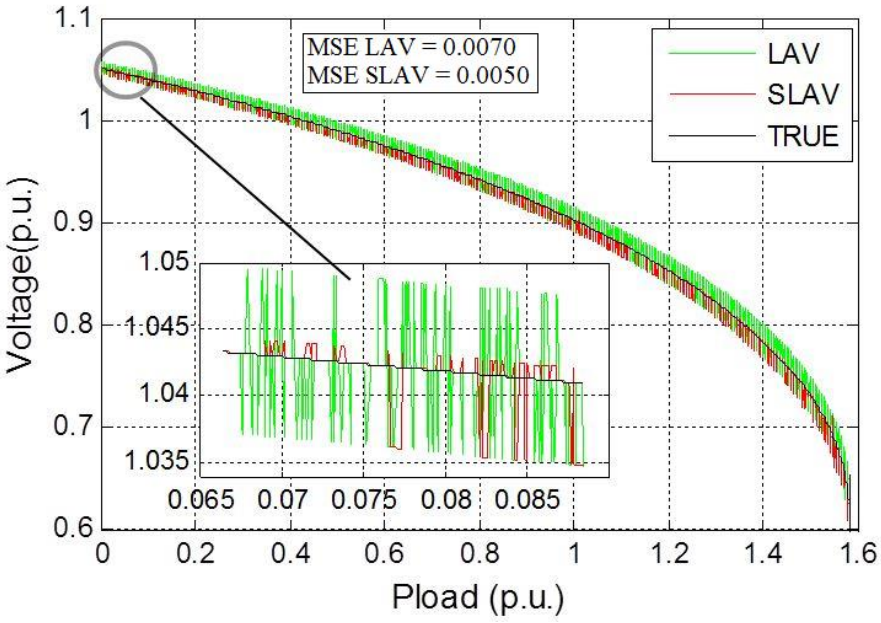

Figure 5.13 Obtained operating point for slow case

showing fast and slow cases. The PMU sampling rate is assumed 30 data per second. The accuracy of voltage instability case of SLAV is compared to traditional LAV as shown in Figure 5.12 and Figure 5.13. Even if the measurement error is high, both LAV and SLAV can still represent the voltage instability occurrence. However, the accuracy level between SLAV and LAV are different. SLAV gives smoother result than LAV does due to the richness of the redundant data. Furthermore, slow system

condition change case has better result than the fast case, which shows that fast cases is more difficult to be monitored. For this aspect, slow or fast even will be relative to the PMU sampling rates and the speed of the estimation problem. On contrary, if the measurement errors were diminished, SLAV would has lesser estimation accuracy than LAV, which the MSE for SLAV become 0.0021 (fast) and 0.0001 (slow) while LAV nearly to 0.

Since some time-slots of series PMU data are utilized, SLAV is best for analyzing the steady state operation. Because utilizing series data is vulnerable under continues system changes, especially in fast case. However, the SLAV has provided the weighting factor to give priority for latest time slot data, which can effectively minimize the estimation error during the momentary disturbance. If the measurement error is assumed exist in the measurement process SLAV will have more benefit than the traditional LAV.

VI. DESIGN OF WAMS HYBRID

6.1. Importance of PMU-SCADA Integration

WAMS is commonly used to monitor system frequency, inter area oscillation, voltage stability and also the assessment as reported in [5], [6], [9], [10], which utilizes PMUs to warrant buses observability, to collect node voltage and line current phasors data and send those data to the control center. Among PMU measurements are synchronized and the system states are estimated in very excellence accuracy as described in the previous section. To confirm the observability, sufficient number of PMU should be installed in power system considering economic aspect, line contingency and some important buses as presented in [20], [85], [101], [105], including in the previous section.

On the other hand, SCADA system has been widely implemented at most of power system in the world and would be used for future power system due to the performance reliability and capability. Power injection, power flow and node voltage magnitude are considered in SCADA system, which called as conventional measurement. However, the SCADA system is vulnerable to the fast system change because of the slow sampling rate of those measurements. Hybridization of SCADA and PMU platform has been conducted in some previous researches for overcoming that vulnerability. A state estimation method that considered the ZIB was proposed in [106] to improve the estimation accuracy in a given number of PMU. Optimal PMU placement (OPP) in given SCADA data for fast load flow calculation was investigated in [107], however, the method was only capable for the simple network. OPP considering ZIB, contingencies and given SCADA data was investigated in [108]. However, that prior research was only considered power flow measurement and omitted injected measurement of existing SCADA.

Transformation of SCADA into WAMS system by determining the OPP in existing SCADA system subject to estimation accuracy improvement is discussed in this chapter. That system is also called as WAMS hybrid. Since the measurement consisted of SCADA and PMU, which has different capability, state estimation procedure needs to be re-evaluated. In conjunction to OPP problem, state estimation procedure, which suitable to hybrid measurement data, is also proposed.

OPP under given existing SCADA system is determined based on estimation accuracy improvement. Consideration related to selected line contingencies scenario and important buses related to voltage stability can be added as a sub-problem.

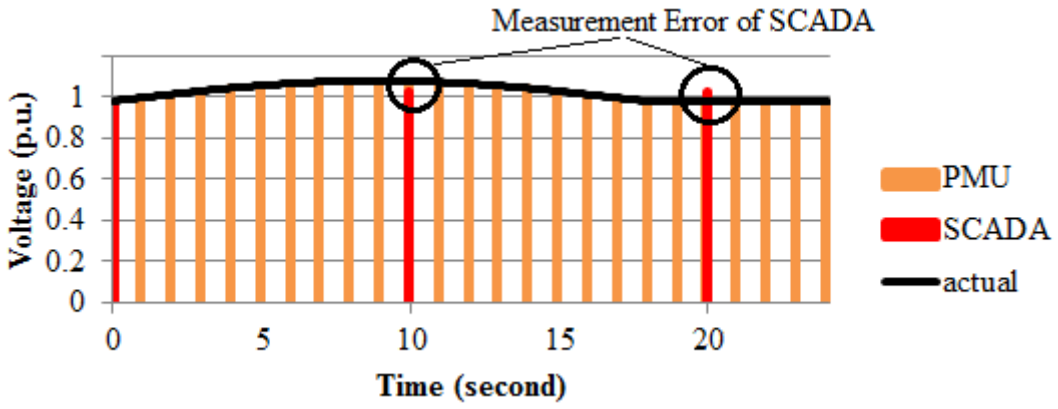

Figure 6.1 Illustration of sampling rates of PMU and SCADA

Different from the OPP for PMU-based WAMS which considers observability only by PMU, the proposed OPP assume that the observability could also be obtained by existing SCADA. Moreover, consideration on important busses makes the corresponding buses observable by PMU, including in some contingencies.

Proposed PMU-SCADA state estimation is based on WLS in [91], [93] with a modification in initial value of state variable and SCADA data's weighting factor adjustment. Modification on the weighting factor is useful for overcoming the different sampling time among SCADA data and different sampling rate between PMU and SCADA. Simulation results show that the proposed WAMS hybrid can improve the estimation accuracy if compared to SCADA-based system. In addition, WAMS hybrid requires less PMU than the fully PMU-based system.

6.2. Illustration of WAMS Hybrid

6.2.1. Consideration of Conventional SCADA Measurement

Compared to the conventional SCADA measurement, PMU has faster sampling rate, typically has 10-30 data per second while SCADA 0.1 – 1 data per second. In addition, the measurement accuracy of PMU was better than SCADA as shown in Figure 6.1. Those characteristic affect an innovative improvement on some applications such as real-time visualization, congestion management, angular, voltage, frequency stability, enhancement in state estimation, design of adaptive protection and control systems as presented in [8]. Moreover, current control actions/strategies need to be adjusted since they are not capable for a fast disturbance. It was cause by response time's difference between PMUs and SCADA as presented in [9], [10]

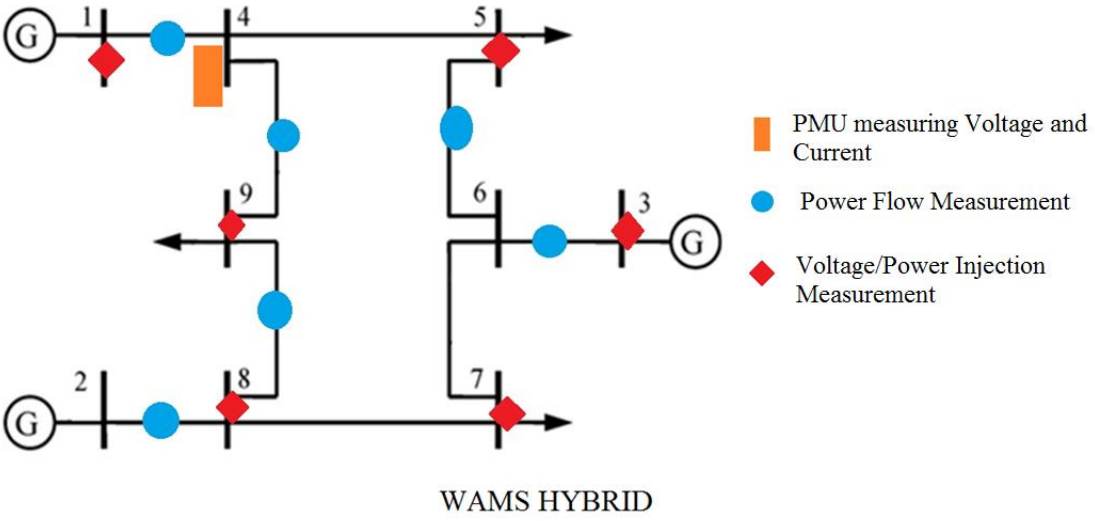

Figure 6.2 Illustration of WAMS hybrid

Considering the role of WAMS for future power system, researches related to OPP has been widely conducted. However, most of the techniques were based on the PMU observability without considering deeper in the existence of SCADA measurement. Actual research on OPP in [108] only considered on some power flow measurements, neglecting the injection measurement. In fact, voltage and power injection measurements may consist in conventional SCADA measurement as illustrated in Figure 6.2. Consideration to all type of conventional measurement becomes one of the contributions of this chapter. Another contribution of this chapter is the utilization of estimation accuracy improvement constraint rather than the network observability by PMUs. Moreover, the network observability could also be achieved by existing conventional SCADA system.

6.2.2. Coordination of PMU and SCADA Measurement

Estimation accuracy improvement by integrating a new measurement technology is developed since the actual system state of power system is remained unknown. WAMS hybrid concept proposes to keep the conventional SCADA measurements while required numbers of PMUs are needed for the sake of estimation accuracy improvement. Effective coordination is needed for WAMS hybrid due to different type of system platform.

Illustration of PMU addition in to existing SCADA system for configuring WAMS hybrid is shown in Figure 6.2, so that the system observability could be

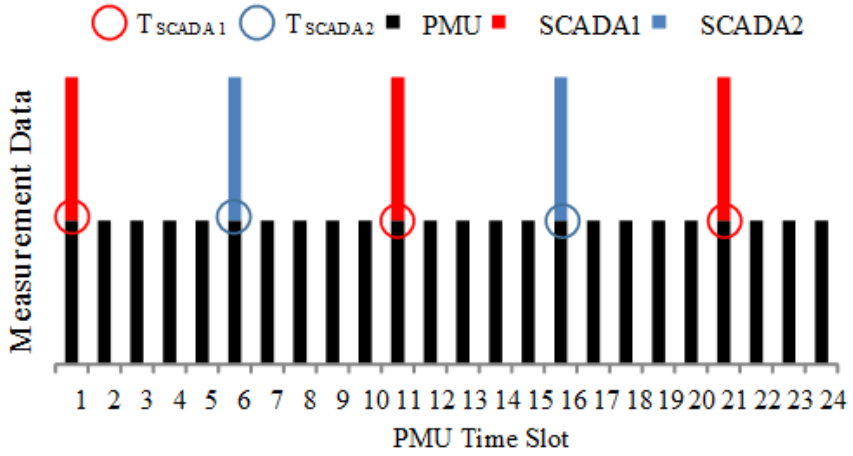

Figure 6.3 Sampling period of PMU and SCADA

increased. Furthermore, the estimation accuracy is also increased due to fast sampling rate of PMU. Since the sampling times of SCADA measurement are not uniform, SCADA data are not synchronized as PMU data are as consequent. Voltage magnitude, nodes power injection and power flow measurement of SCADA system, have the standard error deviation 0.04, 0.01 and 0.08 p.u, respectively, as presented in [7]. On contrary, voltage and current line measurement in phasor form of PMU have standard error deviation 0.00001 p.u, which extremely small compare to SCADA.

Additional PMU installation in the existing SCADA system also increases some buses observability. In example, buses with heavy loading condition could have possibility in voltage stability problem. If continuous load increment happened in the corresponding buses, the estimation accuracy will be gone down. In addition, if the system were in SCADA system platform, state estimation result may represent the actual system incorrectly. In the heavy loading condition, such estimation error might cause improper preventive control output, which can lead some violated scenarios. In WAMS hybrid, the installed PMUs will increase the estimation accuracy of the corresponding buses and the obtained system condition will be similar to actual system condition.

Coordinating the PMU and SCADA measurement is important due to the difference characteristic of sampling and recording time shown in Figure 6.3 with PMU, SCADA 1, SCADA 2, T_{SCADA1}, T_{SCADA2} and PMU represent PMU data, SCADA data and sampling time of SCADA group-1, group-2. As consequent, the existing state estimation procedures need to be re-formulated related to those different characteristics. In WAMS hybrid, the state variables are bus voltage phasor

represented in polar form similar as SCADA system while in PMU based-WAMS are represented in rectangular form. WLS state estimation procedure on PMU-based WAMS can be linearized because of the characteristic of PMU measurement function. On the other hand, WAMS hybrid requires iterative solution since the SCADA data are still used due to their non-linear measurement function. Number of iteration should be considered as important aspect since it will affect the computation length. The non-linear state estimation becomes one of the challenges in the proposed state estimation procedure.

6.3. WAMS Hybrid Configuration

6.3.1. Proposed Modified State Estimation Procedure

Measurement data in WAMS hybrid system are the combination of PMU and SCADA data, of which sampling time and rate are different. PMU sampling processes have higher accuracy than SCADA sampling process with the standard error deviation around 10^{-5} (PMU) and 10^{-3}(SCADA). The advantage of using PMU, the sampling rates are faster and among PMUs data are uniform using global positioning system technologies.

Proposed technique is developed based on classical WLS as formulated in (6.1), which has been widely used for state estimation process of SCADA or WAMS system simultaneously. For compatibility purpose between PMU and SCADA data in the state estimation procedure, the bus voltage as the state variable (x) should be expressed in polar form.

Objective Function

$$Min\ E(x) = [z - h(x)]^T W^{-1}[z - h(x)]$$

Subject to: (6.1)

$$z = h(x) + e$$

with z is a vector of measurement data divided into z_{scada} and z_{pmu} representing SCADA and PMU measurement data, respectively, h is the vector of measurement function, e is the vector of measurement error and W is the weighting matrix, of which the diagonal part corresponds to measurement vector z while the other components are zero. Optimal solution will be obtained if the first order optimally condition is reached. Because the problem is non-linear, iteration based on Gauss-Newton is needed as shown in (6.2). Termination in the iteration is converged when the $(\max|x^{k+1} - x^k|) < \varepsilon$ with ε is the iteration convergence tolerance.

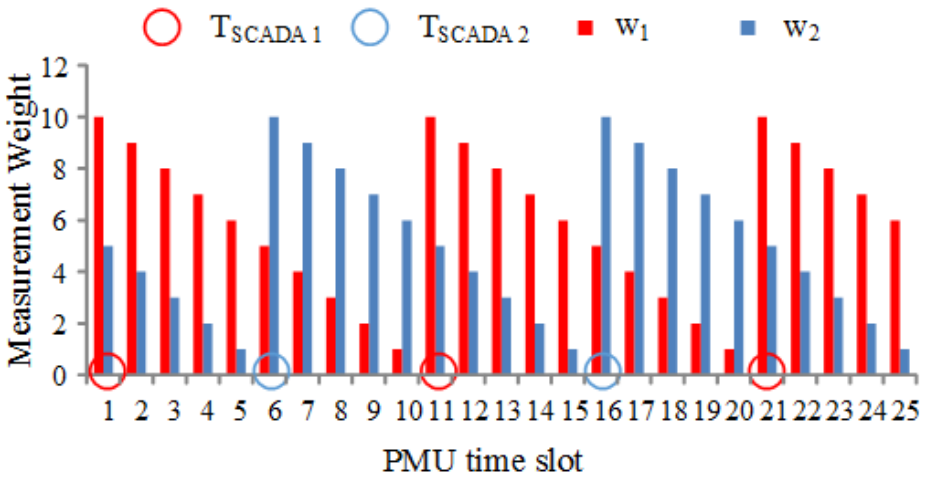

Figure 6.4 Weighting factor of SCADA data in PMU time-slot

$$E'(x^k) = \frac{\partial E(x^k)}{\partial x} = -H(x^k)^T W^{-1}[z - h(x^k)] = 0$$

$$H(x^k) = \frac{\partial h(x^k)}{\partial x} \tag{6.2}$$

$$x^{k+1} = x^k - [E''(x^k)]^{-1} E'(x^k)$$

$$E''(x^k) = \frac{\partial E'(x^k)}{\partial x} = H(x^k)^T W^{-1} H(x^k)$$

For corresponding to the fast system condition changes, modification on state estimation procedure is necessary. State estimation procedure should follow PMU sampling rates for obtaining higher estimation accuracy. The estimation result (x_{t-1}) is set as the initial value (x_{init}) at time-slot–*t*. In WLS estimation procedure, controlling the initial value of state variable is very important since it will affect the convergence speed. Setting the previous time-slot of estimation result as the initial state variables could increase the convergence speed. It will be happened since the power system operation will not change so frequently.

Practically, SCADA measurements are not uniform and scattered into some recording periods. Because of the fast system condition changes, the current SCADA measurement may be not updated so it may be different from the actual condition. For this purpose, serial weighting factor should modify corresponding to this condition as shown in Figure 6.4, which assuming two different sampling groups, with w_1 and w_2 are serial weighting factors of SCADA groups 1 and 2. SCADA data are plotted on PMU sampling rate and only updated in the circle mark (T_{SCADA1}

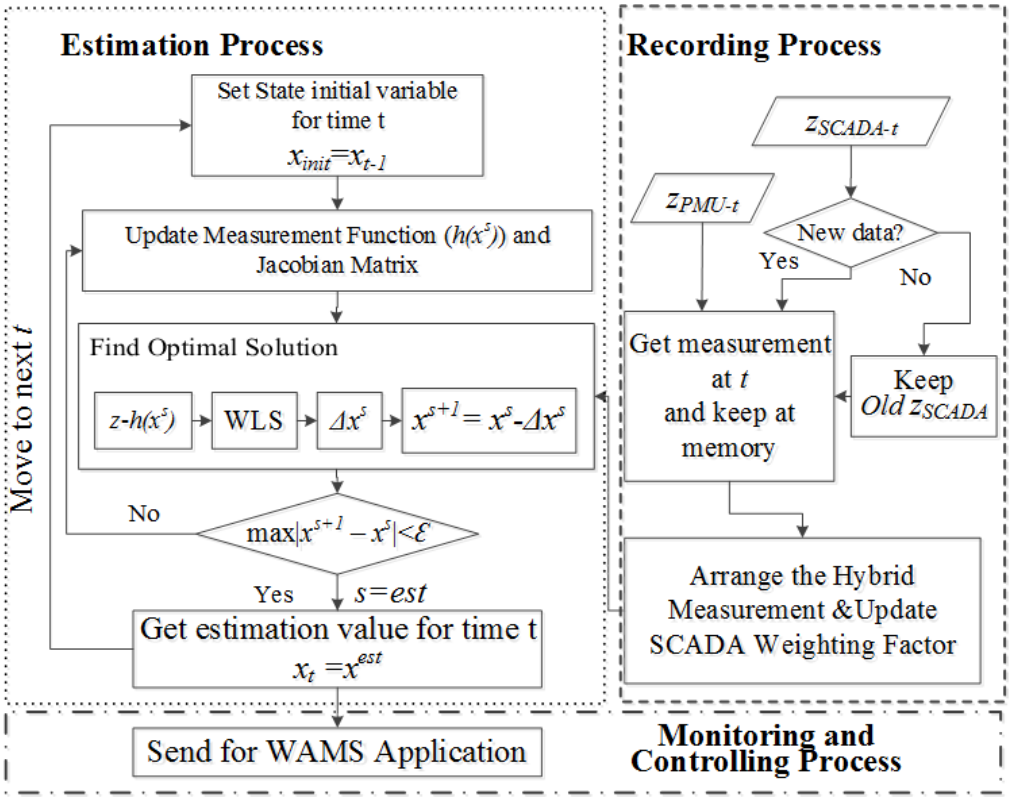

Figure 6.5 Modified state estimation procedure for WAMS hybrid

$_{or}$ T_{SCADA2}) with the color corresponding to each SCADA group as presented in that figure. Other than at the circle mark, old SCADA data are not change and might be different from the actual condition. Corresponding to this matter, the weighting factor modification will be decayed during the sampling processed. At the circle mark, the weighting factor is set at maximum value and decayed for the upcoming time-slot, then repeat periodically for the continuous sampling period.

Because of the weighting factor modification the weighting matrix term W in (6.1), w_1, w_2 and w_N are presented as the function of time as follow:

$$W(t) = [W_{PMU} \quad w_1(t)xW_{SCADA\,1} \quad \cdots \quad w_N(t)xW_{SCADA\,N}] \tag{6.3}$$

with W_{PMU} is the partial of matrix W corresponding PMU data, while $W_{SCADA\,1}$ and $W_{SCADA\,N}$ are the partial of matrix W representing of SCADA group 1 to N.

The whole state estimation procedures are described in Figure 6.5. All of the measurement function is also formulated in polar form. With t, $init$, s and est are indexing the time-slot, initial value of state variable, iteration number and obtained estimation variable. More specifically, the measurement function and

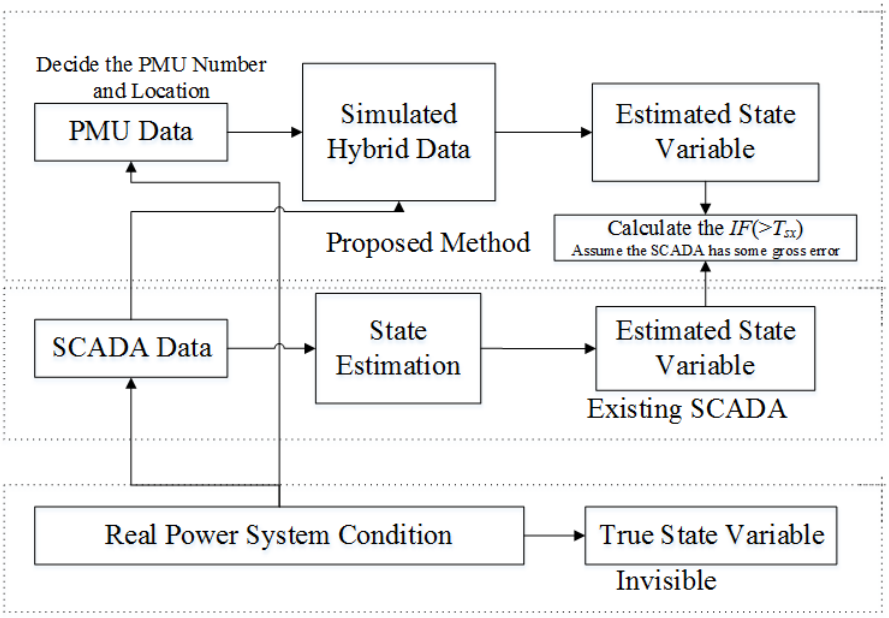

Figure 6.6 OPP procedure of WAMS hybrid design

jacobian matrix component of PMU and SCADA measurement are further described in [109]. In this procedure, iteration process is still necesarry since the problem is non-linear because of the non-linear function.

6.3.2. Proposed Optimal PMU Placement for WAMS Hybrid

Existing SCADA system, the conventional SCADA measurements are used in the state estimation procedure. However, the state estimation result still consists of gross error. PMU based-WAMS warrant better estimation accuracy than the SCADA system as proven in [7]. In this chapter, design of WAMS hybrid is proposed for combining the conventional measurement from SCADA and PMU data, with the objective to increase the system estimation accuracy.

OPP can be determined by estimation accuracy improvement after adding some PMUs in the existing SCADA system. However, the actual operating system condition is remained invisible. Therefore, this paper uses the SCADA estimated values as the reference. More specifically, by installing additional PMU, the difference between WAMS hybrid estimated value and the reference should be increased with any improvement is considered in positive direction. Therefore, it is defined as the improvement factor (IF) as follow:

$$IF = \sqrt{\frac{1}{Nz}\sum_{z=1}^{Nz}(x_z^{WAMS} - x_z^{SCADA})^2} \tag{6.4}$$

with x_z^{WAMS} and x_z^{SCADA} are WAMS hybrid system and SCADA estimation value, respectively. Nz means the number of state variables to be estimated. The state estimation procedure is based on the modified WLS technique as presented on (6.1)-(6.3). The overview of OPP procedures in WAMS hybrid is presented in Figure 6.6.

In WAMS hybrid's OPP, determination of some important nodes, which should be related to the voltage stability level, is important stage. The determination is based on SBRTVSI presented in [15] and equations (2.13)-(2.16). Buses where PMUs were installed can be directly observable by PMU and the other buses (possibly the important bus) might be observable by the adjacent position or ZIB. However, line contingency occurrence may cause the important buses unobservable. For this reason, the PMU installation procedure should consider the network observability during contingencies.

The OPP of PMU for transforming SCADA into WAMS hybrid is defined as follow:

Objective Function:

$$Min \sum_{j=1}^{NB} y_j$$

Subject to:

$$\begin{gathered} IF(y_j) > T_{SX} \\ bvsi_j^k = \begin{cases} 1, if\ VSI_j^k < VSI_{Threshold} \\ 0, for\ others \end{cases} \\ f_j^k = \sum_{i \in I} a_{ij}^k y_j \geq bvsi_j^k \end{gathered} \tag{6.5}$$

with y_j represents the status of the power system node-*j* related to PMU installation, namely, 1 if PMU is installed, otherwise 0. $IF(y_j)$ is the IF status related to WAMS hybrid bus status. T_{SX} is a threshold value of IF, which should be fulfilled after PMUs addition. T_{SX} also indicates the gross error between estimated and true values, which based on the common practice, the estimation accuracy of SCADA system is around 10^{-2}-10^{-3} p.u. The f_j^k is the observability function for node-*j* under the line-k contingency, that is 1 if the node is observable and 0 if not. Here, k = 0 represents non-contingency state. Variable a_{ij}^k is the component of the node incident matrix, which is 1 if the bus-i is connected to bus-*j* and 0 if not. Variable

$bvsi_j^k$ is the observability status value, 1 if the bus-i is important from the viewpoint of voltage stability threshold defined by $VSI_{Threshold}$, otherwise is.

6.4. Numerical Example

6.4.1. System Condition

For demonstrating the effectiveness of the proposed WAMS hybrid design, modified IEEE 57 bus test systems with RES penetration as presented in chapter 2 is used with stressed loading condition case. Observation was conducted for a certain time slot of which power outputs of RES at buses 14, 18 and 56 were predicted as 5, 7 and 3 MW, (RE Expected) respectively with the deviation level 40%. Power system condition at this time-slot is used as the input data for the OPP assuming that the standard error deviation in [7] is distributed evenly within another loading condition.

The existing SCADA system consisted of 132 measurements for making the existing system observable was used as the reference and for comparison purpose after the proposed WAMS hybrid is obtained. For the simulation, the sampling rate of SCADA is 1 data/second and PMU is 10 data/second. For showing the not-uniform characteristic of SCADA measurements, the SCADA measurements were modelled scattered into four different group periods.

Simulation was conducted under MATLAB environment using 64-bit PC with 3.4 GHz CPU and 8 GB memory. MATPOWER toolbox [26] was employed for solving power flow analysis part. For OPP calculation, GA was employed since the non-linear state estimation process is used in the calculation. The population number was set 480, each randomly was set 0 or 1 for every bus of the test system while the iteration number is 300 iterations. In the simulation, 25000 – 30000 seconds were required to complete each OPP simulation. State estimation procedure is built based on WLS technique with the convergence tolerance $\varepsilon = 10^{-4}$ and the weighting factor for each group of SCADA was decay from 10 to 1 following the different sampling time with the most updated data having larger weighting factor while the PMU data weighting factor is set 1000-100 compare to the SCADA's. For the comparison, state estimation procedure of SCADA system was executed following the procedure in Figure 6.5 with the PMU parts is omitted and time-slot-*t* is moved when the new SCADA data is updated. The result of the proposed WAMS hybrid design has been published in [110], [111].

Table 6.1 Important buses selection at different VSI level

$VSI_{Threshold}$	**Number of Important buses**	**Important buses**
0.8	3	18, 31, 33
0.9	9	18, 25, 30, 31, 33, 42, 50, 53, 57

6.4.2. Optimal PMU Placement in WAMS Hybrid

OPP in WAMS hybrid is determined by the equations (6.5). The threshold value T_{SX} is the IF to be achieved by the OPP procedure and the appropriate value of T_{SX} should be determined by the power system planner. In this OPP problem, the value of T_{SX} was set 0.0011 or 0.00155 p.u. by considering the practical gross error of the common SCADA system (no PMU installation) as reported in [7]. For verifying the effectiveness of the estimation result, MSE between SCADA system and actual operating condition is set 0.0016 similar to the common practice that the MSE around $10^{-2} – 10^{-3}$ as reported in [7].

For the planning purposes, the important buses and line contingencies to be considered should be determined before applying the OPP procedure. In the simulations, $VSI_{Threshold}$ for determining the important buses are intentionally set as 0.8 and 0.9, which greater number of $VSI_{Threshold}$ warrant more important buses as presented in Table 6.1. If $VSI_{Threshold}$ were set at 0.8, buses having VSI below this value will be considered as the important buses, which were buses 18, 31 and 33 of VSI 0.5857, 0.7670 and 0.7436, respectively.

Line contingencies scenario to be considered are selected based on the procedure in [24], which occurrence probability and the voltage stability performance are considered, by selecting R_{wams} index. Line contingency occurrence might make the important buses loose the PMU observability. The higher R_{wams} index will warrant more line contingencies for OPP procedure. For the simulation purpose, R_{wams} were set 78 and 92% which cover 4 and 40 line contingencies, respectively.

For T_{SX} = 0.00155, the optimal PMU location determined under various value of $VSI_{Threshold}$ and R_{wams} are reported in Table 6.2. In simulation case without considering line contingencies, OPP procedure results in 6 PMUs to make the important buses observable by PMU within permissible $IF (IF >$ 0.00155) for

Table 6.2 PMU location for T_{SX}= 0.00155

$VSI_{Threshold}$	R_{wams}(%)	PMU Number	PMU Location
0.8	No	6	1, 4, 23, 32, 37, 55
0.9	No	7	1, 4, 25, 32, 49, 53, 56
0.8	78	6	1, 4, 23, 32, 37, 55
0.8	92	7	1, 4, 28,30,32, 44, 56
0.9	78	8	1, 18, 22, 25, 32, 49, 52, 56
0.9	92	9	1, 4, 28, 30, 32, 44, 50, 54, 56

Table 6.3 PMU location at T_{SX} = 0.0011

$VSI_{Threshold}$	R_{wams}(%)	PMU Number	PMU Location
0.8	No	3	1, 18, 32
0.9	No	7	1, 4, 30, 32, 51, 52, 56
0.8	78	3	1, 18, 32
0.8	92	4	1, 19, 30, 33
0.9	78	7	1, 4, 30, 32, 51, 52, 56
0.9	92	8	1, 4, 30, 32, 41, 50, 54, 57

$VSI_{Threshold}$ = 0.8. When more important buses were considered by selecting $VSI_{Threshold}$ = 0.9, 7 PMUs are required. If line contingencies were considered, more PMU are required in WAMS hybrid. For $VSI_{Threshold}$ = 0.8, if R_{wams} = 78 and 92% were considered, 6 and 8 PMUs are required. In R_{wams} = 78%, PMU location is the same as the simulation case without considering any line contingencies. For this situation, OPP results have the role to increase the system estimation accuracy and maintain the observability of the important bus during contingencies. For $VSI_{Threshold}$ = 0.9, 8 and 9 PMUs are required for R_{wams}= 78 and 92%, respectively.

Since selecting the T_{SX} is one of the important step, T_{SX} = 0.0011 is chosen as the IF threshold for comparison purpose. Selecting smaller T_{SX} means that the required IF improvement in OPP is also small, which result in lesser number of PMU. In this situation, the number of required PMU at T_{SX} = 0.0011 is also smaller

compared to T_{SX} = 0.00155 as summarized in Table 6.3. In this table, for all $VSI_{Threshold}$ and R_{wams}, the number of required PMU is also smaller, especially when the $VSI_{Threshold}$ = 0.8 and R_{wams} = 78%, which only requires 3 PMUs.

Simulations are conducted in simulator so the MSE between true and obtained estimated values can be calculated for verifying the OPP procedure as expressed in equation (5.20). Assuming that those MSE could be calculated, MSE of WAMS hybrid with 3 PMUs (by T_{SX} = 0.0011) was 4.0559 x 10^{-4} p.u while that of WAMS hybrid with 6 PMUs (by T_{SX} = 0.00155) was 5.6567 x 10^{-5} p.u. at the $VSI_{Threshold}$ = 0.8 and R_{wams} = 78%. Moreover, in the $VSI_{Threshold}$ = 0.8 and R_{wams} = 92%, MSE of WAMS hybrid with 4 PMUs (T_{SX} = 0.0011) is 3.5122 x 10^{-4} p.u. while that of WAMS hybrid with 7 PMUs (T_{SX} = 0.00155) is 2.8081 x 10^{-5} p.u. At the maximum number of PMU in Table 6.2, 9 PMUs, the estimated value is 1.6297 x 10^{-6} p.u.

Generally, choosing the smaller number of T_{SX} will result in lesser number of PMU and obtain larger MSE. If very large number of T_{SX} were chosen, in example T_{SX} = 0.005, It will require infeasible solution because any selected number of PMU cannot obtained the IF greater than 0.005 p.u.

WAMS hybrid idea utilizes the conventional SCADA measurement to confirm the network observability and keep a power system having acceptable estimation accuracy. If compared to the existing OPP technique which considers N-1 line contingency, as presented in [101] and in chapter 5, which requires 17 PMUs and power flow measurement of conventional measurement [108] which requires 19 PMUs, the OPP procedure of WAMS hybrid is confirmed having more economical advantages by requiring less number of PMU, however, the estimation accuracy is less. If OPP in [101] and [108] were installed, the estimation accuracy will become 4.3618 x 10^{-10} and 3.2902 x 10^{-10} p.u.

In OPP of WAMS hybrid, one of the important procedures is to set the IF. In SCADA system, the estimation results are assumed correct even if there are some gross errors measuring from the actual value. Different from the existing OPP which considering network observability only by PMU, existing SCADA system state estimation results are used as a reference and assumed that the SCADA can also warrant buses observability, which can result in lesser number of required PMU. This aspect becomes another advantage of WAMS Hybrid. For practical use, any difference between estimated value of SCADA and WAMS hybrid (after PMU installation) are considered as estimation accuracy improvement. The estimation

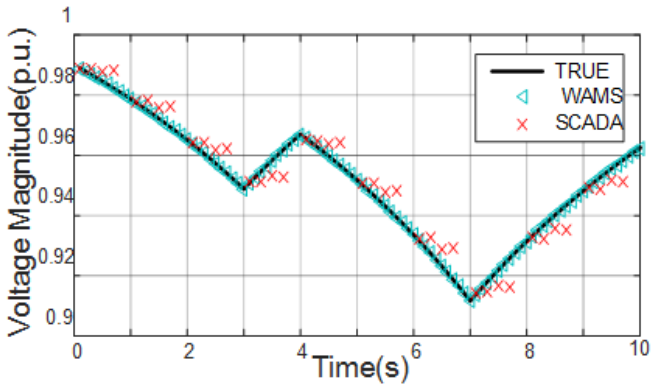

Figure 6.7 Estimation result of SCADA, WAMS Hybrid and true value

Table 6.4 Computation performance of the state estimation procedure

Aspect	**SCADA**	**WAMS Hybrid**
Number of time slot	10 x 4	100
Number of measurement	SCADA : 132 PMU : 0	SCADA : 132 PMU : 34
Average iteration	3.5	2.01
Computation time (ms)	14.786	11.16

accuracy of the power system in line contingency scenario will decrease because of the un-observability of some buses (not the important buses).

6.4.3. Load Fluctuation Case

Load fluctuation is intentionally applied at bus-15 within 10 second, which is relatively short. Simulated in SCADA system, the obtained average MSE is 0.0256 p.u. For comparison, 9 PMUs installed at buses 1, 4, 28, 30, 32, 44, 50, 54 and 56 as the result from T_{SX} = 0.00155, $VSI_{Threshold}$ = 0.9 and R_{wams}= 92% as the result of WAMS hybrid OPP procedure. Installing those PMU in the network, the estimated system accuracy increases with the average MSE of the whole power system became 0.0042 p.u and the estimated voltage at bus-15 is shown in Figure 6.7. WAMS hybrid also obtains more capable computation performance for state estimation procedure. The WAMS hybrid (with 9 PMUs) needs 2.01 iterations (11.16 ms) while the SCADA needs 3.5 iterations (14.786 ms) for each time-slot calculation as presented in Table 6.4. Faster convergence can be achieved because of the quality of measurement data. The measurement data of WAMS hybrid consist of PMU, which gives less measurement error than SCADA system.

Table 6.5 Average MSE for top-10 most severe line contingency scenario

Line Number	Bus From	Bus To	Average MSE (p.u.)	Ratio to non-contingency case
63	49	50	0.03217	7.66
39	27	28	0.01101	2.62
53	22	38	0.01088	2.59
15	1	15	0.00879	2.09
14	13	15	0.00785	1.87
28	14	15	0.00764	1.82
38	26	27	0.00756	1.80
73	40	56	0.00592	1.41
30	19	20	0.00504	1.20
18	3	15	0.00487	1.16

Modification of weighting factor in each time-slot as expressed in (6.3) has improved the system estimation accuracy, especially in fast system condition change in this case. If weighting factors are remained constant, the system estimation accuracy is decreased to 0.0056 p.u. In the load fluctuation case, some SCADA data consist of some errors because their data are not updated for every time-slot. For steady state operation, the estimation accuracy for the both method using weighting factor modification or not are still within acceptable estimation accuracy range, which result the MSE less than 10^{-5} p.u.

For contingency selection using R_{wams} = 92%, 40 line contingencies are selected and if one of those N-1 line contingency cases occur, the estimation accuracies of power system will be changed. The estimation accuracies for each contingency scenario are summarized in Table 6.5, which shows the top-10 scenario having better estimation accuracy. The worst estimation error is at line-63 contingency scenario which has 7.66 times MSE compared to the non-contingency scenario.

Estimation errors comparison of non-contingency and line-63 contingency scenarios for top-10 estimation errors buses voltage are shown in Figure 6.8, which shows that line contingency occurrence have the risk in worsen the system estimation accuracy. The worst estimation error occurs at bus-49, which is connected to bus-50 through line-63. However, the PMU location for this WAMS hybrid case is

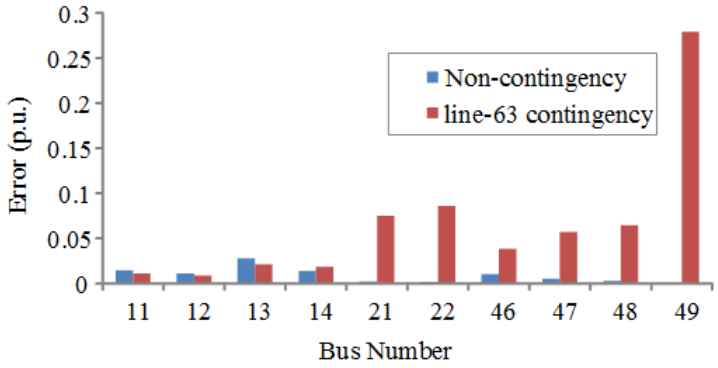

Figure 6.8 Comparison of top-10 individual estimation error of buses voltage

also configured for the observability of some important buses. As shown in this figure, the estimation error for important buses under $VSI_{Threshold}$ = 0.9 selection, which are buses 18, 25, 30, 31, 33, 42, 50, 53 and 57, were resulted below 10^{-4} p.u. even in the worst line contingency scenario.

6.4.4. Performance of Preventive Scheme Control

Preventive scheme strategy for securing uncertainty scenario has been discussed in chapter 2, of which the second-stage is called RBOPF. Considering the uncertainty, all of considered scenario should be secured using the solution strategy of RBOPF. Assuming that there is a difference between actual system operation and estimated data, the solution strategy might fail for securing all scenarios due to the estimation error, which in WAMS hybrid might be higher than in PMU-based WAMS.

State estimation result (bus voltage and load injection), network parameter and generation information are used as the input. RBOPF decides the generator voltage, power, reserve power and compensator taps for securing the voltage stability for selected scenarios. As consequent, the estimation accuracy can affect to the preciseness of those control output. For evaluating this control strategy, WAMS hybrid should be compared to PMU-based WAMS, which is assumed having higher estimation accuracy.

For the simulation, performance of WAMS hybrid with 9 PMUs is compared to PMU-based WAMS, which is called WAMS original in this chapter. In WAMS original, 17 PMUs are installed at buses 1, 4, 6, 9, 15, 20, 24, 28, 31, 32, 36, 38, 39, 41, 47, 51 and 53. That WAMS original has higher estimation accuracy than the WAMS hybrid, which based on previous section the estimation errors at steady state

Table 6.6 Effect on the RBOPF control in heavy loading cases

R_{wams}	Considered line contingency	Total number of scenario	Number of Potential Violated Scenario of WAMS	
			Hybrid	Original
78 %	5, 19, 20, 53	135	0	0
80 %	5, 8, 19, 20, 30, 53, 59, 60, 79	270	9	0

are 3.2902 x 10^{-10} (original) and 1.6297 x 10^{-6} (hybrid). RBOPF is simulated under stressed loading condition with the number of RES scenario is 27 and the numbers of line contingency scenarios are based on the selected contingency decided using R_{wams} = 78 and 80% as presented in Table 6.6.

Under R_{wams} = 78%, 135 scenarios should be considered in RBOP. In this simulation, reactive power compensators for both WAMS are intentionally set at the same values, which the inductive reactive power compensation 0.5 and 0.7 MVar injected to buses 25 and 46 and capacitive reactive power compensation 0.7 and 0.2 MVar injected to buses 18 and 34. As the result, both WAMS hybrid and original can confirm the security of selected scenarios. The most severe scenario obtained when line-20 contingency occurs, which makes bus-18 closer to the voltage stability limit. Obtained operating condition for non-contingency and line-20 contingency scenarios for both systems are plotted in Figure 6.9, which shows that the obtained operating condition are still within safe operating zone. Even if there is a difference result between two systems, it can be seen that the difference is still acceptable, assuming

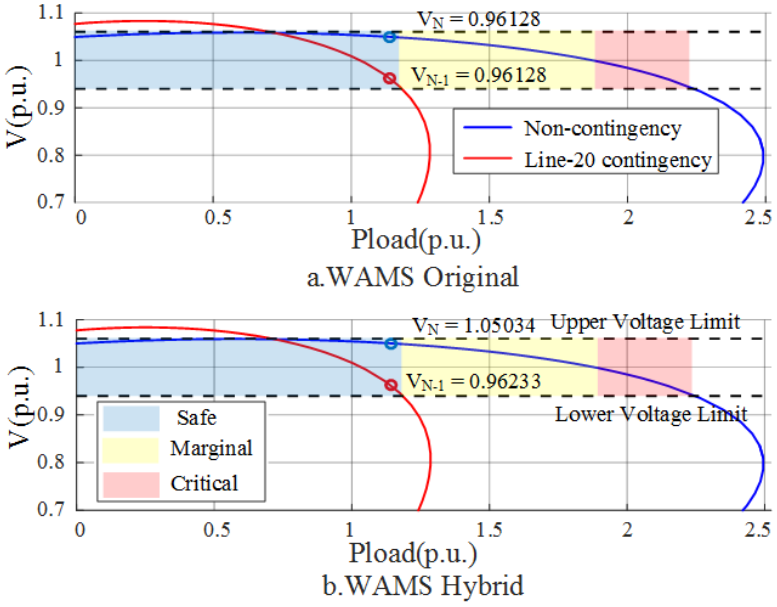

Figure 6.9 Obtained operating condition after RBOPF of WAMS hybrid system

the PMU-based WAMS as the actual value. Since all of 135 scenarios will operate securely, it can be proved that the effect of WAMS hybrid estimation error on the preventive scheme strategy is minor.

However, considering more scenarios will result in more difficult effort for realizing the preciseness of the control strategy, since any estimation error will become more sensitive to the obtained operation condition for each scenario. If R_{wams} = 80% is applied, of which 270 scenarios are selected in the RBOPF control. In the simulation result, there would be a feasible solution of RBOPF for WAMS hybrid even the RBOPF of WAMS hybrid, which means mathematically all of the scenario can be secured. However, if it was subjected to the actual operation condition, there would be 9 potential violated scenarios due to the difference between estimated variable and actual value.

If milder loading condition were applied like the loading profile in [56] as in the moderate RES cases in chapter 2, the load at bus-18 is reduced by 8.5%. In this situation, both systems can secure all selected scenarios for both R_{wams} levels. Generally, the estimation error will have more sensitive effect when the operating condition near to the boundary, especially for voltage stability. As consequent, it becomes irrational to consider so many scenarios for RBOPF.

6.4.5. Voltage Instability Monitoring

In this section, the importance on considering line contingency and VSI constraint on OPP is investigated by considering two types of WAMS hybrid design. Two type of WAMS hybrid with different installation location of PMU are considered. WAMS hybrid type-1 with 6 PMUs are installed at bus 1, 15, 20, 28, 32 and 36 as the result of neglecting the voltage stability and line contingency part of equation (6.5) in the OPP procedure. WAMS type-2 has 9 PMUs as the result in considering $VSI_{Threshold}$ = 0.9 and R_{wams} = 92% level, which PMUs are installed at buses 1, 4, 28, 30, 32, 44, 50, 54 and 56.

Load increment at bus-31 at a rate of 5 MW/second under line-44 contingency is simulated for 20 seconds as shown in Figure 6.10. The bus-31 belongs to the important bus group while line-44 connecting buses 31 and 32 belong to selected contingencies covered by R_{wams} = 92%. In type-1, bus-31 is observable by PMU installed at bus-32 while in type-2 by PMU at buses 30 and 32. If line-44 contingency happen, bus-31 in type-1 becomes unobservable by any PMU. In type-2, bus-31 is still observable by PMU at bus-30 during line-44 contingency scenario.

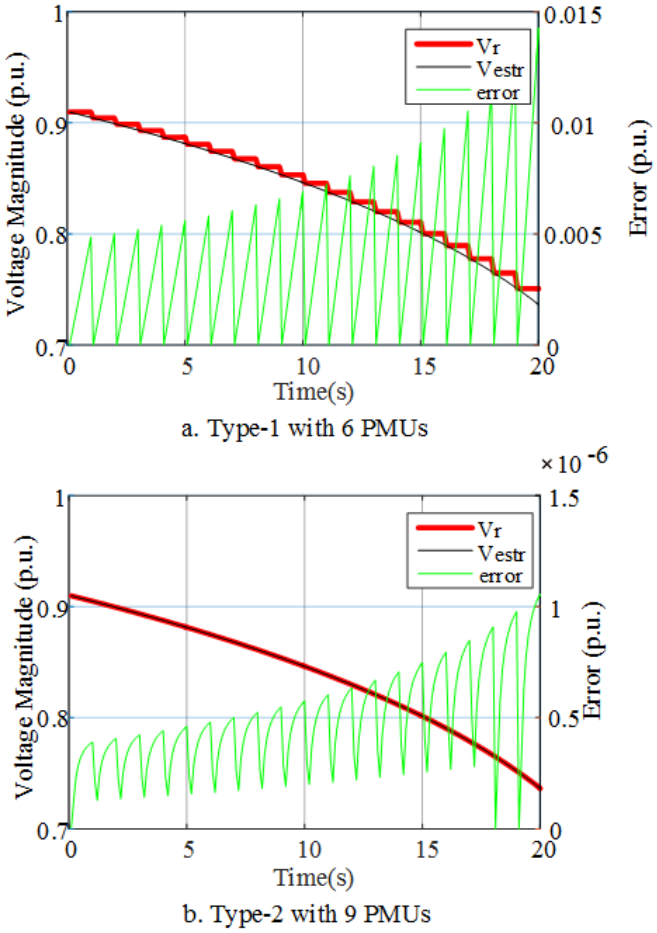

Figure 6.10 Voltage instability case of two different WAMS hybrid types

Both types of WAMS are capable in representing the voltage instability case. However, the estimation accuracy levels are different between those types. Estimation accuracies specific for bus-31 after line-44 contingency are 0.0195 and 7.0482 x 10^{-7} p.u. for types 1 and 2, respectively. After line-44 contingency, estimation accuracy of bus-31 in type-1 is decreased due to loosed observability of the corresponding bus. On contrary, type-2 could still maintain the observability for bus-31 by the PMU install at bus-30. For the whole system, the average MSEs for follows the similar trend, of which MSE becomes 0.0053 and 4.8918 x 10^{-4} p.u. For comparison purpose, the MSE are 2.7380 x 10^{-7} and 1.3475 x 10^{-7} p.u. while the average MSEs were 3.0378 x 10^{-4} and 2.8210 x 10^{-4} p.u, if the contingency is not occurred. In this situation, the estimation accuracies for both WAMS types could still be well maintained since bus-31 was still observable.

The effect of the weighting factor modification on voltage instability

Table 6.7 Effect on weighting factor modification for instability cases

Type	Contingency	MSE for the whole system (p.u.)	
		Without Modification	With Modification
1	non-contingency	3.0422×10^{-4}	3.0378×10^{-4}
2	non-contingency	2.9043×10^{-4}	2.8210×10^{-4}
1	line-44	0.0067	0.0053
2	line-44	5.0567×10^{-4}	4.8918×10^{-4}

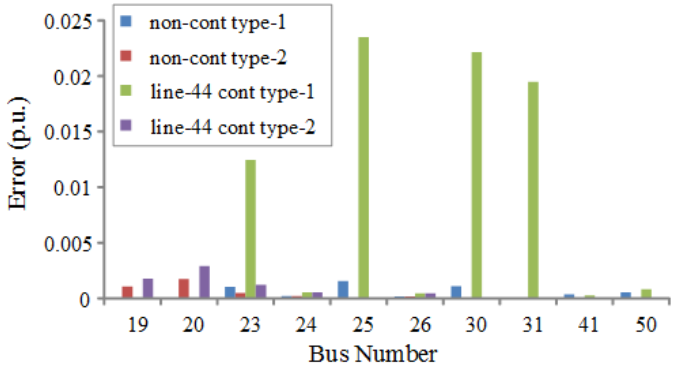

Figure 6.11 Top-10 estimation error for instability case at both WAMS types

monitoring case for both types under non-contingency and line-44 contingency are presented in Table 6.7. It is shown that the estimation accuracy becoming more accurate if modification of weighting factor is applied. Once again the merit of applying the weighting factor is shown in this section.

Top-10 of state estimation errors in buses voltage is summarized in Figure 6.11 for type-1 and type-2 under non-contingency and line-44 contingency condition. The estimation error for non-contingency and contingency condition for WAMS hybrid type-2 is relatively small comparing to contingency scenario of WAMS hybrid type-1. In WAMS hybrid type-1, the line contingency affects the estimation accuracy of some buses with the larger impact on buses 25, 30, 31, 23 and 24 with the error 0.0235, 0.0221, 0.0195, 0.0124 and 0.00052 p.u, respectively. Line-44 contingency directly affects bus-31, which indirectly connected to buses 23, 24, 25 and 30.

VII. CONCLUSION

7.1. Preventive Scheme Strategy Implementation

The multistage preventive scheme is very useful in dealing with an integrated renewable energy system since it can handle uncertainty, heavy stressed loading, and preparation to overcome the associated risks due to the uncertainty for the upcoming time-slot T+1. In addition, the simulation results show the merit of the proposed preventive scheme especially from the voltage stability and security aspects. Considering the uncertainty, the problem size can be very huge which might be difficult for the common computation solver. However, the proposed HC-OPF can estimate the required control output in reasonable computation time. In case of the power system has already installed the ESS, the multistage preventive scheme can be readjusted for rescheduling active and reactive power operation. Installing the ESS into power system can extend the network flexibility, which can increase the loading capacity of the network.

Dealing with the power system uncertainty is correlated to the huge number of scenarios. For larger power system, it will be not rational to consider all of the scenarios from the economic perspective. It has been proven that the preventive strategy requires more operation cost for more number of considered scenarios. Overestimating the uncertainty might be unnecessary since some of the scenario's occurrence probability might be very low, and might be never occurred. For that reason, the preprocessing process should be done by the power system utility to determine the important scenarios. Power system utility should select the selection criteria provided in this paper, in term of R_{wams} and R_{fluct}, which are flexible depending on the characteristics of the power system, including structure, size, and historical data.

Deregulated power systems, of which some power generators are participated, are related to this proposed method of changing generator power output. The generator power output should be scheduled one day ahead owing to the economic considerations. In this situation, agreement between the transmission system utility and the generation company to participate in the proposed method is needed in case that the generator power output needs to be changed under threats to system security. In this case, the idea is to consider the generator coefficients (a_i, b_i, and c_i) as actual bidding curves for each generator.

The proposed preventive scheme is best applied under WAMS technology

which involves several PMUs installed in the specified power system. Bus voltages and powers are required as the input for this application, in which some of them are estimated in the actual situation. Estimation results may consist of gross errors due to the measurement errors of conventional power systems. Poor estimation accuracy caused by the measurement error, especially related to conventional measurement, may result in inaccurate control result. For those reason, both PMU-based WAMS and WAMS hybrid can increase the estimation accuracy, in other word the control accuracy will also increase.

7.2. Optimal PMU Placement in WAMS Design

There are two approaches for defined the WAMS system. The first approach is WAMS based on PMU measurement, which all of the data are collected by PMUs. In this approach, network observability in some consideration is warrant by PMU. The second approach is WAMS hybrid, which combines the conventional SCADA measurement and PMU data. The main objective of this approach is to flexibly transform SCADA into WAMS systems without removing the existing measurement. The role of additional PMU is for increasing the estimation accuracy until a certain level, which could be different for a power system case by case. From the performance aspect, off course PMU-based WAMS will have better performance, which can be observed in the simulated estimation accuracy. However, from the economic perspective, WAMS hybrid will be more economical since the required number of PMU is less than PMU-based WAMS.

Design of WAMS for a power system is unique depending on the power system topography, reliability of component and possible the most severe voltage stability performance, which can be different case by case. Optimal PMU placement in the PMU-based WAMS, should consider some factors such as line contingency selection, ZIB and bus voltage stability performance. For this reason, the proposed OPP for PMU-based WAMS gives flexibility in the decision. Reliability level (R_{cov}) and voltage stability level ($VSI_{threshold}$) can flexibly select the PMU location, which will be useful for a power system utility. R_{cov} value determines a contingency to be considered in WAMS observability, which try to consider line contingency with high occurrence probability. VSI threshold value determines a priority bus, which should be observable during non-contingency and contingency condition. Buses having lower VSI than the threshold will be considered as the priority buses. If a power system want full observability within both condition, it can be obtained by selecting optimum level of R_{cov} and $VSI_{threshold}$, so that it is flexible for power system in

the placement process. For line contingency selection process, the concept of R_{cov} is different purpose from R_{wams} concept in chapter 2, which can result in different line contingency selection. In case of the line contingency occurrence is determined in pre-processing process as the approach in R_{wams}, the formulation of the proposed OPP can be modified so that equation (5.7) is not necessary.

Transformation from existing SCADA system into WAMS system has been accommodated in this work by keeping the existing measurement and adding some required PMUs. Additional PMUs will increase the estimation accuracy of the system. The number of required PMUs can also be flexible to be chosen by a power system. The number of PMU installed on the power system are depend on the determined factors as T_{SX}, $VSI_{Threshold}$ and R_{wams}. The estimation accuracy improvement is defined by the improvement factor (IF). The value of IF is depended on given the T_{SX}, which the ideal condition is as close as possible to the MSE of SCADA system. However, as the common practice the MSE of SCADA system can be assumed around 10^{-2}-10^{-3}. Furthermore, if T_{SX} is set too high, there will be no feasible solution for the PMU placement problem. A pre-processing step in planning stage is needed to find the optimal T_{SX}. Higher $VSI_{Threshold}$ will cover more important buses, which should be observable by PMU during selected line-contingency scenario, which the number is determined by R_{wams}. If both indexes are set at the maximum level, more PMUs are needed and the investment cost is also high.

How to set all of the indexes is basically depend on how the power systems warrant the risk level, which will be unique for each power system, whether for PMU-based WAMS and WAMS hybrid. Risk level management against the investment cost should be analysed beforehand. In case that maximum level of those two indexes cannot be chosen due to economical reason, the OPP procedure for both methods helps the power system utility to choose from the most important one.

7.3. Merit of the Proposed State Estimation Procedure

In WAMS design, adjustment of state estimation is necessary since PMUs, which has linear characteristic of measurement function, are employed. For that purpose, two state estimation techniques have been proposed in this work related to PMU-based WAMS and WAMS hybrid.

SLAV, which has been proposed for PMU-based WAMS, has advantage in maintaining the estimation accuracy even under some measurement error and fast

system condition change. Even though PMU has been warranted has high measurement accuracy, practically measurement error might be occurred in the recording process. SLAV is conveniently applied in PMU-based WAMS since any estimation technique is linear, in other word no iteration process required. Before applying SLAV, the length of data series should be determined by a power system utility. It will be related to the hardware capability, since employing SLAV might result longer computation time compare to WLS and traditional LAV. Another aspect to determine the series length is the estimation/measurement error of the historical data, which can be different case by case.

State estimation in WAMS hybrid is based on WLS technique, of which the measurement function of conventional/SCADA measurement could be modeled with. Since the existing conventional SCADA measurement is remained, state estimation for WAMS hybrid should be modified due to the additional PMUs. Correspond to the fast changes in system condition, different sampling rate and sampling time between PMU and SCADA, weighting factor modification is proposed to adjust the WLS, which should estimate the system variable within PMU sampling rate. Weighting factor modification has effectively increases the estimation accuracy of system variable. Furthermore, with additional PMUs, WAMS hybrid's computation time of the estimation procedure is faster than SCADA's due to the linearity of PMU data measurement function.

7.4. Possible Prospective Research

Even though some contributions have been presented in this work, some prospective work related to this theme could be elaborated related to the preventive scheme strategy, optimal PMU placement and state estimation strategy. Possible future research related to WAMS design can be done related to the proposed methods.

First, related to the preventive scheme strategy, multistage preventive scheme strategy should be work together with the existing emergency control scheme. Some of power system has defined the emergency control for mitigating the post disturbances. For example, in Remedial Action Scheme at Western Electric Coordinating Council of California, United States in [112], some action like generator excitation forcing, advanced reactive support, turbine power ramping, system separation, generator dropping or braking resistor insertion are employed for overcome over frequency, equipment overload, poor oscillation damping, voltage instability, under voltage or overvoltage problems. For a power system, multistage

preventive scheme should be adjusted to the same remedial scheme.

Second, related to OPP of WAMS hybrid, longer planning horizon considering some loading condition need to be evaluated since in this work the planning is mainly focus on heavy loading condition. When longer time horizons are considered, measurement error distribution within the data will be varied in location and magnitude. Moreover, when the uncertainties are considered, the problem sizes could become very huge, which some pre-processing steps might be required for finding the credible uncertainties scenarios and data series. Still related to the planning process, RES and ESS new installation under time horizon planning should consider the existence of multistage preventive scheme. In other words, the RES installation capacity should be evaluated. If high penetration of RES happened in a power system, the planning process might consider the RES curtailment and ESS operation.

Finally, the state estimation procedure for WAMS hybrid still needed to be developed since the iteration process is still required due to the existence of SCADA data. The estimation process of WAMS should follow the PMU sampling rate, faster estimation time is preferable. The improvement of state estimation procedure can be made by processing the SCADA data.

ACKNOWLEDGMENT

Completing the content of the dissertation thesis was very amazing task, which becoming one of my great achievement in my life. However, I want to address deep gratitude for some important people because of their contributions.

First of all, I would like to thank all the member of Power and Energy System Laboratory of Hokkaido University for the help, support and providing a wonderful and enjoyable working environment. Special thank, I want to express my deepest gratitude for my precious supervisor Prof. Hiroyuki Kita for the continuous support of study and my life in Sapporo. Your support, comment, motivation and care are significant to my successes in pursuing this degree including giving the opportunity for me to travel all around the world for presenting the progress of the research in so many conferences. I also really high appreciate Associate Prof. Ryoichi Hara for your huge contribution in my degree completion by giving so many critical comments, experience sharing and so many topics about the future power systems. Your role as my co-supervisor really became one of the crucial factor in this great achievement. I also really appreciate Assistant Prof. Eiichi Tanaka for his tremendous academic support, comment and the facilities for carrying out the research work.

I would also like to thank the rest of my PhD degree committee/referee: Prof. Hajime Igarashi and Prof. Satoshi Ogasawara for their insightful comments and suggestion. It will make me more motivated to widen my understanding of power system research from the various point of view, which will be useful for my future life.

I also want to thank the Japan International Cooperation Agency (JICA) for supporting me in pursuing Ph.D. degree in Hokkaido University by providing so many information and facilities especially for the financial support for conducting the research and insurances.

I would also thank all of my friends in Sapporo, Indonesian and International community, which has regarded me as your family. Thank you for providing me good life environment, delicious cooking and nice entertainment.

Finally, I would like to my family members (parents, brothers, and girlfriends), which have given me the energy to run again, again and again for facing the research challenges in pursuing the Ph.D. degree. It strengthens my belief that behind the great achievement, it must be the great family support.

REFERENCE

[1] V. Cutsem and Vournas, *Voltage stability of electric power systems*. Boston:Kluwer academic publisher, 1998.

[2] M. Begovic *et al.*, "Summary of System protection and voltage stability," *IEEE Trans. Power Deliv.*, vol. 10, no. 2, pp. 631–638, Apr. 1995.

[3] P. Kundur, *Power System Stability And Control by Prabha Kundur.* New York: McGraw-Hill, 1994.

[4] J. Machowski, J. W. Bialek, and J. R. Bumby, *Power system dynamics : stability and control*. Wiley, 2008.

[5] M. Begovic, D. Novosel, D. Karlsson, C. Henville, and G. Michel, "Wide-Area Protection and Emergency Control," *Proc. IEEE*, vol. 93, no. 5, pp. 876–891, May 2005.

[6] M. Zima, M. Larsson, P. Korba, C. Rehtanz, and G. Andersson, "Design Aspects for Wide-Area Monitoring and Control Systems," *Proc. IEEE*, vol. 93, no. 5, pp. 980–996, May 2005.

[7] H. A. Sangrody, M. T. Ameli, and M. R. Meshkatoddini, "The Effect of Phasor Measurement Units on the Accuracy of the Network Estimated Variables," in *2009 Second International Conference on Developments in eSystems Engineering*, 2009, pp. 66–71.

[8] V. Terzija *et al.*, "Wide-Area Monitoring, Protection, and Control of Future Electric Power Networks," *Proc. IEEE*, vol. 99, no. 1, pp. 80–93, Jan. 2011.

[9] M. M. Eissa, M. E. Masoud, and M. M. M. Elanwar, "A Novel Back Up Wide Area Protection Technique for Power Transmission Grids Using Phasor Measurement Unit," *IEEE Trans. Power Deliv.*, vol. 25, no. 1, pp. 270–278, Jan. 2010.

[10] D. Westermann and H. Sauvain, "Experience with wide area monitoring and facts control in a real time simulator," in *2005 IEEE Russia Power Tech*, 2005, pp. 1–6.

[11] M. A. Mustafa, N. S. N. Yusuf, and V. V. Terzija, "Development of wide area

monitoring and control applications in Malaysia," in *2009 IEEE Power & Energy Society General Meeting*, 2009, pp. 1–8.

[12] J. Wen, W.-H. E. Liu, P. L. Arons, and S. K. Pandey, "Evolution Pathway Towards Wide Area Monitoring and Protection—A Real-World Implementation of Centralized RAS System," *IEEE Trans. Smart Grid*, vol. 5, no. 3, pp. 1506–1513, May 2014.

[13] H. E. Brown, S. Suryanarayanan, S. A. Natarajan, and S. Rajopadhye, "Improving Reliability of Islanded Distribution Systems With Distributed Renewable Energy Resources," *IEEE Trans. Smart Grid*, vol. 3, no. 4, pp. 2028–2038, Dec. 2012.

[14] R. S. Al Abri, E. F. El-Saadany, and Y. M. Atwa, "Optimal Placement and Sizing Method to Improve the Voltage Stability Margin in a Distribution System Using Distributed Generation," *IEEE Trans. Power Syst.*, vol. 28, no. 1, pp. 326–334, Feb. 2013.

[15] Y. Gong, N. Schulz, and A. Guzman, "Synchrophasor-Based Real-Time Voltage Stability Index," in *2006 IEEE PES Power Systems Conference and Exposition*, 2006, pp. 1029–1036.

[16] A. Monticelli, S. Deckmann, A. Garcia, and B. Stott, "Real-Time External Equivalents for Static Security Analysis," *IEEE Trans. Power Appar. Syst.*, vol. PAS-98, no. 2, pp. 498–508, Mar. 1979.

[17] G. C. Ejebe, G. D. Irisarri, S. Mokhtari, O. Obadina, P. Ristanovic, and J. Tong, "Methods for contingency screening and ranking for voltage stability analysis of power systems," in *Proceedings of Power Industry Computer Applications Conference*, pp. 249–255.

[18] E. Vaahedi, C. Fuchs, W. Xu, Y. Mansour, H. Hamadanizadeh, and G. K. Morison, "Voltage stability contingency screening and ranking," *IEEE Trans. Power Syst.*, vol. 14, no. 1, pp. 256–265, 1999.

[19] S. Greene, I. Dobson, and F. L. Alvarado, "Contingency ranking for voltage collapse via sensitivities from a single nose curve," *IEEE Trans. Power Syst.*, vol. 14, no. 1, pp. 232–240, 1999.

[20] O. Gomez, G. Anders, and M. A. Rios, "Reliability-based phasor measurement

unit placement in power systems considering transmission line outages and channel limits," *IET Gener. Transm. Distrib.*, vol. 8, no. 1, pp. 121–130, Jan. 2014.

[21] R. Billinton and R. N. Allan, *Reliability Evaluation of Power Systems*, 1st ed. Boston, MA: Springer US, 1996.

[22] P. Pinson, "Uncertainties in Renewable Power Generation and Electric Loads," in *Tutorial material at Power System Computation Conference*, 2016.

[23] L. L. Freris and D. G. Infield, *Renewable energy in power systems*. John Wiley & Sons, 2008.

[24] L. M. Putranto, R. Hara, H. Kita, and E. Tanaka, "Risk-based voltage stability monitoring and preventive control using wide area monitoring system," in *2015 IEEE Eindhoven PowerTech*, 2015, pp. 1–6.

[25] M. Mitchell, *An introduction to genetic algorithms*. MIT Press, 1996.

[26] R. D. Zimmerman, C. E. Murillo-Sanchez, and R. J. Thomas, "MATPOWER: Steady-State Operations, Planning, and Analysis Tools for Power Systems Research and Education," *IEEE Trans. Power Syst.*, vol. 26, no. 1, pp. 12–19, Feb. 2011.

[27] L. M. Putranto, R. Hara, H. Kita, and E. Tanaka, "Multistage Preventive Scheme for Improving Voltage Stability and Security in an Integrated Renewable Energy System," *IEEJ Trans. Power Energy*, vol. 137, no. 1, 2017.

[28] L.-A. Dessaint, I. Kamwa, and T. Zabaiou, "Preventive control approach for voltage stability improvement using voltage stability constrained optimal power flow based on static line voltage stability indices," *IET Gener. Transm. Distrib.*, vol. 8, no. 5, pp. 924–934, May 2014.

[29] T. V. Menezes, L. C. P. da Silva, C. M. Affonso, and V. F. da Costa, "MVAR management on the pre-dispatch problem for improving voltage stability margin," *IEE Proc. - Gener. Transm. Distrib.*, vol. 151, no. 6, p. 665, 2004.

[30] F. Capitanescu *et al.*, "State-of-the-art, challenges, and future trends in security constrained optimal power flow," *Electr. Power Syst. Res.*, vol. 81, no. 8, pp. 1731–1741, 2011.

[31] R. Jabr, N. Martins, and S. Karaki, "Contingency constrained VAr planning using penalty successive conic programming," in *2012 IEEE Power and Energy Society General Meeting*, 2012, pp. 1–1.

[32] K. Karoui, H. Crisciu, A. Szekut, and M. Stubbe, "Large Scale Security Constrained Optimal Power Flow," in *Power System Computation Conference*, 2008, pp. 1–7.

[33] L. Platbrood, F. Capitanescu, C. Merckx, H. Crisciu, and L. Wehenkel, "A Generic Approach for Solving Nonlinear-Discrete Security-Constrained Optimal Power Flow Problems in Large-Scale Systems," *IEEE Trans. Power Syst.*, vol. 29, no. 3, pp. 1194–1203, May 2014.

[34] Y. Xu, Z. Y. Dong, R. Zhang, K. P. Wong, and M. Lai, "Solving Preventive-Corrective SCOPF by a Hybrid Computational Strategy," *IEEE Trans. Power Syst.*, vol. 29, no. 3, pp. 1345–1355, May 2014.

[35] W. Wood, "Spinning Reserve Constrained Static and Dynamic Economic Dispatch," *IEEE Trans. Power Appar. Syst.*, vol. PAS-101, no. 2, pp. 381–388, Feb. 1982.

[36] A. Y. Abdelaziz, S. F. Mekhamer, M. Z. Kamh, and M. A. L. Badr, "A hybrid Hopfield neural network-quadratic programming approach for dynamic economic dispatch problem," in *2008 12th International Middle-East Power System Conference*, 2008, pp. 565–570.

[37] C.-L. Chen, "Simulated annealing-based optimal wind-thermal coordination scheduling," *IET Gener. Transm. Distrib.*, vol. 1, no. 3, p. 447, 2007.

[38] J.-P. Chiou, "A variable scaling hybrid differential evolution for solving large-scale power dispatch problems," *IET Gener. Transm. Distrib.*, vol. 3, no. 2, pp. 154–163, Feb. 2009.

[39] N. Yorino, H. M. Hafiz, Y. Sasaki, and Y. Zoka, "High-Speed Real-Time Dynamic Economic Load Dispatch," *IEEE Trans. Power Syst.*, vol. 27, no. 2, pp. 621–630, May 2012.

[40] L. M. Schmitt, "Theory of genetic algorithms," *Theor. Comput. Sci.*, vol. 259, no. 1, pp. 1–61, 2001.

[41] U. Bodenhofer, "Genetic Algorithms: Theory Applications," in *Lecture Notes of*

Fuzzy Logic Laboratory Johannes Kepler University in Linz, Winter Semester, p. 2003.

[42] Zwe-Lee Gaing and Rung-Fang Chang, "Security-constrained optimal power flow by mixed-integer genetic algorithm with arithmetic operators," in *2006 IEEE Power Engineering Society General Meeting*, 2006, p. 8 pp.

[43] Ying-Hong Liao and Chuen-Tsai Sun, "An educational genetic algorithms learning tool," *IEEE Trans. Educ.*, vol. 44, no. 2, p. 20 pp., May 2001.

[44] M. Marseguerra and E. Zio, "Genetic Algorithms: Theory and Applications in the safety domain," in *Meeting on Nuclear Reaction Data and Nuclear Reactors, pt. 2*, 2000, pp. 655–696.

[45] S. Granville, "Optimal reactive dispatch through interior point methods," *IEEE Trans. Power Syst.*, vol. 9, no. 1, pp. 136–146, 1994.

[46] Yu-Chi Wu, A. S. Debs, and R. E. Marsten, "A direct nonlinear predictor-corrector primal-dual interior point algorithm for optimal power flows," *IEEE Trans. Power Syst.*, vol. 9, no. 2, pp. 876–883, May 1994.

[47] A. J. Wood, B. F. Wollenberg, and G. B. Sheblé, *Power generation, operation, and control*. .

[48] G. L. Torres and V. H. Quintana, "On a nonlinear multiple-centrality-corrections interior-point method for optimal power flow," *IEEE Trans. Power Syst.*, vol. 16, no. 2, pp. 222–228, May 2001.

[49] E. D. Castronuovo, J. M. Campagnolo, and R. Salgado, "On the application of high performance computation techniques to nonlinear interior point methods," *IEEE Trans. Power Syst.*, vol. 16, no. 3, pp. 325–331, 2001.

[50] Wei Qiu, A. J. Flueck, and Feng Tu, "A new parallel algorithm for security constrained optimal power flow with a nonlinear interior point method," in *IEEE Power Engineering Society General Meeting, 2005*, pp. 2422–2428.

[51] H. Wang, "On The Computation and Application of Multi-Period Security-Constrained Optimal Power Flow for Real-Time Electricity Market Operations," Cornell University, 2007.

[52] "Optimization Toolbox 4 Users's Guide." Incorporation, The MathWorks, 2008.

[53] "GNU General Public License." .

[54] Y. Wotao, "A MATLAB interface for Gurobi." Gurobi Mex, 2011.

[55] Siemens, "PSSE Program Application Guide v.31." Siemens Power Transmission & Distribution Inc., Power Technologies International, 2007.

[56] L. M. Putranto, R. Hara, H. Kita, and E. Tanaka, "Hybrid computation approach for SCOPF considering voltage stability and penetration of renewable enegy," in *2016 Power Systems Computation Conference (PSCC)*, 2016, pp. 1–7.

[57] M. S. Whittingham, "History, Evolution, and Future Status of Energy Storage," *Proc. IEEE*, vol. 100, no. Special Centennial Issue, pp. 1518–1534, May 2012.

[58] T. Yau, L. Walker, H. Graham, A. Gupta, and R. Raithel, "Effects of Battery Storage Devices on Power System Dispatch," *IEEE Trans. Power Appar. Syst.*, vol. PAS-100, no. 1, pp. 375–383, Jan. 1981.

[59] H. Ibrahim and A. Ilinc, "Techno-Economic Analysis of Different Energy Storage Technologies," in *Energy Storage - Technologies and Applications*, InTech, 2013.

[60] A. Ulbig and G. Andersson, "On operational flexibility in power systems," in *2012 IEEE Power and Energy Society General Meeting*, 2012, pp. 1–8.

[61] A. Ulbig and G. Andersson, "Analyzing operational flexibility of electric power systems," *Int. J. Electr. Power Energy Syst.*, vol. 72, pp. 155–164, 2015.

[62] P. Denholm and M. Hand, "Grid flexibility and storage required to achieve very high penetration of variable renewable electricity," *Energy Policy*, vol. 39, no. 3, pp. 1817–1830, 2011.

[63] P. D. Brown, J. A. Peas Lopes, and M. A. Matos, "Optimization of Pumped Storage Capacity in an Isolated Power System With Large Renewable Penetration," *IEEE Trans. Power Syst.*, vol. 23, no. 2, pp. 523–531, May 2008.

[64] K. Dvijotham, M. Chertkov, and S. Backhaus, "Storage Sizing and Placement through Operational and Uncertainty-Aware Simulations," in *2014 47th Hawaii International Conference on System Sciences*, 2014, pp. 2408–2416.

[65] M. Ghofrani, A. Arabali, M. Etezadi-Amoli, and M. S. Fadali, "A Framework for Optimal Placement of Energy Storage Units Within a Power System With

High Wind Penetration," *IEEE Trans. Sustain. Energy*, vol. 4, no. 2, pp. 434–442, Apr. 2013.

[66] S. Wogrin and D. F. Gayme, "Optimizing Storage Siting, Sizing, and Technology Portfolios in Transmission-Constrained Networks," *IEEE Trans. Power Syst.*, vol. 30, no. 6, pp. 3304–3313, Nov. 2015.

[67] S. Akita, "Future Technology in Power Systems," *International Workshop on Construction of Low-Carbon Society using Superconducting and Cryogenics Technology*, pp. 1–24, 2016.

[68] I. Wasiak, R. Pawelek, and R. Mienski, "Energy storage application in low-voltage microgrids for energy management and power quality improvement," *IET Gener. Transm. Distrib.*, vol. 8, no. 3, pp. 463–472, Mar. 2014.

[69] N. R. Tummuru, M. K. Mishra, and S. Srinivas, "Dynamic Energy Management of Renewable Grid Integrated Hybrid Energy Storage System," *IEEE Trans. Ind. Electron.*, vol. 62, no. 12, pp. 7728–7737, Dec. 2015.

[70] B. Olek and M. Wierzbowski, "Local Energy Balancing and Ancillary Services in Low-Voltage Networks With Distributed Generation, Energy Storage, and Active Loads," *IEEE Trans. Ind. Electron.*, vol. 62, no. 4, pp. 2499–2508, Apr. 2015.

[71] K. Christakou, D.-C. Tomozei, M. Bahramipanah, J.-Y. Le Boudec, and M. Paolone, "Primary Voltage Control in Active Distribution Networks via Broadcast Signals: The Case of Distributed Storage," *IEEE Trans. Smart Grid*, vol. 5, no. 5, pp. 2314–2325, Sep. 2014.

[72] L. M. Putranto, R. Hara, H. Kita, and E. Tanaka, "Multistage-based Preventive Scheme Considering Energy Storage System Operation in an Integrated Renewable Energy System for Securing Voltage Stability," in *Power Engineering and Power Systems Engineering Joint Technical Meeting*, 2016, p. PE-16-157, PSE-16-177.

[73] S. C. Muller, A. Kubis, S. Brato, U. Hager, C. Rehtanz, and J. Gotze, "New applications for wide-area monitoring, protection and control," in *2012 3rd IEEE PES Innovative Smart Grid Technologies Europe (ISGT Europe)*, 2012, pp. 1–8.

[74] B. Milosevic and M. Begovic, "Nondominated sorting genetic algorithm for optimal phasor measurement placement," in *2003 IEEE Power Engineering Society General Meeting (IEEE Cat. No.03CH37491)*, p. 639.

[75] M. Hajian, A. M. Ranjbar, T. Amraee, and A. R. Shirani, "Optimal Placement of Phasor Measurement Units: Particle Swarm Optimization Approach," in *2007 International Conference on Intelligent Systems Applications to Power Systems*, 2007, pp. 1–6.

[76] X. Bian and J. Qiu, "Adaptive Clonal Algorithm and Its Application for Optimal PMU Placement," in *2006 International Conference on Communications, Circuits and Systems*, 2006, pp. 2102–2106.

[77] A. H. Al-Mohammed, M. A. Abido, and M. M. Mansour, "Optimal PMU placement for power system observability using differential evolution," in *2011 11th International Conference on Intelligent Systems Design and Applications*, 2011, pp. 277–282.

[78] F. Aminifar, C. Lucas, A. Khodaei, and M. Fotuhi-Firuzabad, "Optimal Placement of Phasor Measurement Units Using Immunity Genetic Algorithm," *IEEE Trans. Power Deliv.*, vol. 24, no. 3, pp. 1014–1020, Jul. 2009.

[79] B. Gou, "Optimal Placement of PMUs by Integer Linear Programming," *IEEE Trans. Power Syst.*, vol. 23, no. 3, pp. 1525–1526, Aug. 2008.

[80] B. Gou, "Generalized Integer Linear Programming Formulation for Optimal PMU Placement," *IEEE Trans. Power Syst.*, vol. 23, no. 3, pp. 1099–1104, Aug. 2008.

[81] B. K. Saha Roy, A. K. Sinha, and A. K. Pradhan, "An optimal PMU placement technique for power system observability," *Int. J. Electr. Power Energy Syst.*, vol. 42, no. 1, pp. 71–77, 2012.

[82] F. Aminifar, A. Khodaei, M. Fotuhi-Firuzabad, and M. Shahidehpour, "Contingency-Constrained PMU Placement in Power Networks," *IEEE Trans. Power Syst.*, vol. 25, no. 1, pp. 516–523, Feb. 2010.

[83] X. Tai, D. Marelli, E. Rohr, and M. Fu, "Optimal PMU placement for power system state estimation with random component outages," *Int. J. Electr. Power Energy Syst.*, vol. 51, pp. 35–42, 2013.

[84] F. Aminifar, M. Fotuhi-Firuzabad, M. Shahidehpour, and A. Khodaei, "Observability enhancement by optimal PMU placement considering random power system outages," *Energy Syst.*, vol. 2, no. 1, pp. 45–65, Mar. 2011.

[85] F. Aminifar, M. Fotuhi-Firuzabad, M. Shahidehpour, and A. Khodaei, "Probabilistic Multistage PMU Placement in Electric Power Systems," *IEEE Trans. Power Deliv.*, vol. 26, no. 2, pp. 841–849, Apr. 2011.

[86] Xiaolin Gao, "An optimal PMU placement method considering bus weight and voltage stability," in *2013 12th International Conference on Environment and Electrical Engineering*, 2013, pp. 124–129.

[87] L. Huang, Y. Sun, J. Xu, W. Gao, J. Zhang, and Z. Wu, "Optimal PMU Placement Considering Controlled Islanding of Power System," *IEEE Trans. Power Syst.*, vol. 29, no. 2, pp. 742–755, Mar. 2014.

[88] F. Broussolle, "State Estimation in Power Systems: Detecting Bad Data through the Sparse Inverse Matrix Method," *IEEE Trans. Power Appar. Syst.*, vol. PAS-97, no. 3, pp. 678–682, May 1978.

[89] A. M. Erisman and W. F. Tinney, "On computing certain elements of the inverse of a sparse matrix," *Commun. ACM*, vol. 18, no. 3, pp. 177–179, Mar. 1975.

[90] K. Takahashi, J. Fagan, and M. Chen, "Formation of a sparse bus impedance matrix and its application to short circuit study," in *Proceeding of PICA*, 1973, pp. 63–69.

[91] P. W. Holland and R. E. Welsch, "Robust regression using iteratively reweighted least-squares," *Commun. Stat. - Theory Methods*, vol. 6, no. 9, pp. 813–827, Jan. 1977.

[92] R. C. Pires, A. Simoes Costa, and L. Mili, "Iteratively reweighted least-squares state estimation through Givens Rotations," *IEEE Trans. Power Syst.*, vol. 14, no. 4, pp. 1499–1507, 1999.

[93] A. Abur and A. Gomez-Exposito, *Power System State Estimation: Theory and Implementation*. New York: Marcel Dekker, 2004.

[94] L. Mili, M. G. Cheniae, N. S. Vichare, and P. J. Rousseeuw, "Robust state estimation based on projection statistics [of power systems]," *IEEE Trans.*

Power Syst., vol. 11, no. 2, pp. 1118–1127, May 1996.

[95] M. B. Do Coutto Filho, J. C. Stacchini de Souza, and M. A. Ribeiro Guimaraens, "Enhanced Bad Data Processing by Phasor-Aided State Estimation," *IEEE Trans. Power Syst.*, vol. 29, no. 5, pp. 2200–2209, Sep. 2014.

[96] M. Gol and A. Abur, "LAV Based Robust State Estimation for Systems Measured by PMUs," *IEEE Trans. Smart Grid*, vol. 5, no. 4, pp. 1808–1814, Jul. 2014.

[97] F. Aminifar, M. Shahidehpour, M. Fotuhi-Firuzabad, and S. Kamalinia, "Power System Dynamic State Estimation With Synchronized Phasor Measurements," *IEEE Trans. Instrum. Meas.*, vol. 63, no. 2, pp. 352–363, Feb. 2014.

[98] C. Zheng, V. Malbasa, and M. Kezunovic, "Regression tree for stability margin prediction using synchrophasor measurements," *IEEE Trans. Power Syst.*, vol. 28, no. 2, pp. 1978–1987, May 2013.

[99] R. F. Nuqui and A. G. Phadke, "Phasor measurement unit placement based on incomplete observability," in *IEEE Power Engineering Society Summer Meeting*, vol. 2, pp. 888–893.

[100] G. Venugopal, R. Veilumuthu, and P. A. Theresa, "Optimal PMU Placement and Observability of Power System using PSAT," in *International Journal of Computer Network and Security*, 2010.

[101] L. M. Putranto, R. Hara, H. Kita, and E. Tanaka, "Voltage stability-based PMU placement considering N- 1 line contingency and power system reliability," in *The 2nd IEEE Conference on Power Engineering and Renewable Energy (ICPERE) 2014*, 2014, pp. 120–125.

[102] L. M. Putranto, R. Hara, H. Kita, and E. Tanaka, "Series PMU Data-based State Estimation Technique for WAMS Application," in *2016 IEEE Power and Energy Society General Meeting*, 2016, pp. 1–5.

[103] "IBM ILOG CPLEX System version 12.1 User's Manual for CPLEX." 2009.

[104] "IEEE Standard for Synchrophasors for Power Systems," in *IEEE Std C37.118-2005*, 2006, pp. 1–57.

[105] B. Gou and R. G. Kavasseri, "Unified PMU Placement for Observability and

Bad Data Detection in State Estimation," *IEEE Trans. Power Syst.*, vol. 29, no. 6, pp. 2573–2580, Nov. 2014.

[106] D. Li, R. Li, Y. Sun, and H. Chen, "State estimation with WAMS/SCADA hybrid measurements," in *2009 IEEE Power & Energy Society General Meeting*, 2009, pp. 1–5.

[107] A. M. Glazunova, I. N. Kolosok, and E. S. Korkina, "PMU placement on the basis of SCADA measurements for fast load flow calculation in electric power systems," in *2009 IEEE Bucharest PowerTech*, 2009, pp. 1–6.

[108] S. Azizi, G. B. Gharehpetian, and A. S. Dobakhshari, "Optimal Integration of Phasor Measurement Units in Power Systems Considering Conventional Measurements," *IEEE Trans. Smart Grid*, vol. 4, no. 2, pp. 1113–1121, Jun. 2013.

[109] G. N. Korres and N. M. Manousakis, "State estimation and bad data processing for systems including PMU and SCADA measurements," *Electr. Power Syst. Res.*, vol. 81, no. 7, pp. 1514–1524, 2011.

[110] L. M. Putranto, R. Hara, H. Kita, and E. Tanaka, "WAMS hybrid configuration for real time voltage stability monitoring application," in *2016 17th International Scientific Conference on Electric Power Engineering (EPE)*, 2016, pp. 1–6.

[111] L. M. Putranto, R. Hara, H. Kita, and E. Tanaka, "Optimal WAMS Hybrid Configuration for Voltage Stability Monitoring Application considering the Existence of Conventional Measurement," *IEEJ Trans. Power Energy (Under Rev.*

[112] WECC, "Remedial action scheme design guide," 2006.

APPENDIX

APPENDIX A Modified IEEE 57-bus test system

Modified IEEE 57-bus test system is used as the test system. The system is equipped by the additional controllable reactive power compensators in buses 25 and 46 (inductive) and at buses 18 and 34. For describing the RE generation, RE generator are penetrated at buses 14, 18, and 56. The topography of the test systems are described in Figure A.1 and Table A.1. Then, the generator cost, alfa coefficient and reactive power limit is presented in Table A.2

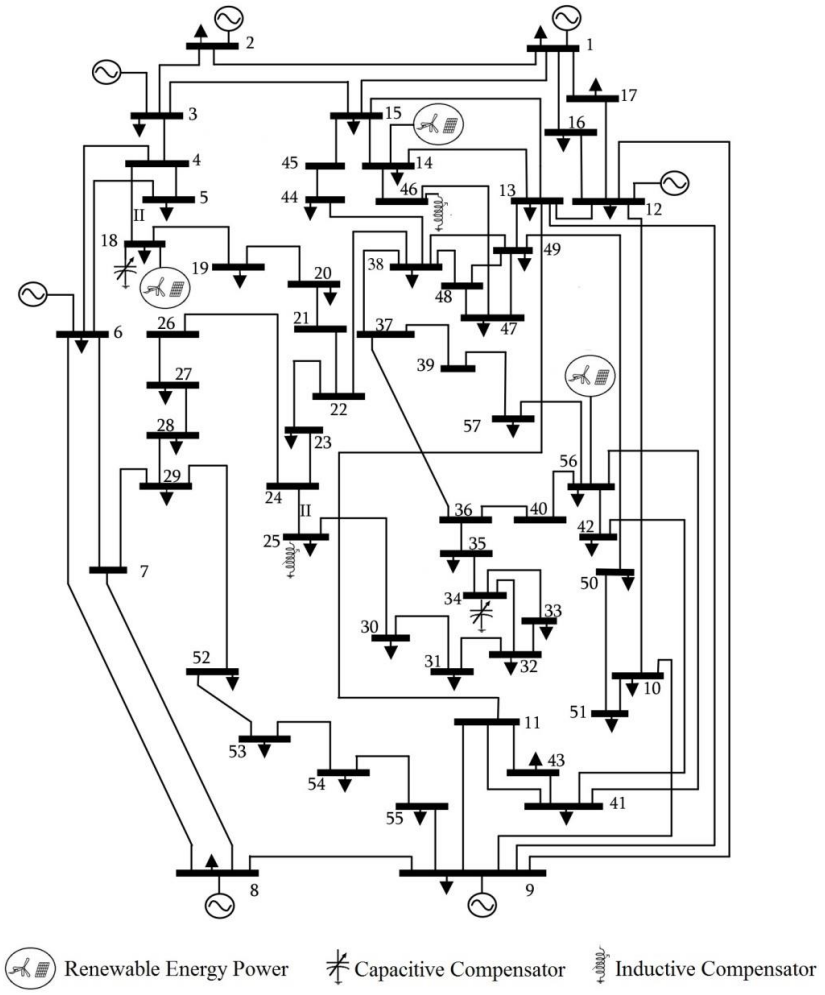

Figure A.1 Modified IEEE 57-bus Test System

Table A.1 Line Numbering in IEEE-57 bus test system

Line Number	From bus	To bus	Line Number	From bus	To bus
1	1	2	41	7	29
2	2	3	42	25	30
3	3	4	43	30	31
4	4	5	44	31	32
5	4	6	45	32	33
6	6	7	46	34	32
7	6	8	47	34	35
8	8	9	48	35	36
9	9	10	49	36	37
10	9	11	50	37	38
11	9	12	51	37	39
12	9	13	52	36	40
13	13	14	53	22	38
14	13	15	54	11	41
15	1	15	55	41	42
16	1	16	56	41	43
17	1	17	57	38	44
18	3	15	58	15	45
19	4	18	59	14	46
20	4	18	60	46	47
21	5	6	61	47	48
22	7	8	62	48	49
23	10	12	63	49	50
24	11	13	64	50	51
25	12	13	65	10	51
26	12	16	66	13	49
27	12	17	67	29	52
28	14	15	68	52	53
29	18	19	69	53	54
30	19	20	70	54	55
31	21	20	71	11	43
32	21	22	72	44	45
33	22	23	73	40	56
34	23	24	74	56	41
35	24	25	75	56	42
36	24	25	76	39	57
37	24	26	77	57	56
38	26	27	78	38	49
39	27	28	79	38	48
40	28	29	80	9	55

Table A.2 Generator cost, reduction coefficient and reactive power range

Gen	Gen Cost Coefficient (Unit Cost)			Generator Reduction Coefficient (α)	Reactive Power Limit (Mvar)	
	a	b	c		$Q_{G_{imin}}$	$Q_{G_{imax}}$
1	0.0776	20	0	0.2578	-140	200
2	0.0100	40	0	0.0671	-40	60
3	0.2500	20	0	0.0752	-30	50
6	0.0100	40	0	0.0537	-50	80
8	0.0222	20	0	0.2955	-140	200
9	0.0100	40	0	0.0671	-80	90
12	0.03226	20	0	0.1835	-150	155